FLUIDIZED-BED ODH OF ETHANE TO ETHYLENE: OPTIMIZATION MODELING AND CATALYST DEVELOPMENT

BY

Abd Alwadood Hassan Elbadawi

A Thesis Presented to the

DEANSHIP OF GRADUATE STUDIES

KING FAHD UNIVERSITY OF PETROLEUM & MINERALS

DHAHRAN, SAUDI ARABIA

In Partial Fulfillment of the
Requirements for the Degree of

MASTER OF SCIENCE

In

CHEMICAL ENGINEERING

November 2014

KING FAHD UNIVERSITY OF PETROLEUM & MINERALS

DHAHRAN- 31261, SAUDI ARABIA

DEANSHIP OF GRADUATE STUDIES

This thesis, written by **Abd Alwadood H. Elbadawi** under the direction his Thesis advisor

and approved by his Thesis committee, has been presented and accepted by the Dean of

Graduate Studies, in partial fulfillment of the requirements for the degree of **MASTER**

OF SCIENCE IN CHEMICAL ENGINEERING.

Dr. Mohammed S.Ba-Shammakh
(Advisor)

Dr. Mohammed S.Ba-Shammakh
Department Chairman

Dr. Mohammad M. Hossain
(Co-Advisor)

Dr. Salam A. Zummo
Dean of Graduate Studies

Dr. Sameer Al-Ghamdi
(Member)

12|1|15
Date

Dr. Shaikh A.Razzak
(Member)

Dr. Abdalla A. Al-Shammari
(Member)

Dedicated

To my parents who love me unconditionally
to my supportive family and
to my teachers

ACKNOWLEDGMENT

TABLE OF CONTENTS

LIST OF TABLES

LIST OF FIGURES

x

LIST OF SYMBOLES

M_{WV} molecular weight of vanadium g/mol

E_{des} energy of desorption, kJ/mol

k_{d0} pre-exponential factor

k_d adsorption constant

T_m centering temperature K

T desorption temperature, K

r_{des} rate of desorption ml-NH_3/g.s

V_d volume of ammonia desorbed, ml/g

V_m volume of ammonia adsorbed at saturation conditions, ml/g

n order of the desorption rate

R the universal gas constant J/k.mol or cm^3 atm K^{-1} mol^{-1}

VO_x vanadium oxide surface species

Greek letters

β rate of temperature increase, °C/min

θ_{des} surface coverage of adsorbed species

ν stoichiometric number

Abbreviations

ODH oxidative dehydrogenation

XRD X-ray diffraction

TPR temperature-programmed reduction

TPO temperature-programmed oxidation

TPD temperature-programmed desorption

ABSTRACT

Full Name   : [Abd Alwadood Hassan Elbadawi Babikir]

Thesis Title   : [Fluidized-bed ODH of ethane to ethylene: optimization modeling and catalyst development]

Major Field   : [Chemical Engineering]

Date of Degree : [November 2014]

Oxidative dehydrogenation (ODH) of ethane to ethylene is investigated in a fluidized-bed with a gas phase oxygen free environment over $VO_x/\gamma\text{-}Al_2O_3\text{-}ZrO_2$ catalysts. In catalyst formulation, both ZrO_2 and VO_x loading are varied to obtain optimum catalytic performance. TPR/TPO results show that $VO_x/\gamma\text{-}Al_2O_3\text{-}ZrO_2$ catalyst is very reactive and stable in repeated reduction and oxidation cycles. NH_3-TPD analysis and desorption kinetics modeling indicate that the modification of ZrO_2 gives an intermediate catalyst acidity and medium metal-support interaction. The estimated energy of ammonia desorption is found to be 75.4, 77.8 and 80.5 kJ/g for Al_2O_3/ZrO_2 ratio of 2:1, 1:1 and 1:2, respectively. The increasing energy of desorption is due to the increased metal support interaction for the additional ZrO_2 content. XRD, Raman and FTIR analysis indicate the presence of crystal phases and VO_x phases. The catalysts are evaluated in a fluidized CREC Riser Simulator in temperature range of 525-600 ^{o}C and 20-50 seconds contact time. The catalyst with Al_2O_3/ZrO_2 ratio of 1:1 and 10 % VO_x loading displays highest ethylene selectivity (91.3%) and minimum CO_x formation (9.7 %). The kinetics of gas phase oxygen free ODH of ethane is established by using a modified Langmuir-Hinshelwood type model considering all the series-parallel reactions. The reducibility of the catalysts is also incorporated in kinetic models. It appears that the specific reaction rate constant for ethylene formation is almost 10 times higher than that of the formation of CO_x which is consistent to the product selectivity data. Finally, reaction conditions are optimized with GAMS using kinetic parameters and proposed reaction network. Optimum ethylene selectivity found to be 92 % at 5.6% ethane conversion and these two are slightly higher than what obtained by experiment. Theoretical optimum operating conditions found to be 600 ^{o}C using 0.2 g catalyst and reaction time of 20 seconds.

ملخص الرسالة

الاسم الكامل: عبد الودود حسن البدوى بابكر

عنوان الرسالة: أكسدة غاز الايثان المتميعة الى الايثلين بانتزاع الأوكسجين : النمذجة الامثل وتطوير الحفاز

التخصص: الهندسة الكيميائية

تاريخ الدرجة العلمية: نوفمبر 2014

في هذه البحث تمت دراسة اكسدة غاز الايثان الى الايثلين بانتزاع الهيدروجين بانتزاع الهيدروجين باستخدام $VO_x/\gamma\text{-}Al_2O_3\text{-}ZrO_2$ كحفاز في بيئة خالية من الاوكسجين، حيث تم تغيير نسب كل من ZrO_2 و VO_x لتحديد نسب الحفاز التي تعطي افضل اداء. نتائج تحليل TPR/TPO اظهرت ان الحفاز $VO_x/\gamma\text{-}Al_2O_3\text{-}ZrO_2$ نشط ومستقر اثناء دورات الاكسدة والاختزال. دراسة $NH_3\text{-}TPD$ و تحليل حركيات التفاعل في هذه الاختبار اعطت مؤشر الى ان حموضة الحفاز منخفضة بالاضافة الى ان تفاعلا المعدن مع الداعم متوسط. تم حساب الطاقه اللازمة لامتزاز الامونيا ووجد انها تعادل 75.4 ، 77.8 و80.5 ك.جول للنسب ZrO_2 الى Al_2O_3 (2:1) ، (1:1) و(2:1) على التوالي. الزيادة في طاقة امتزاز الامونيا نسبة الى اضافة مركب اوكسيد الزركونيوم. ايضا تحليل الحفاز بواسطة XRD، Raman و FTIR اثبت وجود طور كريستالي من مركبات VO_x . تم اختبار الحفاز باستخدام مفاعل CREC Riser Simulator المتميع في درجة حرارة من 525 الى 600 درجة مئوية وزمن تفاعل من 20-50 ثانية. الحفاز المكون من نسبة (1:1) ZrO_2 الى Al_2O_3 والذي يحتوي على 10% VO_x اعطى افضل نتائح من حيث انتقائية الايثلين والتي تعادل 91% واقل انتقائية لغازات اوكسيد الكربون والتي تعادل 9.7 % . في هذا البحث ايضا تم دراسة حركيات التفاعل لاكسدة الايثان الى الايثلين في بيئة خالية من الاوكسجين باستخدام ميكانيكية Langmuir- Hinshelwood المعدلة اخذين في الاعتبار كل التفاعلات المتوازية والمتزامنة وكذلك درجة اختزال الحفاز. نائج دراسة حركيات التفاعل اظهرت ان ثابت معدل تفاعل انتاج الايثلين 10 اضعاف ثابت معدل تفاعل انتاج CO_x وذلك يتوافق مع نتائج التفاعل التجريبية. وبالاضافة تم امثلة التفاعل باستخدام برنامج GAMS ونتائج دراسة حركيات التفاعل ووجد ان الانتقائية المثلى للايثلين 92% عند نسبة تحويل 5.6% للايثان. والظروف المثلى لتحقيق هذه النتائج النظرية هي 600 درجة مئوية و0.2 جم من الحفاز ومدة تفاعل تقدر ب 20 ثانية.

CHAPTER 1

INTRODUCTION

1.1. Background

Ethylene is a valuable feed stock for the petrochemical industries. It is used as starting chemical to produce wide range of chemicals and products [1]. The major applications of ethylene include in (i) polymerization, (ii) oxidation, (iii) halogenation and hydro-halogenation, (iv) alkylation, (v) oxo reactions, (vi) hydration, (vii) dimerization to n-butenes and (viii) niche uses. Ethylene derivatives are used in the production of textiles, plastics, food packaging, antifreeze, and ethylene oxide glycol ether solvents. Ethylene is also used to produce polyethylene with linear higher olefins. These olefins are used to manufacture detergents, plasticizers, synthetic lubricants, additives, as co-monomers in the production of poly-ethylene. With rapid urbanization and increasing quality of human life, the global demand for ethylene is ever increasing. Figures 1.1 and 1.2 show ethylene production and top producer countries. One can see that Asia, Europe and North America are the top ethylene producing regions. In Asia region, China and the Middle Eastern countries are major ethylene producer.

Steam cracking of petroleum hydrocarbons is the conventional source of ethylene. These steam cracking processes are energy intensive which contribute to the high ethylene production cost. The use of petroleum feed stocks, also the main source of energy, makes

1
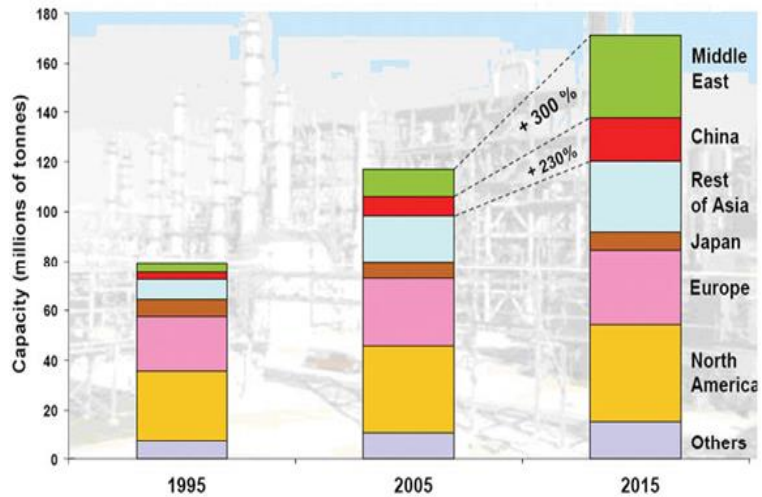
Figure 1.1. World production of ethylene [Parpinelli Tecnon]
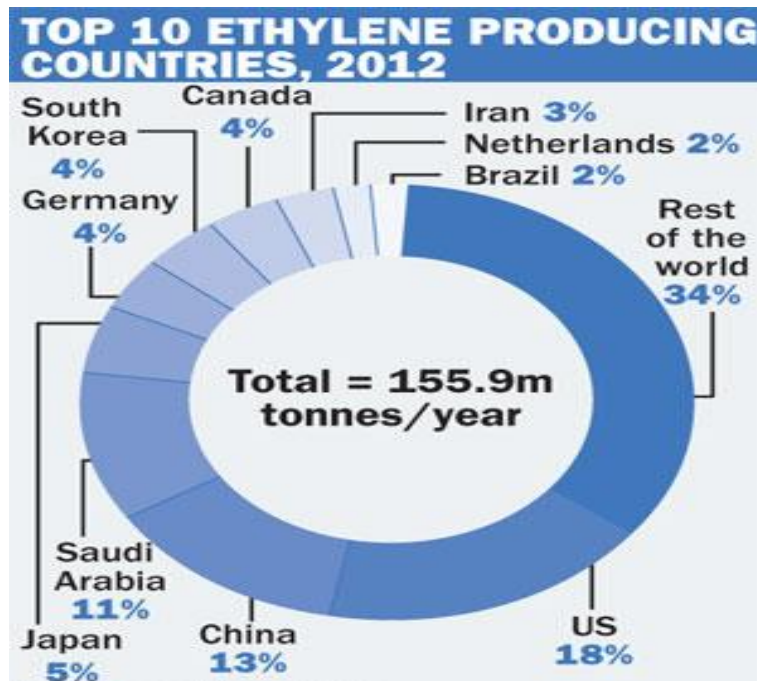
Figure 1.2. Top producing countries [OGJ and GPCA 2013]

the steam cracking approach further costly for producing ethylene. On the other hand, oxidative dehydrogenation (ODH) has a potential to produce ethylene from relatively cheaper gaseous feed stocks such as natural gas and refinery gas. The use of a suitable

catalyst can efficiently process the gaseous feeds to produce ethylene. Due to the fact, in recent years the ODH research has received great deal of attentions both in the industrial and academic settings.

1.2.   ODH of ethane to ethylene

In oxidative dehydrogenation (ODH) process, both the feed ethane and oxidizing air streams are introduced to the reactor as shown in Figure 1.3.

C_2H_4, CO_2, CO
,H_2O ,N_2

Catalyst

C_2H_6, Air
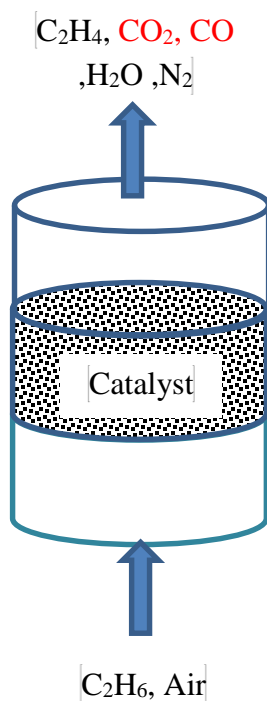
Figure 1.3. Schematic diagram of fixed bed ODH process

Ethylene is produced by a combination of simple dehydrogenation of ethane coupled with combustion of hydrogen to give water (Equation 1.1).

$$C_2H_6 + \tfrac{1}{2}\,O_2 \leftrightarrow C_2H_4 + H_2O \qquad\qquad (1.1)$$

In this process, the presence of oxygen also favors the complete combustion of feed ethane and the product ethylene, which are undesired.

$$C_2H_6 + (1.5 + x)\, O_2 \leftrightarrow 2CO_x + 3H_2O \tag{1.2}$$

$$C_2H_4 + (4x - 2)\, O_2 \leftrightarrow 2CO_x + 2H_2O \tag{1.3}$$
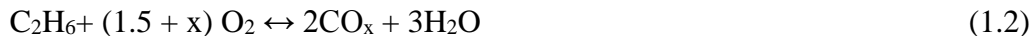
Therefore, the control of consecutive oxidation reactions leading to the formation of undesired by-products are the main challenge of ODH of ethane using gas phase oxygen. In this context, a gas phase oxygen free ODH in a circulating fluidized bed has been considered as a very promising alternative (Figure 1.4). This process consists of two interconnected fluidized bed reactors: (i) ODH reactor and (ii) catalyst regenerator and the solid catalysts is being circulated between the reactors. In this approach, ethane is dehydrogenated in the presence of a solid oxide catalyst which furnishes oxygen to the reactant and this is accompanied by simultaneous reduction of the catalyst. The reduced catalyst is then sent to a regenerator to be re-oxidized in contact with air and recycle back to the ODH reactor. In the overall process, the catalyst is continuously circulated between the ODH reactor and the regenerator. The major advantages of this process is the possibility of achieving higher ethylene selectivity by proper controlling of the reaction temperature given the two exothermic reactions are separated into two less exothermal steps. The remaining outstanding challenge for this process is the development of a fluidizable catalyst capable of satisfying wide variations in the normal metal oxidation state without suffering any structural failure.
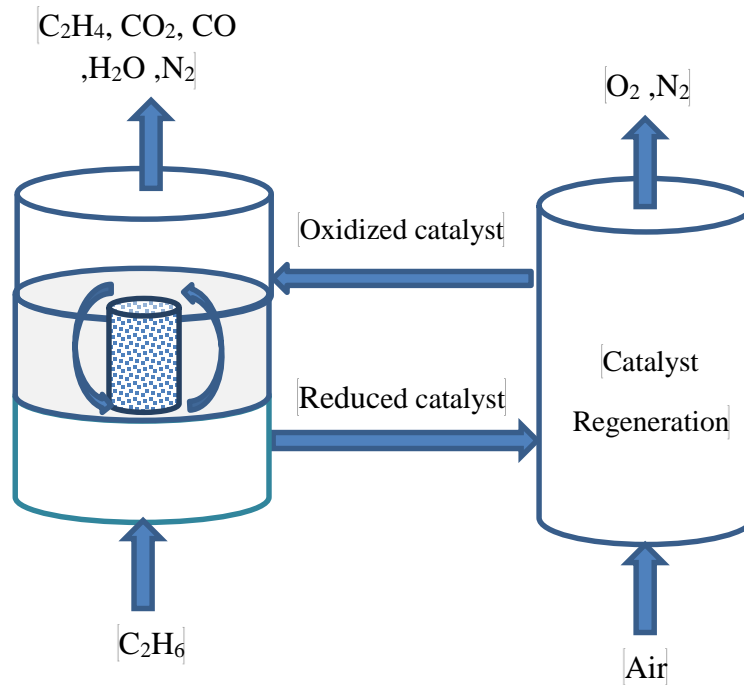
Figure 1.4. Schematic diagram of fluidized bed ODH process

Keeping the above into consideration, the present research has been focused upon investigating ZrO_2 modified fluidizable VO_x/γ-Al_2O_3-ZrO_2 catalysts for ODH of ethane to ethylene under gas phase oxygen free environment. Following are the major contributions of this research:

i. Developed highly active ZrO_2 modified VO_x/γ-Al_2O_3-ZrO_2 catalyst,

ii. Investigated the effects of ZrO_2 on the VO_x/γ-Al_2O_3-ZrO_2,

iii. Investigated the variation of VO_x loading on the VO_x/γ-Al_2O_3-ZrO_2,

iv. Evaluated the reactivity and stability of the synthesized fluidizable VO_x/γ-Al_2O_3-ZrO_2 in a CREC Riser Simulator under the expected conditions of an industrial scale ODH reactor,

v.   Developed mechanism based (Langmuir-Hinshelwood) kinetic model taking into account of catalyst reduction kinetics model,

vi.   Optimized reaction conditions with GAMS using kinetic parameters and proposed reaction network.

CHAPTER 2

LITERATURE REVIEW

The available articles in the open literature are been focused on different aspects of catalysis such as active metal phases, structure and morphology. These components are important for catalyst performance. Moreover, in ODH reaction catalyst selectivity is the most important parameter together with catalyst stability and other parameters. Kinetic modeling as well is a major tool to understand reaction mechanisms. The understanding reaction mechanism can also help to increase ethylene selectivity. In addition these models can be useful to optimize the reaction conditions to maximize the desired product yields. Literature review in this chapter covers catalyst composition, ODH kinetic modeling and optimization.

2.1. ODH Catalyst structure

2.1.1. Catalyst support

Like other conventional heterogeneous catalytic reactions, both the support and the active metal components play important roles in ODH reactions. The most commonly studied metals are V and Cr, using different type of support materials [2]. For example, the phosphate supported V catalysts are more active and provides better ethylene selectivity than that is reported for $(VO)_2 P_2O_7$ [3]. For a Cr containing catalyst, it was shown that at equivalent conversion level, ethylene selectivity varies according to different supports $(VO)_2P_2O_7 > CrPO_4 > Cr/\alpha\text{-}ZrP > Cr/\beta\text{-}ZrP$. Iron phosphate phases such as $FePO_4$, $Fe_2P_2O_7$, $\alpha\text{-}Fe_3(P_2O_7)$ and $\beta\text{-}Fe_3(P_2O_7)$, and nonstoichiometric (mixed) iron phosphate phases with

P:Fe ratios of 1.2:1 and 2:1 have been also reported to be active for ODH reactions [4]. The nickel based Ni–Co/Al$_2$O$_3$ catalysts are active but shows low ethylene selectivity (less than 30 %) [5].

There are some studies investigated different acidic SAPO-34 support materials such as AlPO-34, SAPO-34, NaAPSO-34 and LaAPSO-34 in ODH catalysts [6]. It was demonstrated that the cracking reactions were inhibited with SAPO-34 catalysts. The deactivation effects were practically absent even in a longer period of operation in a laboratory scale reactor. Upon introduction of an active metals such as V, Co, Mg and Mn, the ALPO-5 supported catalysts showed improved activity. However, the ethylene selectivity did not exceed 65% [6]. There are some studies dealt with the acidic and basic Y zeolites supported transition metal (Ni, Cu, and Fe) catalysts in ODH reactions [7]. Among these catalysts, the nickel based catalyst shows better activity and selectivity. Based on the catalyst activity and ethylene selectivity, these metal-loaded Y zeolites samples were ranked as Ni/Y-zeolite > Cu/Y-zeolite > Fe/Y-zeolite [8]. In order to improve the activity and selectivity sometimes Li, Mg, Al, Ga, Ti, Nb and Ta have been used as promoter [9, 10] .

2.1.2. Catalyst active phase

Mo and V are the most commonly used metals for ODH of lighter hydrocarbons. In some cases a third metal has been employed as promoter. The phosphorous promoted bimetallic catalysts were found to be effective, especially when both V and phosphorous were added together [11]. Vanadium with Ti, Sn or Zr pyrophosphates support were studied in ODH reaction [12]. Catalyst exhibited a good conversion with selectivity up to 90%. Cr containing oxide pillared zirconium phosphate materials was synthesized using

the fluoro-complex method which enhanced catalyst activity [13]. A multi component $BaCl_2$–TiO_2–SnO_2 showed high selectivity of ethylene and low CO_x selectivity [14]. It was believed that the presence of Cl^- ions in the catalyst play vital and positive roles in ODH reaction. Although, this catalyst displayed promising result (92.6% ethylene selectivity), the deactivated rate was very high. The catalyst activity was sharply declined during the initial time on stream. The other types of metals tested are La, Nd, Sm and Gd. In catalyst synthesis modified sol-gel method were employed [15]. Among, the synthesized catalysts, Gd-NiO showed the best catalytic performance for ODH reaction, with 56% ethane conversion and 51% ethylene selectivity at 375 ℃. Cobalt–titania (anatase) catalysts was also investigated alone and with the addition of Phosphorous [16].

It was shown that the addition of vanadium and phosphorous can enhance the ethane conversion, ethylene selectivity and catalyst stability although Mo is more effective in the same aspects[17]. NiO–CeO_2 mixed oxides were also investigated. The addition of cerium oxide to NiO also improve the catalytic performance [13]. V_2O_5/Nb_2O_5 catalysts with various V_2O_5 contents was studied [18], it gave 38% selectivity and 28 % yield although pure Nb_2O_5 has very little activity by itself.

It is important to mention here that all the above studies conducted in fixed reactors using air as oxidizing source, which contribute to the CO_x formation due to complete oxidation of feed ethane and product ethylene. Consequently, the ethylene selectivity is low. The other drawback of the fixed bed ODH are the separation of product form CO_x and nitrogen associated with oxidizing air.

Combustion reactions can be controlled by controlling the availability of gas phase oxygen. One of the possible alternative is the gas phase oxygen free ODH in a circulating fluidized bed reactor system as proposed by the present research group [19, 20]. In this approach, the oxidized form of the catalyst will be the source of lattice oxygen. The oxygen depleted catalyst can be re-oxidized by circulating them to a regenerator maintaining a continuous air flow and suitable temperature. It was showed that up to 84.5% ethylene selectivity can be obtained in the range of 550–600 $^{\circ}$C. The selectivity of the VO_x based catalyst can be further improved with MoO_x modification [20]. MoO_x enhanced the reducibility of VO_x therefore ethane conversion was increased. Despite some interesting results both the VOx and VO_x-MoO_x catalyst shows decreased ethylene selectivity at higher temperature and conversion levels which was due to the consecutive oxidation of product ethylene.

2.1.3. Reactor type

In literature mainly fixed bed reactors are employed for oxidative dehydrogenation of lighter hydrocarbons to produce olefins. There are also few studies considered fluidized bed and fluidized bed membrane reactors. Fluidized bed membrane reactor (FLBMR) was studied experimentally in comparison to the conventional operation as a fluidized bed reactor (FLBR) for the catalytic oxidative dehydrogenation of ethane using a g-alumina supported vanadium oxide catalyst. For both reactor configurations, the influence of process parameters such as temperature and contact time was investigated. Further, the experimental data obtained were compared to previous experiments with a fixed-bed reactor (FBR) and a packed-bed membrane reactor (PBMR) operated with a similar catalyst. For identical overall feed rates, the distributed oxidant feeding in the FLBMR

improves the selectivity to ethylene significantly. The beneficial effect of oxidant dosing over the membrane is most pronounced at high temperatures and long contact times. Under limiting oxidant supply the FLBMR and the PBMR show a similar performance, but under moderate oxygen excess the FLBMR outperforms the PBMR significantly. The maximum ethylene yield observed in the FLBMR was 37% compared to 35% for the PBMR. Beside a high productivity, for the FLBMR a broader favorable operation range with respect to the oxygen–hydrocarbon ratio was observed, what indicates a lower sensitivity against oscillations and disturbances in the reactant feed, corresponding to a higher operational safety. Due to excellent heat transfer characteristics, the fluidized bed membrane reactor concept is very promising for maximizing the yield of the desired intermediates also in large-scale plants, especially for strongly exothermic reactions [26].

Oxidative dehydrogenation of ethane to ethylene in a large-scale multi-tubular reactor has been analyzed. The results suggest that the reactor operation would be feasible, provided that high heat transfer areas per unit volume and low to moderate oxygen partial pressures are maintained. Egg-shell-type catalysts lead to a feasible operation through the moderation of the heat generation rate. Although operation with spherical catalyst pellets is realistic, the introduction of catalyst geometries providing higher bed void fractions (e.g., hollow cylinders) would lead to a minimization of the pressure drop and would allow the processing of higher gas flow-rates, leading consequently to increased ethylene production rates. Low operation pressures, a few bars over atmospheric, should be selected resulting from a compromise between an increase in gas density to satisfy both pressure drop and productivity constraints and the drop of selectivity with the increase in pressure. The oxygen distribution along the reactor axial coordinate has a positive impact on the reactor

performance due to an improvement in the selectivity based on the operation with lower oxygen partial pressures. A membrane reactor for the continuous axial feed of oxygen is currently under study for the ODH of ethane to ethylene over Ni-based mixed oxide catalysts [27].

2.2. Kinetics modeling

Short-chain olefin have been produced from several reactions such as cracking and oxidative dehydrogenation (ODH). Kinetics of these reactions were investigated in literature to determine the reaction networks and reaction mechanisms. For example, propane on VO_x/ZrO_2 catalysts kinetic were studied using isotopic tracer, and elementary reaction steps were successfully determinate [28]. A similar study used the same techniques to study elementary steps and their reversibility in the oxidative dehydrogenation of propane over ZrO_2-supported MoO_x catalysts [29]. Study showed that propane is the major product and CO_x gases were produced by secondary combustion of propane. C_4 hydrocarbons ODH reaction over VMgO catalyst investigated and its kinetics were studied, using intermediate products reaction network proposed. Catalyst showed significant activity in absence of oxygen[30]. Kinetic and isotopic tracer and exchange measurements were used to determine elementary steps of ethane ODH over vanadium oxide catalyst. The study suggested that oxygen, OH groups, and oxygen vacancies are the most reactive species during ethane ODH. Furthermore ethane ODH over MoO_3/Al_2O_3 kinetics studied using in-situ FTIR to determine role of the support as well as selective and unselective pathways of the ODH [31]. Mars-Van Krevelen mechanism and Langmuir-Hinshelwood equations were used to investigate reaction networks of ethane ODH over $VO_x/\gamma\text{-}Al_2O_3$ catalyst [32]. Eley–Rideal steady-state mechanism was applied to ODH reaction of ethane

and propane over vanadia-silica catalyst doped by potassium. It was shown that taking into account water adsorption on catalyst surface makes the increases model accuracy [33]. Ethane ODH kinetics over Ni–Nb–O mixed oxides kinetics were studied [34]. Study considered Mars–Van Krevelen mechanism and the kinetic model was able to successfully predict the catalytic performance. Temperature-programmed reaction (TP-reaction) was used to study reaction pathways of oxidative and non-oxidative dehydrogenation of ethane over MoO_3/γ-Al_2O_3 [35]. It was found Al_2O_3 enhance the unselective oxidation of ethane to carbon oxides, and MoO_3 phase is involved in the selective oxidative dehydrogenation (ODH) of ethane to ethylene and over-oxidation of ethylene to CO_x. Vanadium oxide supported on silica (SBA-15) was used for a kinetic study of the ODH of propane in a fixed bed reactor[36]. Moreover, partial oxidation of ethane to ethylene and acetic acid over MoV investigated using two-site Eley-Rideal-Redox (ERR) model which predicted experimental data with good accuracy [37].

Only a few studies investigated ODH reaction in oxygen-free environment. It was reported that ODH reactions can occurs in oxygen-free environment and oxygen could be provided by the catalyst lattice[38]. Furthermore a kinetic model that can be applied using oxygen and oxygen-free environment presented to describe partial oxidation of n-butane to maleic anhydride [39,40]. The proposed kinetic model assumes that there are three sources of oxygen; adsorbed oxygen, surface lattice oxygen and subsurface lattice oxygen. Moreover the degree of catalyst oxidation was taken into account. It was found that lattice oxygen has the major effect on selective oxidation and adsorbed oxygen lead to non-selective oxidation. Propane ODH in oxygen-free environment investigated [41,42],

however there are no reported studies on kinetic of propane ODH in oxygen free environment.

There are several studies on ODH catalysts, there are a few studied that deal with light olefin ODH in dense fluidized beds, using riser or downer reactors. Moreover the majority of these studies in "dense fluidized beds" have been limited to butane ODH [43,44].

The motivation to use the fluidized-bed conditions that it is close to isothermal conditions, in contrast with Fixed-bed reactor which operates at non-isothermal conditions and that may damage the catalyst. Additionally, catalyst has better performance in fluidized conditions in ODH reaction of short-chain hydrocarbons and that bring us to investigate ODH reaction kinetics in such conditions especially ethane ODH to ethylene. The kinetic study of ethane ODH reaction over $VO_x/\gamma\text{-}Al_2O_3$ catalyst is reported [45], using CREC-riser simulator in absence of oxygen feed. Langmuir-Hinshelwood rate expression was used and degree of catalyst oxidation also considered. Model gives good results which in agreement with experimental data.

2.3. Optimization of ethane ODH reaction

Catalyst properties and reaction mechanism are used in the area of reaction conditions modeling and optimization. A representative model should be developed describing what is actually happening during the reaction under study as well as the reactor. Some of these reactors as well as reaction conditions are modeled and optimized in literature, for examples fixed-bed multi-tubular reactor system for ODH of ethane is modeled by examining a variety of parameters affecting reactor performance [46]. Multi-

tubular reactor system which is being used to model ODH reaction of ethane in an industrial-scale reactor for ethylene production was modeled to test a variety of parameters affecting reactor performance. The model showed that a double-bed multi-tubular reactor with intermediate air injection scheme was better than a single-bed design. That is because of the increased ethylene selectivity while operating under lower oxygen partial pressures. The optimized reactor length for 100% oxygen conversion was theoretically determined for both reactor designs. Distributed oxygen feed with a limited number of injection points showed an important improvement on the reactor performance in terms of ethane conversion and ethylene selectivity. This concept also enhances the reactor runaway temperature problem, and enabled operations over a wider range of conditions to obtain enhanced ethylene production.

Another modeling work done considering fluidized bed reactor for the oxidative dehydrogenation of ethylbenzene to styrene[47]. A dynamical model is proposed for a fluidized bed catalytic reactor for the production of styrene by oxidative dehydrogenation of ethylbenzene. The static and dynamic bifurcation of the reactor model conducted, it showed that the reactor is to be operated in a multiplicity region in order to yield a maximum production rate of styrene. Ethylene yield also optimized in oxidative coupling of methane over Li/MgO catalyst [48], the central composite design and the response surface method was effective to estimate the optimum C_2H_4 yield for OCM over Li/MgO (Li/Mg = 0.1). A second order polynomial equation models were developed to estimate the values of C_2H_4 yield, C_2H_4 selectivity and CH_4 conversion by utilizing the experimental data. Neural network modeling method used to model the effect of oxygenate additives on the performance Pt-Sn/γ-Al_2O_3 catalyst in propane dehydrogenation[49]. The

dehydrogenation reaction carried out in fixed bed quartz reactor, steady reports modeling were performed in three different levels of oxygenate additives, and the results gave the optimum amounts of water and ethanol for the reaction.

Regarding oxidative dehydrogenation of ethane to ethylene in fluidized bed reactor, literature review revealed that there are only few studies were focused on the fluidized bed systems. It is required to investigate this case study and to model the reaction to optimize ethylene yield. On the other hand in this study a mathematical model is developed based on temperature programmed reduction characterization technique. The objective is to correlate catalyst properties (metal loading, oxygen carrying capacity) to its performance during oxidation reaction. The model explicitly is a function of temperature and implicitly is a function of metal loading and other catalyst properties.

2.4. Conclusion of literature review

ODH of ethane is a very promising alternative technology for ethylene production. The exothermic nature of the ODH reactions requires less energy as compared to the cracking process. It is economically attractive given it uses comparatively cheaper natural/refinery gas as feed stock. There are significant number of articles available in the open literature dealing with various aspects of ODH of ethane. Followings are the main observations based on the literature review as presented in this Chapter 2:

- Developing a suitable catalyst still a challenge for commercial scale application of ODH of ethane to ethylene. Only few catalysts reported in the open literature show good ethylene selectivity which drastically decreases with increasing ethane

conversion. Complete oxidation of ethane/ethylene to CO_x is mainly responsible for decreasing ethylene selectivity.

- Most of the catalysts are mixed metal oxides with low metal dispersion. The metal-support interaction plays a major role in ethylene selectivity.

- The present research group investigated the novel gas phase oxygen free ODH of ethane to ethylene using a fluidized bed system. This process shows encouraging ethylene selectivity at high ethane conversion. The complete oxidation is significantly decreased due to the unavailability of oxygen in the gas phase.

- There are only a few reported studies presented phenomenological kinetic modeling ODH of ethane, especially in the fluidized bed conditions.

- Only few studies reported the optimization of the ODH process.

Table 2.1. Summary of literature review

Topic	Author	Selectivity ,yield and conversion %	Notes
Ferrous and its oxides	Miller et al 2002	S=65% c=56%	A mixture of $fepo_4$ and $fe_2p_2o_7$
Mo and oxides + (zr, v ,ti) promoter phosphorous support	l. Lisi et al 2005 and haddad et al 2007	S= 90% c= 20%	At 560^oc when vanadium added as promoter
Moo_x	haddad et al , 2009	S=less than in mo based catalyst	Vanadium and phosphorous added to enhance the performance
Vo_x/ c-al$_2$o$_3$	Sameer et al 2012	27.6% conversion and 57.6–84.5% selectivity	Metal–support interactions and as a result, a well dispersed vo_x ,500-600∘c
Ni-o +(la ,nd and gd)	Qin et al 2013	S =51% c=56 %	375^oc using sol-gel method
Vo_x-moo$_x$/ c-al$_2$o$_3$	Bakare et al 2014	S=80% c=24 %	Moo_x improved vo_x isolation
Kinetics of odh over vo_x/ c-al$_2$o$_3$	Sameer et al 2013	-	Langmuir hinshelwood kinetics were applied
Optimization of propane dehydrogenation over pt-sn/γ-al$_2$o$_3$	Mitra et al 2006	-	Neural network modeling method used

CHAPTER 3

OBJECTIVES

3.1 Major objectives

I. Development of a highly active fluidizable VO_x-based catalyst suitable for oxidative dehydrogenation (ODH) of ethane to ethylene in a gas phase oxygen free reaction conditions. In this regard a ZrO_2 modified γAl_2O_3-ZrO_2 is used as support.

II. Establishment of phenomenological based kinetics model to describe the kinetics of ODH ethane using the developed $VO_x/\gamma Al_2O_3$-ZrO_2 catalyst.

III. Optimization ODH of ethane reaction conditions to maximize ethylene selectivity and to minimize CO_2 formation.

3.2 Specific objectives

i. To investigate the effects of ZrO2 modification on the activity and stability of $VO_x/\gamma Al_2O_3$-ZrO_2 catalysts at various $\gamma Al_2O_3/ZrO_2$ ratios and constant VO_x loading.

ii. To optimize the VO_x loading on ZrO_2 modified γAl_2O_3-ZrO_2 supports.

iii. To characterize the catalysts using different techniques such as XRD, N_2 adsorption, FTIR, Raman, NH_3-TPD and TPR/TPO to understand the physiochemical properties of the catalysts and their stability.

iv.   To evaluate the performances (ODH of ethane to ethylene) of the $VO_x/\gamma Al_2O_3$-ZrO_2 catalysts in a fluidized CREC Riser Simulator under different reaction conditions as expected in a large scale ODH unit.

 v.   To construct the reaction network based on experimental data, to develop the reaction mechanisms and to formulate phenomenogical based kinetic model for the fluidized ODH of ethane to ethylene using $VO_x/\gamma Al_2O_3$-ZrO_2.

vi.   To optimize the reaction conditions based on ODH of ethane data in the CREC Riser Simulator, kinetic model and reduction model.   The objective functions are formulated using GAMS software and evaluated by utilizing nonlinear programs solver CONOPT.

CHAPTER 4

EXPERIMENTAL METHODS

4.1. Catalyst synthesis

Impregnation by soaking (excess of solvent) technique was used to prepare catalyst samples [40]. Before metal loading, the support alumina was calcined under pure N_2 flow at 500 ºC for 4 hours to remove moisture and volatile compounds. The calcined sample was placed in a beaker and toluene was added. Zirconium tetra-chloride was then added to the beaker and the mixture was left under stirring for 12 h. The sample was filtered from the solvent and dried under ambient conditions. After complete drying, the sample was calcined again at 500ºC for 5 hours also to remove the solvent. Three support samples prepared with different γ-Al_2O_3 to ZrO_2 weight ratios (2:1, 1:1 and 1:2).

Two sets of sample were prepared using impregnation. In the first set of samples, V loading was kept at 15 wt% on the above three ZrO_2 modified samples. The second set of samples were prepared by successive impregnation to load 5%, 10% and 15% on γ-Al_2O_3/ZrO_2 = 1:1. Vanadyl acetylacetonate $V(AcAc)_3$ (Aldrich, 97%) was used as vanadium precursor. The V loading was also accomplished by the same approach as Zr loading. The Zr modified Al_2O_3 support and $ZrCl_2$ was added to a beaker containing toluene. The mixture was stirred for 24 hours to obtain homogenous mixture which facilitate better metal dispersion. The solid sample was separated by vacuum filtration and dried at ambient temperature. The dried sample was then reduced by hydrogen (10% H_2

and 90% Ar) at 500 °C in a fluidized bed reactor. Finally, the reduced sample was calcined under air at 500 °C for 4h the oxide form of the catalyst was obtained. After this treatment catalyst color became yellow indicating the presence of V_2O_5 on support surface.

4.2. Catalyst characterization

4.2.1. X-Ray Fluorescence (XRF)

XRF analysis was used to determine elements and compounds ratios in each sample. A Bruker Tornado M4 micro-ed XRF analyzer, equipped with a single high performance XFlash detector and 25 μm diameter spot size, employed for XRF analysis.

4.2.2. BET surface area

The nitrogen adsorption and BET surface area of the VO_x/Al_2O_3-ZrO_2 catalyst samples was determined in a Quantachrome ASIQwin. The nitrogen adsorption was carried out at 77 K. For each experiment, 0.4–0.50 g of catalyst sample degassed at 350 °C for 2h. The adsorption isotherms were measured in the 0.04 to 1 relative pressure range.

4.2.3. X-ray diffraction (XRD)

X-ray diffraction (XRD) analysis was conducted to identify the crystallographic structure of catalyst samples. XRD patterns of all catalysts reported in this study were recorded on a Rigaku MiniFlex Diffractometer with monochromatic Cu Kα radiation (λ = 0.15406 nm, 30 kV, 15 mA) using the normal scan rate of 4°/min. X-rays were collected using a 1.25° divergent scattering slit, and a 0.13 mm receiving slit. Samples were scanned within the 2θ range of 20–80° with a step size of 0.005°.

4.2.4. Temperature programmed reduction-oxidation (TPR/TPO)

(TPR/TPO) experiment were conducted using AutoChemII ASAP 2920 analyzer as shown in Figure 4.1. The purposes of TPR/TPO cycles are to determine catalyst activity temperature ranges, maximum activity temperature and catalyst stability during reduction-oxidation cycles. Its reported that during reduction/oxidation at high temperature vanadium dispersion changes[23] and that changes VO_x phases on support surface [24] , and that affects the catalyst activity[25].

At the beginning of the experiment Argon (99.9%) introduced at rate of 50 ml/min while temperature increased to 300 ℃ for period of 3 hours. temperature cooled to ambient and H_2 Argon gas mixture (10% H_2) circulated to reduce the sample at rete of 50 ml/min and temperature elevated to 750 ℃ at heating rate of 10 ℃/min, meanwhile H_2 concentration measured using thermal conductivity detector (TCD) and the signal later calibrated to volume of H_2 consumed cc/g catalyst . Plot of H_2 volume versus time and temperature obtained and total H_2 volume consumed obtained by numerical integration.

4.2.5. Temperature programmed desorption (TPD)

The purposes of NH_3-TPD test was to determine catalyst total acidity. The metal–support interactions were also evaluated by TPD kinetics analysis. Furthermore, NH_3-TPD was utilized to determine the quantity and strength of acid sites available on the surface of the prepared catalyst samples. NH_3-TPD experiments were conducted using a Micromeritics AutoChem II 2029 analyzer. The catalyst sample (0.15-0.20 g) was placed in a U-shaped quartz container and degassed for 2 h at 300 ℃ in a flow of helium at 30 ml/min. The samples were then cooled to 120 ℃ and brought to saturation with ammonia using a NH_3/He gas mixture (5% NH_3/He) for one hour at

a rate of 50 ml/min. After that, the ammonia flow was stopped, and replaced by a He purge gas, fed at the rate of 50 ml/min. This was done for 1 h at 120 ◦C to remove the physically adsorbed ammonia. Following this step, the temperature was raised up to 500 ◦C at different heating rates (10, 20 and 30 ◦C/min). As the temperature was increased, ammonia desorbed as it gained enough energy to overcome the activation energy barrier.
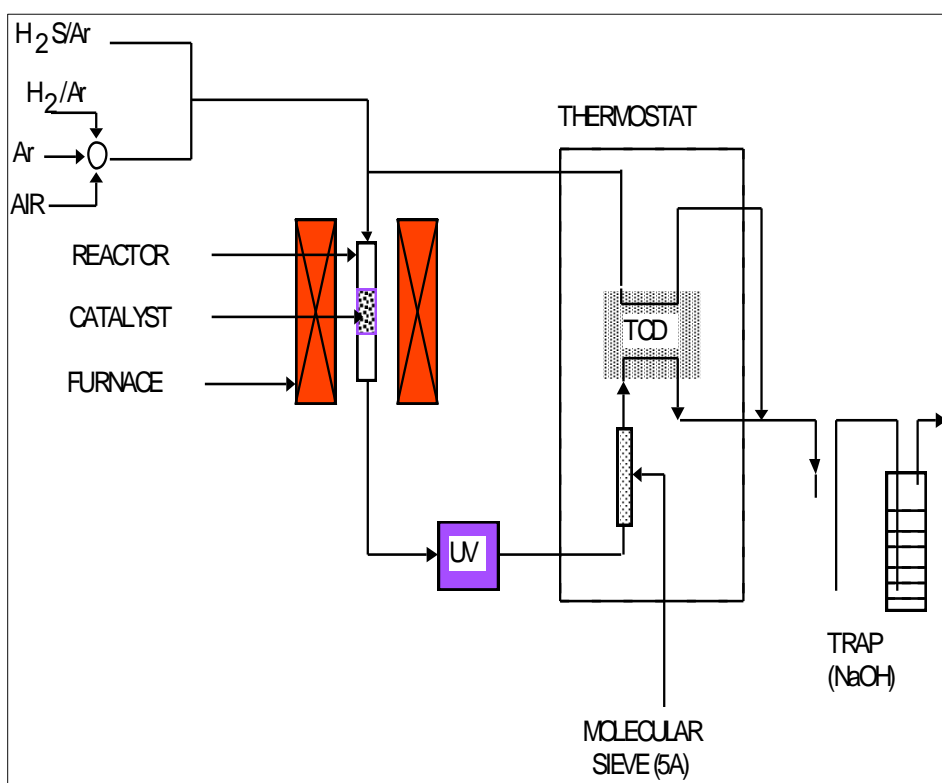
Figure 4.1. Schematic diagram of AutoChemII ASAP 2920 analyzer for TPR test

4.2.6. Scanning electron microscopy (SEM)

Shape and morphology of the active metals phases were examined by SEM (Tescan Lyra-3) with high performance focused ion beam (FIB) at various magnifications (up to 500 kx) using 20 kv voltage. For SEM analysis the samples were prepared by 5 nm Au coating.

4.2.7. Raman spectroscopy

The Raman spectra were collected using Yvon Jobin equipment with a cooled iHR320 Horiba spectrometer with CCD detector that removes the elastic laser scattering, laser source is green type at 532 nm and laser intensity of 50%, with 96 slit width and 50 to 2500 spectrum window. The samples were maintained in powder form to minimize mass transfer limitations and ensure that all catalytic material in the cell is exposed to the flowing gases.

4.2.8. Fourier transform infrared spectroscopy (FTIR)

FTIR spectroscopy of prepared samples was recorded using Nicolet 6700 Thermo Fischer Scientific instrument. For each experiment 3 mg of powdered samples were mixed thoroughly with 400 mg KBr. Thereafter, infrared spectra of pelletized samples were collected in the range 400 cm^{-1} to 4000 cm^{-1}.

4.3. Catalyst evaluation in fluidized CREC riser simulator

4.3.1. Reactor set-up

The reactivity and the stability of the VO_x/γ-Al_2O_3-ZrO_2 catalyst samples were tested using the CREC riser simulator Figure 4.2a [19]. The batch reactor with a capacity of 53 cm^3, has been designed for catalyst evaluation and kinetic studies under fluidized bed

reactor conditions. The major components of the CREC riser simulator in shown in Figure. 4.2a which includes a vacuum box, series of sampling valves, a timer, two pressure transducers and three temperature controllers. The product gas was analyzed by gas chromatography (GC) with thermal conductivity detector (TCD) and a flame ionization detector (FID).

4.3.2. Fluidized bed ODH of ethane experimental runs

The ODH of ethane to ethylene experiments were conducted at various temperatures and contact times. The selected temperature should be consistent to the reduction temperature of the catalysts as observed in the TPR analysis. In a typical run, 0.4 g of oxidized catalyst sample was loaded in the reactor basket and leak test was conducted. Following the leak test, the system was purged by flowing argon. The temperature program was started to heat the reactor to the desired temperature. The argon flow was maintained to keep the reactor from any interference of gas phase oxygen. Once the reactor temperature reached to the desired temperature, the argon flow was discontinued. The reactor isolation valve was closed when it reached the desired pressure level.

The vacuum pump was started to evacuate the vacuum box until it reached 20.7 kPa (3.75 psi). The catalyst was fluidized by rotating the impeller. At this point, feed ethane was injected into the reactor by using preloaded gas tight syringe. The reaction continues for a pre-specified time. At termination point, the isolation valve between the
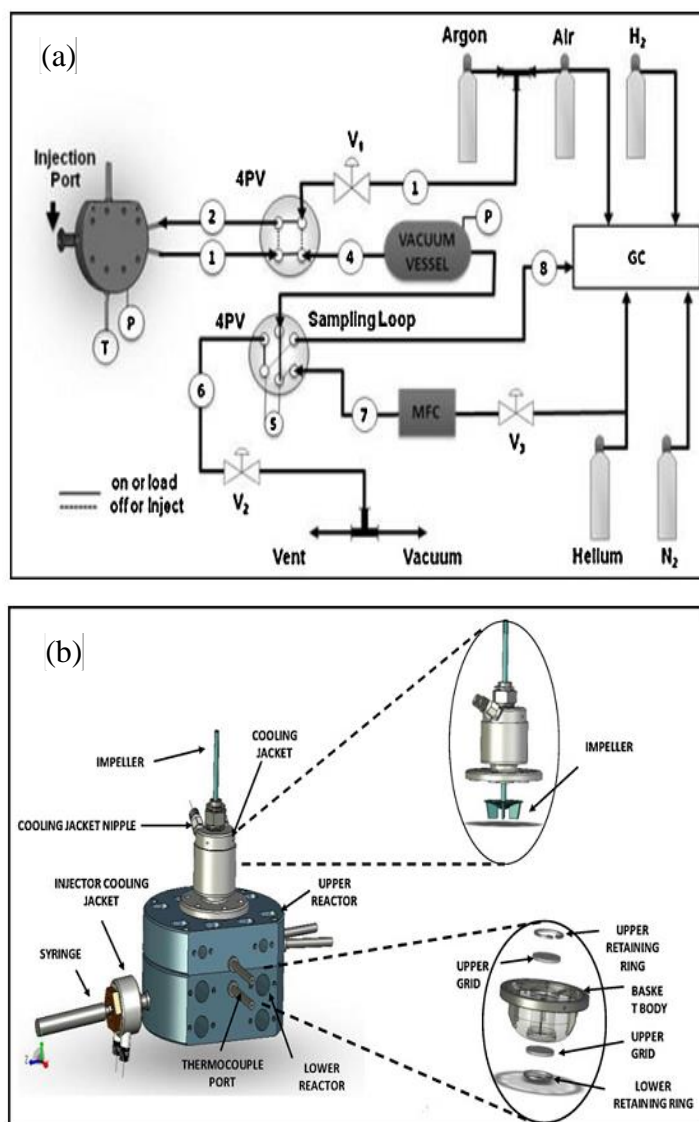
Figure 4.2. (a) Schematic diagram of the CREC riser simulator experimental set-up (b) Overview of the CREC riser simulator reactor body.

reactor and vacuum box opened automatically and transferred all the reactant and products into the vacuum box. The gas samples in the vacuum bottle were analyzed using an Agilent 7890A GC equipped with both a TCD and a FID detector. For each catalytic run, the product samples were analyzed three times to ensure the accuracy of the analysis. Finally, the product analysis data were used to calculate conversion and selectivity of

various products. The following definitions were used in calculating the conversion and selectivity, respectively:

$$\text{Conversion of ethane} = \frac{\text{Moles of ethane converted}}{\text{Moles of ethane fed}} \times 100 \text{ \%} \qquad (4.1)$$

$$\text{Selectivity of product i} = \frac{\text{Moles of product i}}{\text{Total moles of products} - \text{Moles of i}} \times 100 \text{ \%} \quad (4.2)$$

CHAPTER 5

RESULTS AND DISCUSSION - EFFECTS OF ZrO$_2$

This chapter presents the effects of ZrO$_2$ modification on VO$_x$/γ-Al$_2$O$_3$-ZrO$_2$ catalysts. The support γ-Al$_2$O$_3$ was modified using different amount of ZrO$_2$. The VO$_x$ was then dispersed on the ZrO$_2$ modified γ-Al$_2$O$_3$-ZrO$_2$ supports. It is hypothesized that the addition of ZrO$_2$ alters the surface acidity and the metal-support interaction which has significant influence on the ethylene selectivity [12]. The effects of ZrO$_2$ modification was assessed by different characterization techniques such as XRF, XRD TPR/TPO, TPD and Raman. The metal support interaction was demonstrated by NH$_3$ desorption kinetics analysis. The catalysts were evaluated in a fluidized CREC riser simulator at various reaction conditions as expected in a large scale ODH reactors using ethane as a feed.

5.1. Catalyst characterization

5.1.1. XRF and nitrogen adsorption/desorption analysis

XRF analysis was used to quantify sample compositions after synthesis. XRF results are shown in Table 5.1 which indicates compound percentages are equal to what was targeted with slight deviation. The nitrogen isotherm analysis was conducted to understand the adsorption/desorption characteristics of the catalyst sample. The isotherm data was further processed to determine the BET surface of ZrO$_2$ modified VO$_x$/γ-Al$_2$O$_3$-ZrO$_2$ sample. Figure 5.1 shows the adsorption/desorption isotherms of a ZrO$_2$ modified VO$_x$/γ-Al$_2$O$_3$-ZrO$_2$ sample synthesized for this study. The sample shows a Type-V

isotherm indicating narrow size mesoporosity [22]. The calculated BET surface area and monolayer volume are presented in Table 5.1. The BET surface area of the ZrO_2 modified sample is lower than the surface of the bare γ-Al_2O_3 support (141 m^2/g). The dispersed ZrO_2 and the vanadium species occupied the support pores, which contributed to the decrease of the surface area. The monolayer volume of the adsorbed nitrogen can be calculated by Equation 5.1

$$n_m = \frac{S_{BET}}{A_m \times N} \tag{5.1}$$
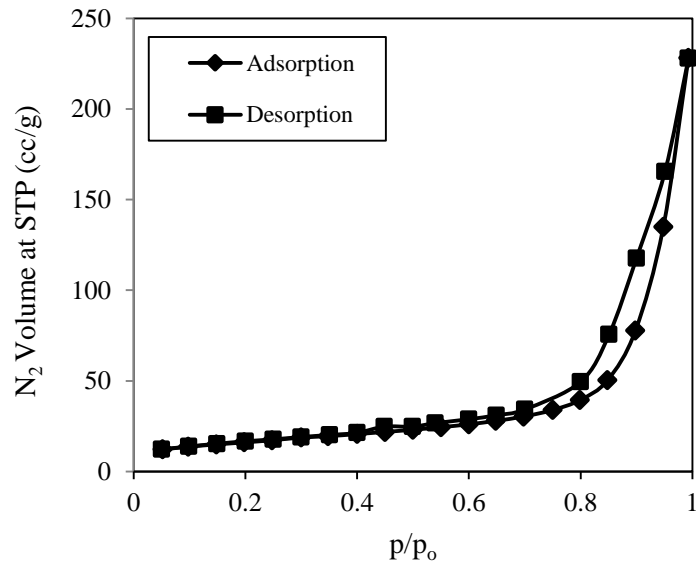
Figure 5.1. N$_2$ adsorption/desorption isotherms of 15%VO$_x$/Al$_2$O$_3$-ZrO$_2$ (2:1) catalyst sample

where, S_{BET} is the BET surface area m^2, N represents Avogadro's constant and molecule/mol, A_m stands for the volume occupied by one N$_2$ gas molecule (0.162 m^2), and n_m denotes the monolayer volume per gram catalyst. The monolayer coverage occurs after 0.75 relative pressure indicates good dispersion of active sites and their availability for

adsorption. This was expected as the catalyst was synthesized by soaking impregnation which provided good metal dispersion and thus, a satisfactory monolayer volume.

Table 5.1. XRF[a] and BET surface area characterization results

Sample	VO_x%	Al_2O_3%	ZrO_2%	BET surface area (m^2/g.cat)	Monolayer volume (cm^3/g)
15%VO_x/Al_2O_3-ZrO_2(2:1)	14.4	57.2	28.4	24.17	2.47×10^{-4}

[a] Catalyst elements percentages are within ±2% accuracy

5.1.2. X-ray diffraction (XRD)

Figure 5.2 shows the XRD patterns of the various γ-Al_2O_3/ZrO_2 containing support samples and the VO_x/γ-Al_2O_3-ZrO_2 catalyst after VO_x loading. The V_2O_5 was detected in the range of 2θ from 10 to 40° are relevant to V_2O_5[26]. T-ZrO_2 peaks can also be found at 2θ of 30°, 48° and 65° while γ-Al_2O_3 peaks appeared at 2θ of 45° and 60°. One can see in Figure 5.3 that the V_2O_5 peak intensity was sharply decreased with decreasing the γ-Al_2O_3 to ZrO_2 ratios (increasing in ZrO_2 contents). Only VO_2 was obtained on the support surface, which resulted in lower oxygen-carrying capacity and therefore lower catalyst activity. Furthermore, ZrO_2 introduced a crystal phase to the catalyst, in comparison with the catalyst sample without ZrO_2 [19].

Increasing ZrO_2 contents reduced V_2O_5 peaks sharpness in samples with (2:1) and (1:1) γ-Al_2O_3 to ZrO_2 weight ratio, and further increasing ZrO_2 content in Al_2O_3-ZrO_2 (1:2) sample only VO_2 was obtained on support surface which results in lower oxygen carrying capacity and therefore catalyst activity. Furthermore ZrO_2 introduced crystal phase to the catalyst in comparison with catalyst sample without ZrO_2 [19], this crystal phase is not
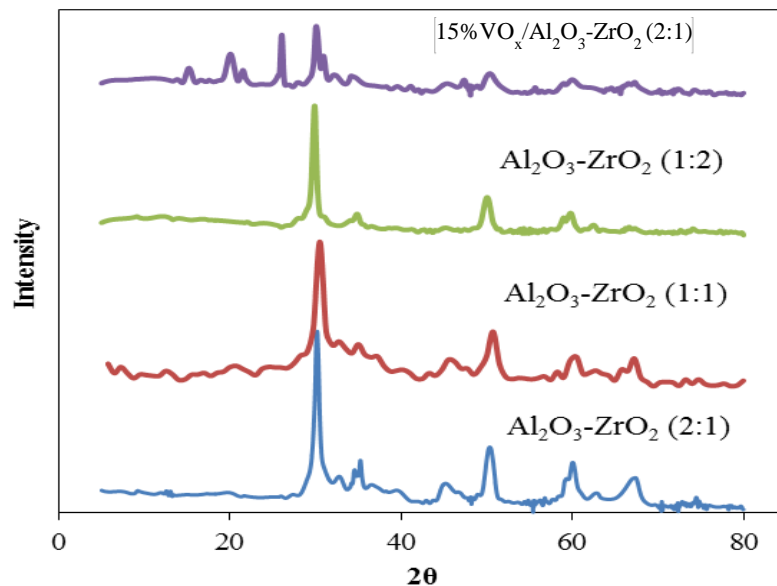
Figure 5.2. XRD patterns of Al_2O_3-ZrO_2 with various ZrO_2 ratios and 15%VO_x/ Al_2O_3-ZrO_2 (2:1)

detected by XRD and may reduce oxygen carrying capacity and catalyst activity by enhancing active site agglomeration.

5.1.3. Reducibility and oxygen carrying capacity

TPR/TPO characterization is an important technique for oxygen free ODH because it simulates the actual ODH reaction as compared in Equation 5.2 and 5.3.

Reduction of catalyst during TPR,

$$V_2O_5 + 2\,H_2 \rightarrow V_2O_3 + 2\,H_2O \qquad\qquad (5.2)$$

Reduction of catalyst during gas phase oxygen free ODH of ethane

$$2CH_3\text{-}CH_3 + V_2O_5 \rightarrow V_2O_3 + 2CH_2{=}CH_2 + 2H_2O \qquad\qquad (5.3)$$
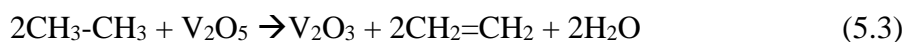
One can easily see that both in the ODH of ethane and in the TPR with hydrogen, the gaseous reactant reduces the V_2O_5 into V_2O_3. Consequently, the TPR evaluation of the catalyst sample clearly indicates the activity (reactivity) of the catalyst at various temperature ranges. The TPR/TPO test also determines the oxygen-carrying capacity and the redox properties of the catalysts. The oxygen-carrying capacity eventually determines the circulation rate of the catalyst between the ODH reactor and the catalyst regenerator.

Figure 5.3 a and b shows the TPR profiles and H_2 consumption for different ZrO_2 containing catalyst samples. In all catalysts, the V loading maintained at 15 wt% of the catalyst. Presence of 3 peaks indicates that the reduction proceeds in several steps [49,53]. Introduction of ZrO_2 reduced support surface acidity and that enhance the formation of isolated mono-vanadate species on support surface [54,55]. During vanadium oxide reduction, oxygen vacancies are formed at the surface. As the reduction proceeds, the concentration of these vacancies gradually decreases. They aggregate and part of vanadium oxide edges may shear producing a new structure (non-isolated species). This may also occur, as a result of increasing the vanadium loading [51].

TPR results may also point to the catalyst oxygen-carrying capacity and the oxygen releasing rate. This is the case, since the oxygen-carrying capacity of the catalyst can be determined according to Equation 5.1(two moles of hydrogen reduce one mole of oxygen). Figure 5.3b shows the histogram plots of hydrogen consumption at different Al_2O_3 to ZrO_2 ratios with same 15% VO_x. It appears that the hydrogen consumptions were comparable between the catalyst samples containing γ-Al_2O_3/ZrO_2 ratios of 2 to 1 and 1 to 1. The catalyst reducibility was significantly decreased with 1:2 γ-Al_2O_3/ZrO_2: 1:2 ratio (Figure 5.3 a and b).
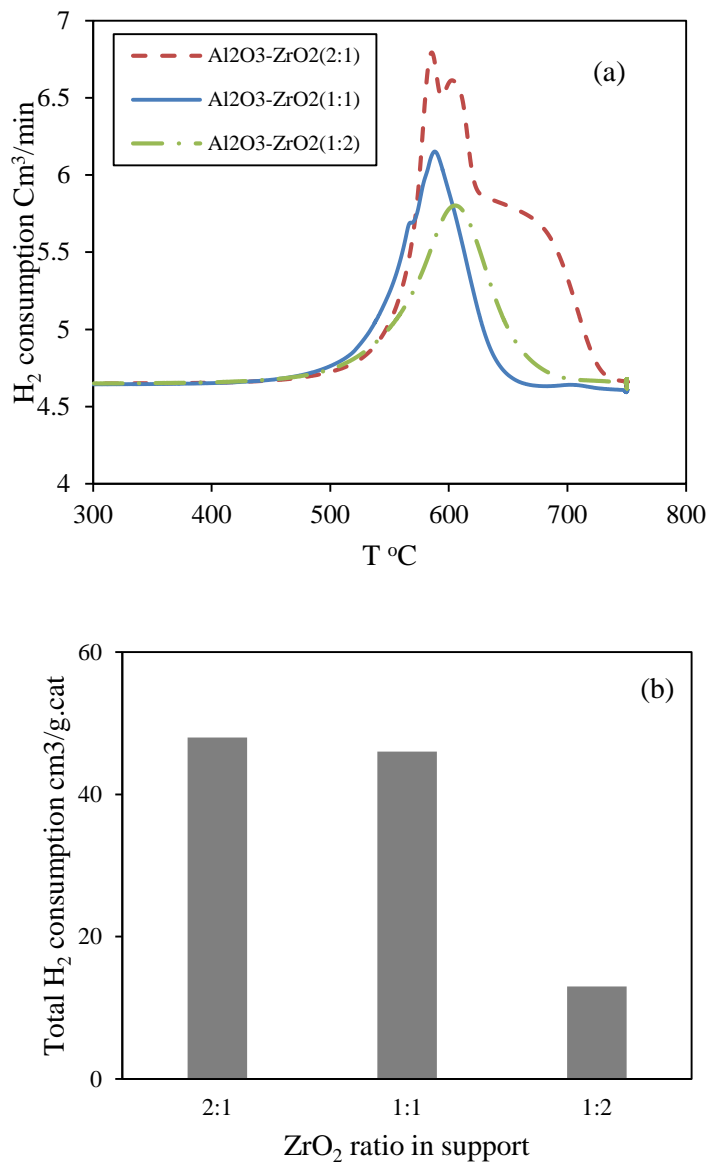
Figure 5.3. (a)TPR profile for catalyst $VO_x/Al_2O_3-ZrO_2$ with various ZrO_2 loading (b) H_2 consumption versus ZrO_2 ratio

The repeated TPR/TPO experiments were conducted to confirm catalyst reducibility and reoxidation ability in the multiple cycles. This also indicates any possibility of thermal sintering in the high temperature redox cycles. The $VO_x/\gamma-Al_2O_3-ZrO_2$ (2:1) sample was selected due to its high oxygen-carrying capacity as revealed in

hydrogen consumption analysis. Figure 5.4 shows the TPR profiles of the VO_x/ γ-Al_2O_3-ZrO_2 (2:1) sample under repeated TPR/TPO cycles. One can see that the TPR profiles remained almost unchanged after first cycle. The decomposition of the residual metal precursors possibly contributed to the first cycle. Once they were removed, the hydrogen consumption of the sample became stable over the repeated TPR/TPO cycles. Calcination temperature directly affected redox properties, since in this scenario, all samples were calcinated at same temperature. Only composition of ZrO_2 affected the reduction and oxidation ability, as well as new surface species such as polyvanadate. It can be formed during the reduction cycle, when oxygen vacancies are created [51]. In reduced sample, γ-Al_2O_3 and ZrO_2 remain in their original phases after reduction and that can be interpreted as good thermal stability[24]. Reduced vanadium over redox cycles was calculated as in Equation 5.4.

$$\text{fraction reduced (f)\%} = \frac{Mw_V \times V_{H_2}}{v \times V_g \times W_o} \times 100\% \tag{5.4}$$

where, W_V is the amount of reduced vanadium (g), Mw_V is the molecular weight of vanadium (g/mol), V_{H_2} is the volume of reacted hydrogen (cm^3 at STP), Vg is the molar volume of gas(mol/cm^3 at STP), W_o is initial weigh of vanadium and v is the stoichiometric number of hydrogen based on the following reaction stoichiometry. Assuming that V_2O_5 is the initial reducible catalyst species present on the support [19], V_2O_5 reduction percentages was found to be 59% for first cycle and 57.7% for the following cycles remain almost constant. In reduced sample, γ-Al_2O_3 and ZrO_2 remain in their original phases after reduction and that can be interpreted as good thermal stability[24]. Reduced vanadium over redox cycles was calculated as in Equation 5.5.

$$\text{Fraction reduced (f)\%} = \frac{Mw_V \times V_{H_2}}{v \times V_g \times W_o} \times 100\% \qquad (5.5)$$

where, W_V is the amount of reduced vanadium (g), Mw_V represents the molecular weight of vanadium (g/mol), V_{H_2} stands for the volume of reacted hydrogen (cm^3 at STP), V_g denotes the molar volume of gas(mol/cm^3 at STP), W_o is initial weigh of vanadium and v represents the stoichiometric number of hydrogen of the VO_x reduction reaction ($H_2 + VO_x = H_2O + V_2O_3$). Assuming that V_2O_5 is the initial reducible catalyst species present on the support [19], V_2O_5 reduction percentages was found to be 59% for first cycle and 57.7% for the following cycles remain almost constant.
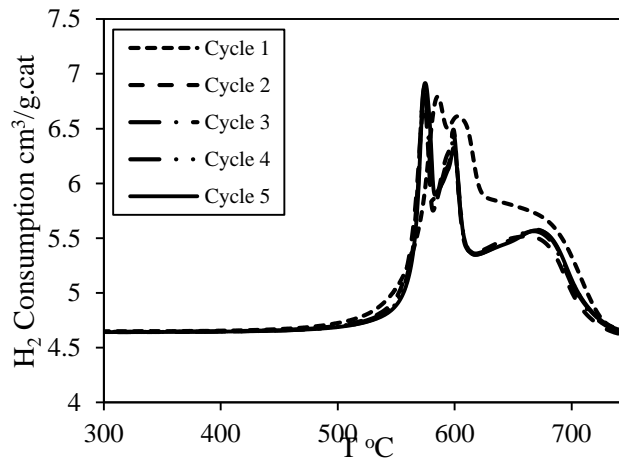
Figure 5.4. TPR /TPO cycles of 15% VO_x/Al_2O_3-ZrO_2 (2:1) catalyst

5.1.4. Scanning electron microscopy (SEM)

SEM characterization was conducted to investigate the size and the shape of the metal crystals of the catalyst before and after reduction in TPR. Figure 5.5a shows SEM images with magnification of 50 kx of fresh samples of VO_x/Al_2O_3-ZrO_2 (2:1) catalyst which calcinated at 500 °C. The images reveals that impregnation of vanadium oxide resulted in non-uniform size and shape particles. The pH of the impregnation solution and

support surface affects the nature of vanadium oxide on the support, Al_2O_3 has Surface pH of 8.9 which will results in polyvanadate formation (V-O-V bond) but thermal treatment converts polyvnadate into monovanadate[54]. Therefore, the fresh sample has isolated and bulk phase VO_x as indicated by XRD peaks. This observation is consistant to the literature for VO_x species to by pure isoladed, peaks in XRD pattern will disappear[19]. Figure 5.5b shows SEM images for the reduced samples of VO_x/γ-Al_2O_3-ZrO_2 (2:1), which reduced at 500 ^{o}C under H_2 flow. Since there are many form of VO_x can appear on support surface , such as V_2O_5 and VO_2, these reduced oxides are mostly present in crystalline and aggolomorated form due to lake of oxygen and will be oxidized again in regeneration process.

Reduction of samples at 500 ^{o}C did not affect alumina and zirconia phases, however slight weight loss migh occure, γ-alumina tends to transfer into θ-alumina when temperature rises to 700 ^{o}C and that will results in loss of serface area. Therefore the support can be considered stable similar results were concluded in literature [57]. The major change happens after reduction on the support surface and it is reversable .
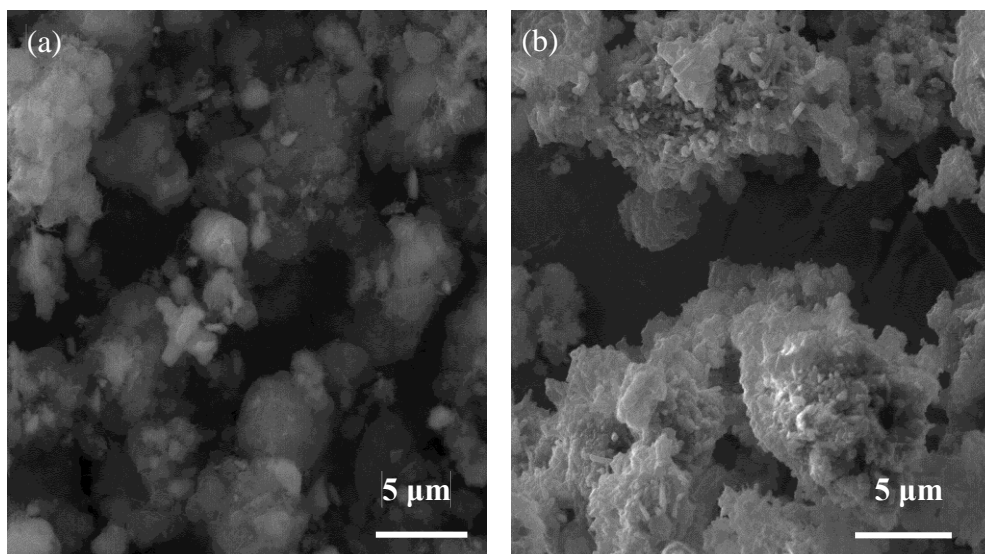
Figure 5.5. SEM images of 15%VO_x/Al_2O_3-ZrO_2 (2:1) (a) Fresh sample (b) Reduced sample

5.1.5. Acidity and metal-support interaction

NH_3-TPD was conducted to determine the catalyst acidity and its strength. Catalyst acidity affects metal-support interactions. Ammonia was used in TPD analysis due to its strong basicity and small molecular size. Furthermore, ammonia allows to determine the total acidity and strength of acid sites, for wide range of temperatures. For all samples, ammonia was firstly adsorbed at 120 ^{o}C and desorbed in a temperature range from 120 to 500 ^{o}C. Following this, the sample was heated at a heating rate of 10 ^{o}C/min and the desorbed concentration of ammonia was recorded using a TCD detector. Figure 5.6 shows the NH_3-TPD profiles of catalyst samples with various Al_2O_3/ZrO_2 ratios. ZrO_2 affect metal-support interaction specially at low and intermediate metal loading[55]. One can see from Figure 5.6 that desorption profiles of the samples have not significantly changed after the ZrO_2 modification.

Total acidity was calculated by calibrating TCD signal to volume of NH_3 desorbed and the area under the curve calculated using numerical integration. Heating rate of 10 °C/min was used and samples weight during TPD test which in all samples was 0.2 g, Equation 5.6 was used to calculate samples total acidity calculations.

$$\text{Total acidity (ml NH}_3/\text{g)} = \frac{a}{w\beta} \qquad (5.6)$$
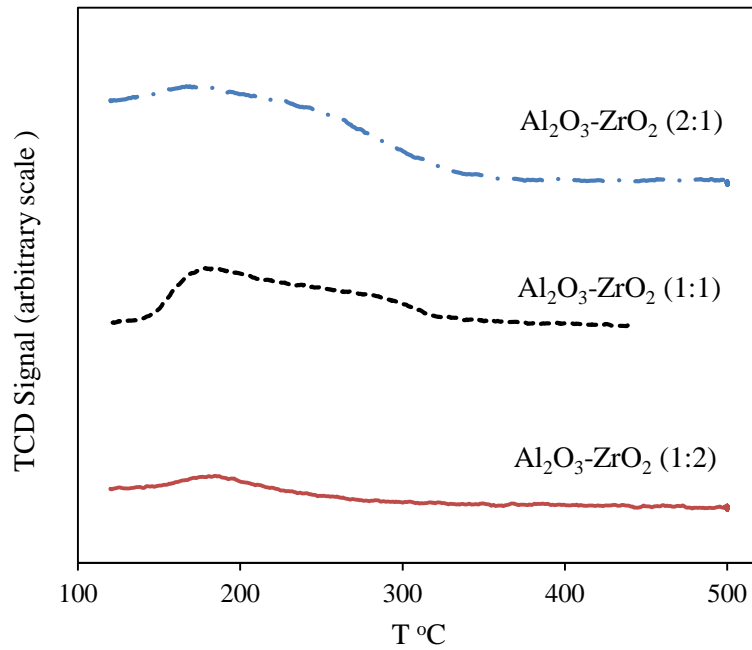
Figure 5.6. NH_3-TPD profiles of $VO_x/\gamma Al_2O_3$-ZrO_2 samples various amount of ZrO_2 loading (constant 15 wt% VO_x loading)

where, (1) a is the area under the curve after TCD signal calibration (ml NH_3 °C/min), (2) w is sample weight and β is the heating rate °C/min. Samples total acidity was found to be in the range between 2 and 6 (mlNH$_3$/g.cat). The total acidity was decreased with decreasing the Al_2O_3/ZrO_2 ratios (increasing the ZrO_2 content). Zirconia and metal loading reduces samples acidity by blocking acid sites[57], however samples acidity is almost

39

constant when metal loading is further increased. This observation indicates that ZrO_2 enhances vanadia species isolation on the surface which created more active sites, since ZrO_2 as mentioned before has lower acidity than alumina[19].

The NH_3-TPD data was further treated to estimate the desorption kinetics parameters such as desorption energy E_{des} and frequency factors $k_{des,0}$. These kinetic parameters are very important to assess the metal-support interaction. The NH_3-TPD data can be modeled as described in [37] used to estimate these parameters under the following assumptions;

i-   Homogeneous catalyst surface, $k_d= (-E_{des}/RT)$.

ii-   Ammonia doesn't re-adsorb during experiment.

iii- Uniform adsorbate concentration in the gas flow.

iv-   First order adsorption rate in surface coverage.

A high gas flow rate maintained together with appropriate conditions to satisfy the previous assumptions , and by performing species balances on desorbing NH_3 as and following same steps mention in [24], E_{des} and $k_{des,0}$ can be obtained ;

$$r_{des} = -V_m \left(\frac{d\theta_{des}}{dt}\right) = k_{d,0}\theta_{des}\exp\left[\frac{-E_{des}}{R}\left(\frac{1}{T}-\frac{1}{T_m}\right)\right] \qquad (5.6)$$

where, θ_{des} is the surface coverage, K_d, k_d are the desorption constant and pre-exponential factor, respectively, T_m is centering temperature, and by rising the temperature gradually with a constant value β the following equation applies:

$$T = T_o + \beta t \qquad (5.7)$$

$$\frac{dT}{dt} = \beta \qquad (5.8)$$

$$\left(\frac{d\theta_{des}}{dt}\right) = \left(\frac{d\theta_{des}}{dT}\right)\left(\frac{dT}{dt}\right) = \beta\left(\frac{d\theta_{des}}{dT}\right) \tag{5.9}$$

Equations 5.6 and 5.7 give:

$$\left(\frac{d\theta_{des}}{dt}\right) = \frac{k_{des,0}}{V_m \times \beta}\theta_{des}\exp\left[\frac{-E_{des}}{R}\left(\frac{1}{T} - \frac{1}{T_m}\right)\right] \tag{5.10}$$

where,

$$\theta_{des} = 1 - \frac{V_{des}}{V_m} \tag{5.11}$$

Combining Equations 5.10 and 5.11 results in

$$\left(\frac{dV_{des}}{dT}\right) = \frac{k_{des,0}}{\beta}(1 - \frac{V_{des}}{V_m})\exp\left[\frac{-E_{des}}{R}\left(\frac{1}{T} - \frac{1}{T_m}\right)\right] \tag{5.12}$$

Equation 5.12 was fitted to experimental data using Mathematica NonlinearModelFit built-in function at heating rate of 10 °C/min for all samples. Ammonia pre-adsorbed at 120 °C and samples weigh was 0.2 g, parameters obtained are shown in Table 5.2.

Table 5.2. Estimated[b] TPD model parameters for catalyst samples at 10 °C/min heating rate

Sample	$K_{des,0}$ (cm³/min)	E_{des} kJ/mol	R^2	AIC	V_{des}(ml NH₃/g.cat)
15% VO$_x$ Al$_2$O$_3$-ZrO$_2$(2:1)	3.9×10-6	75.44±3.5	0.99	-64252	5.87
15% VO$_x$ Al$_2$O$_3$-ZrO$_2$(1:1)	5.6×10-6	77.88±3.8	0.99	-64055	3.4
15% VO$_x$/Al$_2$O$_3$-ZrO$_2$(1:2)	14.9×10-6	80.52±4	0.99	-51751	2.75

[b] Confidence interval was set to be 95%

Coefficient of determination R^2 found to be above 0.99 in all cases which indicates a good regression. Akaike information criterion (AIC) was also used as a measure of the relative

quality of a statistical model to data set, the large negative AIC values indicate goodness of the fitting as can be seen in Table 5.2.

One can see from Table 5.2 activation energies for some samples are higher than bare Al_2O_3 and VO_x/Al_2O_3 which indicates stronger interaction between vanadium species and the support [19] which confirm the presence of isolated vanadium oxide species, on the other hand vanadium species interaction may results in formation of VO_2 [60] which will lead to lowering catalyst O_2 carrying capacity. On the whole, the intermediate interaction between active sites and supports is favorable. TPD kinetics show increased metal-support interaction, indicated by high desorption energy due to the introduction of ZrO_2. Higher metal-support interaction decreases the VO_x reducibility. Thus, catalyst activity is consistent with TPR results. Furthermore, decreased catalyst activity can reduce conversion of ethane. However, it is expected to increase ethylene selectivity by controlling O_2 release.

5.2. ODH of ethane in a fluidized CREC Riser Simulator

The fluidized ODH of ethane experiments were conducted in a CREC-Riser Simulator using pure ethane feed (99.95% ethane). For comparison, all three catalysts (VO_x/γ-Al_2O_3-ZrO_2) with different γ-Al_2O_3/ZrO_2 ratios (constant 15 % VO_x loading) were evaluated under same experimental conditions. The catalyst activity and product selectivity was evaluated using 0.4 g of oxidized catalysts and 2 ml of ethane injection. The product analysis of the preliminary experiments shows that C_2H_6, C_2H_4, CO_2 and CO are the major products of the gas phase oxygen free ODH of ethane reaction. Based on this product analysis, one can consider the following possible reactions to be involved under the studied reaction conditions:

42

Desired reaction:

Ethane to ethylene: $C_2H_6 \xrightarrow{\text{VOx/Al2O3-ZrO2}} C_2H_4 + H_2O$

Undesired reactions:

Complete oxidation of ethane: $C_2H_6 \xrightarrow{\text{VOx/Al2O3-ZrO2}} CO_2 + CO + 3H_2O$

Complete oxidation of ethylene: $C_2H_4 \xrightarrow{\text{VOx/Al2O3-ZrO2}} CO_2 + CO + 2H_2O$
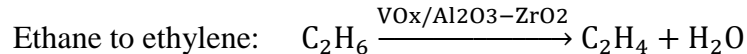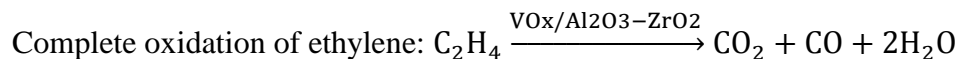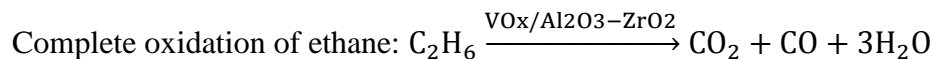
Therefore, the reaction between the catalyst and the feed ethane has to be developed at the reaction conditions maximizing the desired ethylene product selectivity and minimizing complete combustion of CO_x. Keeping the above in mind, the temperature during the experiments were varied from 525 to 600 °C, while the contact time was adjusted between 20 and 50 sec. After each ODH run, the catalyst was regenerated by supplied air at 550 °C for 10 min.

In order to demonstrate the effects of ZrO_2 the conversion and product data are presented as per gram of VO_x loading on the Al_2O_3-ZrO_2 support. Figure 5.7 displays the product selectivity at various Al_2O_3/ZrO_2 ratios. All the catalyst samples gives good selectivity to ethylene although the ethane conversion is relatively low. This low conversion was due to the low catalyst/feed ratio used for the evaluation. The ethane conversion further decreased with the increase of the ZrO_2 content (decreasing γ-Al_2O_3/ZrO_2 ratio). This was expected after the TPR analysis of the samples which showed that the oxygen carrying capacity of the samples decreased with the increase of the ZrO_2 content on the support. Interestingly, ethane selectivity slightly increased between when the γ-Al_2O_3/ZrO_2 ratio was decreased form 2:1 to 1:1. At this level up to 90% ethylene selectivity was achieved 600 °C reaction temperature. Further increment of ZrO_2 decreased

the ethylene selectivity was sharply decreased which is directly related to the scarcity of oxygen in the high ZrO_2 containing sample (γ-Al_2O_3/ZrO_2 1:2 to 1:1).

Overall, both the ethane conversion and ethylene selectivity were increased by augmenting the ZrO_2. This is due to enhanced catalyst activity via the formation of reducible polyvanadates [42, 54]. This agrees with the TPR results. However, at high ZrO_2 content, crystalline VO_x species are also formed. This results in a decreasing ethane conversion and ethylene selectivity. TPD kinetics also show an increased metal-support interaction due to high desorption energies. This high desorption energies were likely caused by an increased surface heterogeneity, which can favour catalyst ethylene selectivity by controlling the lattice O_2 released [64].
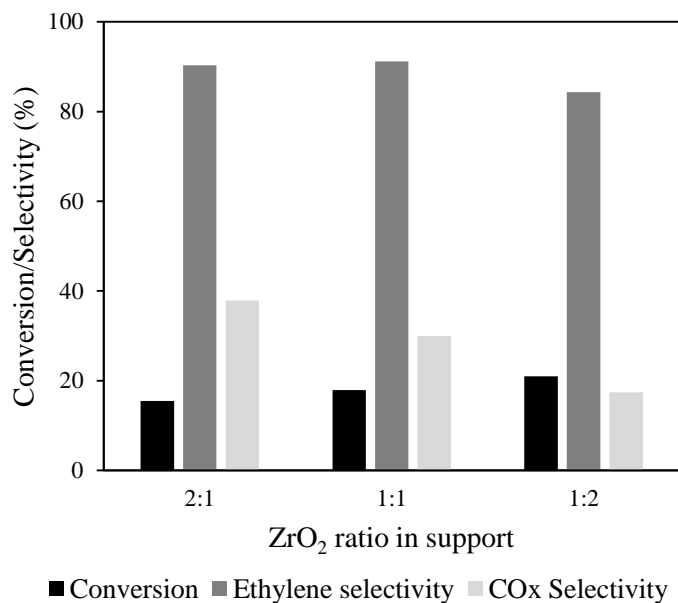
Figure 5.7. Effect of ZrO_2 on C_2H_6 conversion and product selectivity (per gram of VO_x, t=40 sec, T=600°C, W=0.4, feed= 1 ml)

Figure 5.8 shows ethane conversion and ethylene selectivity over 3 reduction and oxidation cycles for VO_x/Al_2O_3-ZrO_2 (2:1) catalyst sample. Stable performance was

obtained which indicates sample thermal stability and ability to be regenerated. Ethane conversion is shown in Figure 5.9 which becomes high at catalyst activity temperature range and lower outside this region. Sample without ZrO_2 gives higher ethane conversion and the addition of ZrO_2 lowered catalyst conversion by decreasing VO_x reducibility. Figure 5.9 displays the relationship between ethane conversion and ethylene selectivity with reaction temperature.
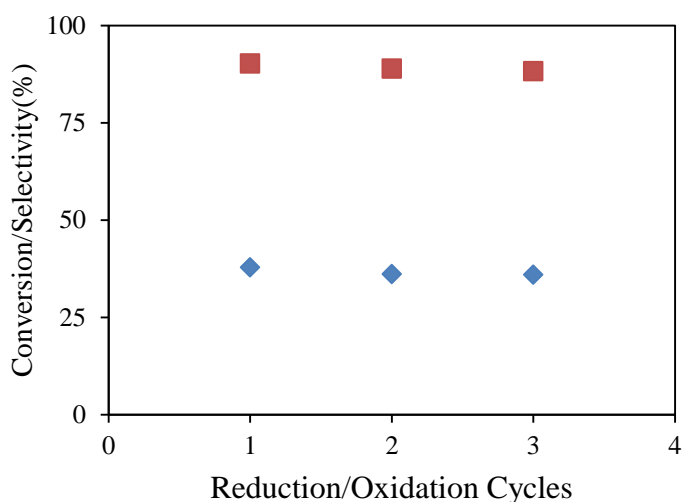
Figure 5.8. Conversion and selectivity over redox cycles for $VO_x/Al_2O_3-ZrO_2$ (2:1)
■Ethylene selectivity, ♦ Conversion (per gram VO_x, t=40 sec T=600 ${}^{o}C$, feed= 1 ml)

It can be seen that as the reaction temperature increases, with the unprompted $VO_x/c-Al_2O_3$ catalyst the conversion of ethane increased from 13.75 % at 550 ${}^{o}C$ to 18.80 % at 600 ${}^{o}C$. On the contrary, with the $VO_x/\gamma-Al_2O_3-ZrO_2$, the ethane conversion was slightly decreased from 13.75 % at 550 ${}^{o}C$ to 11.45 % at 600 ${}^{o}C$.
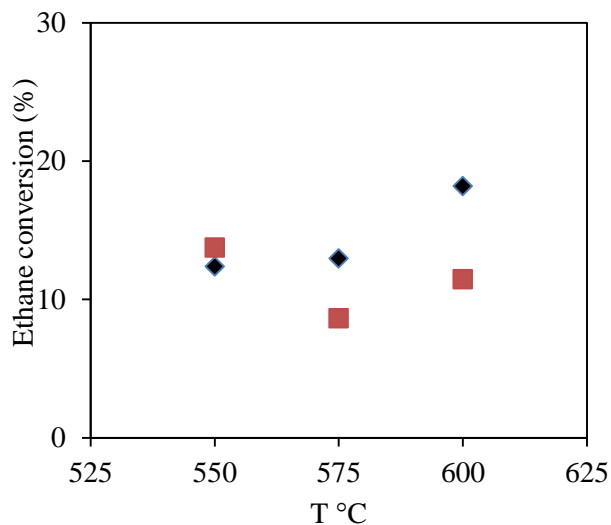
Figure 5.9. Effect of temperature on C_2H_6 conversion per gram VO_x (t=45 sec, feed= 1 ml, ■γ-Al_2O_3-ZrO_2 (2:1), ♦Al_2O_3)
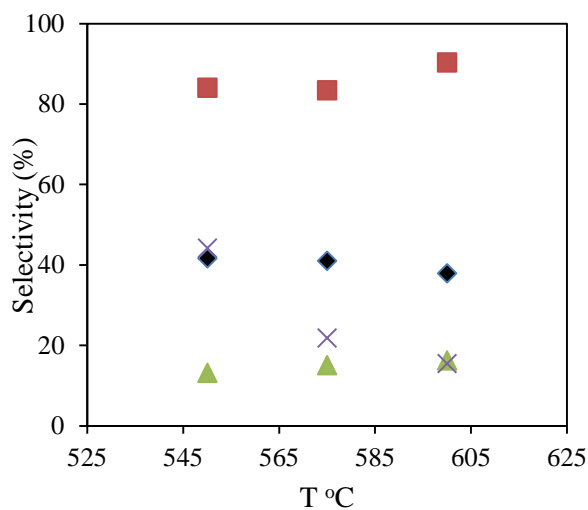
Figure 5.10 Effect of temperature on product selectivity per gram VO_x (t=40 sec, feed= 1 ml, ■ethylene γ-Al_2O_3-ZrO_2 (2:1), ♦ethylene Al_2O_3, x CO_x γ-Al_2O_3-ZrO_2 (2:1), ▲CO_x Al_2O_3 (2:1)

Figure 5.10 shows products selectivity per gram VO_x for VO_x/Al_2O_3 and VO_x/γ-Al_2O_3-ZrO_2 (2:1) catalyst samples. Ethylene selectivity reaches 90.3 % for VO_x/γ-Al_2O_3-ZrO_2 (2:1) catalyst sample and only 42% for VO_x/Al_2O_3 sample. This can be attributed to

ZrO_2 effect which enhances metal support interaction as mentioned earlier. Lower V reducibility decrease O_2 availability for combustion reactions which lead to production of CO_2 and CO gases.

Catalyst selectivity to CO_x gases versus temperature is shown in Figure 5.10. Highest CO_2 selectivity obtained was 44.2% for $VO_x/\gamma-Al_2O_3-ZrO_2$ (2:1) sample and 15.5% for sample without ZrO_2. Furthermore, in the sample containing ZrO_2 formation of CO_x is decreasing with temperature indicating ZrO_2 enhanced catalyst activity and selectivity at high temperature of 600 °C. This agrees with TPR results in Figure 5.3a. On the other hand, VO_x/Al_2O_3 sample produces more CO_x at high temperature due to combustion of produced ethylene.

The time effect is shown in Figure 5.11 for VO_x on $\gamma-Al_2O_3-ZrO_2$ (1:2) and Al_2O_3 at fixed reaction temperature of 550 °C. For sample without ZrO_2, combustion effect appears as CO_x production which is increasing over time. However ZrO_2 addition results in stable reactivity with temperature and time as shown. Combustion reaction leads to CO_x production, and CO_2 selectivity reaches 50%. In fact also increasing ZrO_2 contents in the support decrease catalyst reducibility which will result in lower conversion.

In general, the introduction of ZrO_2 to the support, enhanced ethylene selectivity and stability. ZrO_2 lowers support total acidity and also reduces Lewis acidity which leads to cracking reactions and CO_x production as shown in NH_3-TPD analysis. Similar results were obtained when the SAPO-34 catalyst was used in the ethane ODH reaction, where CH_4 traces were detected, as a result of cracking reactions [6].
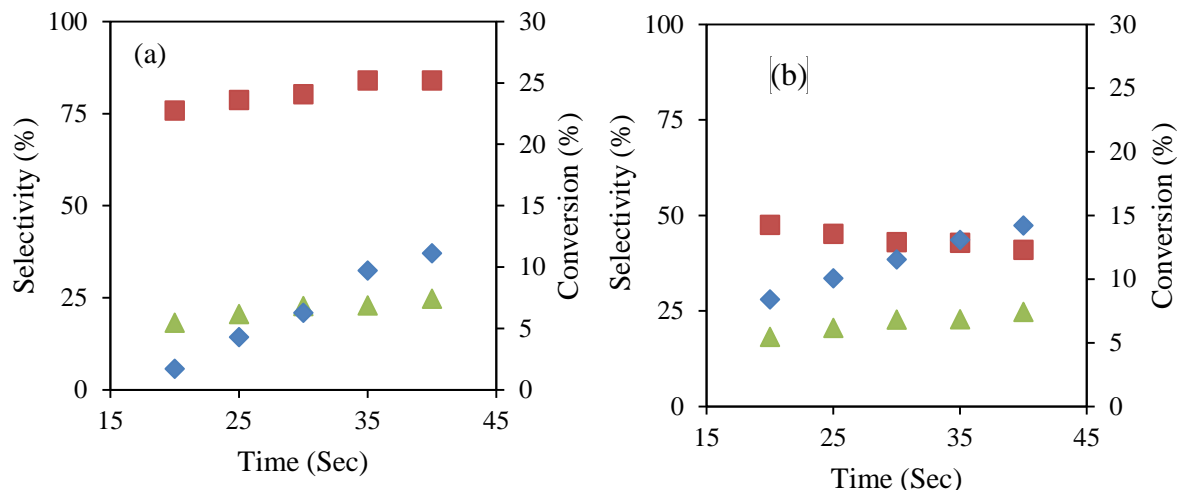
Figure 5.11. Effect of time on products selectivity per gram VO_x loaded on (a) Al_2O_3-ZrO_2 (2:1) (b) Al_2O_3 (t=40 sec, feed= 1 ml, ♦Conversion ■, Ethylene selectivity, ▲CO_x selectivity)

Following are the conclusions of the effects of ZrO_2 study:

i.   Metal loading and stirring for long period reduced the specific surface area due to blockage of support pores.

ii.   XRD indicates the presence of V_2O_5 and ZrO_2 in the VO_x/Al_2O_3-ZrO_2 catalysts. XRD pattern of VO_x/Al_2O_3-ZrO_2 showed that VO_x are present in crystalline phase, this phase introduced by ZrO_2. VO_x/Al_2O_3 sample shows only the amorphous phase.

iii. The TPR results show good catalyst activity, also reduction of V_2O_5 which occurs in two steps at low ZrO_2 contents. Increasing ZrO_2 contents decreased metal reduction. Also, TPR/TPO cycles shows excellent catalyst stability in repeated reduction and re-oxidation process.

iv. NH$_3$-TPD measurement indicates the presence of weak acid sites on the VO$_x$/γ-Al$_2$O$_3$-ZrO$_2$. The desorption kinetics analysis suggests a medium interaction between VO$_x$ and support which enhances the metal reducibility as seen in TPR.

v. The gas phase oxygen free ODH ethane in presence of VO$_x$/Al$_2$O$_3$-ZrO$_2$ shows ethylene, CO and CO$_2$ are the major products. The high temperature and longer contact time favor the CO$_x$ formation due to consecutive oxidation of ethane to ethylene and finally to CO$_x$.

vi. ZrO$_2$ additions enhanced catalyst performance by enhancement of metal support interaction. Higher ethylene selectivity even after ten repeated reduction runs.

CHAPTER 6

RESULTS AND DISCUSSION - EFFECTS OF VO$_x$

This chapter deals with the effects of the variation of vanadium loading on a ZrO$_2$ modified γ-Al$_2$O$_3$-ZrO$_2$ support. In this regards, the vanadium loading was varied between 5 to 15 wt% while γ-Al$_2$O$_3$/ZrO$_2$ ratio was kept at 1:1. The prepared samples were characterized using XRF, nitrogen adsorption, temperature programmed reduction/oxidation, XRD, FTIR, and Raman analysis. The reduction kinetics of the catalyst samples were established using a nucleation and nuclei growth model. The reducibility of the catalysts were further correlated with the ODH of ethane to ethylene performance of the VO$_x$/γ-Al$_2$O$_3$-ZrO$_2$ catalysts.

6.1. Catalyst characterization

6.1.1. XRF and N$_2$ adsorption/desorption

The compositions of the various component of the VO$_x$/γ-Al$_2$O$_3$-ZrO$_2$ catalysts are measured by XRF analysis and are presented in Table 6.1. The XRF analysis shows that the percentages of different species are closed to targeted values with slight deviation.

Figure 6.1 shows the adsorption/desorption isotherms of three different catalysts with various VOx loading. One can see that all the samples follow type (v) isotherm indicating narrow size meso-porosity[51]. The monolayer coverage occurs after 0.75 relative pressures which indicates a good dispersion of active site and availability for adsorption.

Table 6.1. XRF and BET surface area characterization results[a]

Sample	V%	O_2 %	Al%	Zr%	BET surface area m^2/g.cat
5% VO_x/γ-Al_2O_3-ZrO_2(2:1)	4.6	48.81	27.2	7	24.17
10% VO_x/γ-Al_2O_3-ZrO_2(1:1)	9.3	40.4	27.2	7	16.5
15% VO_x/γ-Al_2O_3-ZrO_2(1:2)	14.46	22.94	27.2	7	11.24

[a] samples composition is within ± 2% error
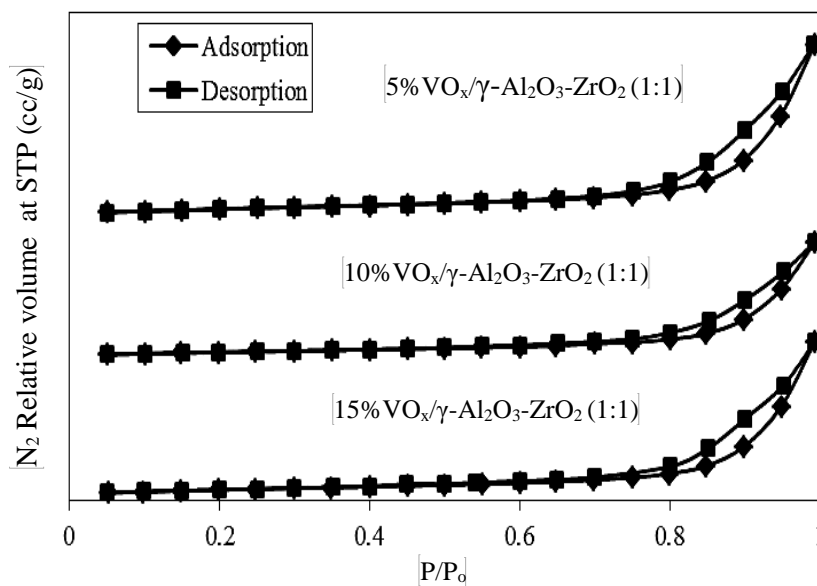
Figure 6.1. N_2 adsorption/desorption isotherms of catalyst samples

BET surface area was determined from N_2 adsorption desorption/desorption isotherms. Table 6.1 also shows the BET surface area and monolayer volume. As expected, the surface area of the catalyst samples were decreased with the increase of VO_x loading. The pore blockage by the increased amount of VO_x is mainly responsible for the decreased

surface area. Previous studies also showed that catalyst synthesis using impregnation by soaking reduces surface area although it gives good metal dispersion.

6.1.2. X-ray diffraction (XRD)

XRD analysis was conducted to identify the crystallographic structure of catalyst samples. Figure 6.2 shows XRD patterns of $VO_x/\gamma-Al_2O_3-ZrO_2$ (1:1) catalyst with different VO_x loading together with the support. VO_x species were obtained after oxidation and reduction peaks in the range of 2θ from 10 to $40°$ are relevant to V_2O_5[18]. The t-ZrO_2 peaks can also be found at 2θ of $30°,48°$ and $65°$, $\gamma-Al_2O_3$ peaks appears at 2θ of $45°$ and $60°$. Amorphous phase is present and it has been changed toward crystallinity by increasing metal loading and the repeated thermal treatment at 500 °C. $\gamma-Al_2O_3$ and ZrO_2 peaks appear in the support in contrast with pure $\gamma-Al_2O_3$ and ZrO_2, support crystallinity as shown in Figure 6.2.
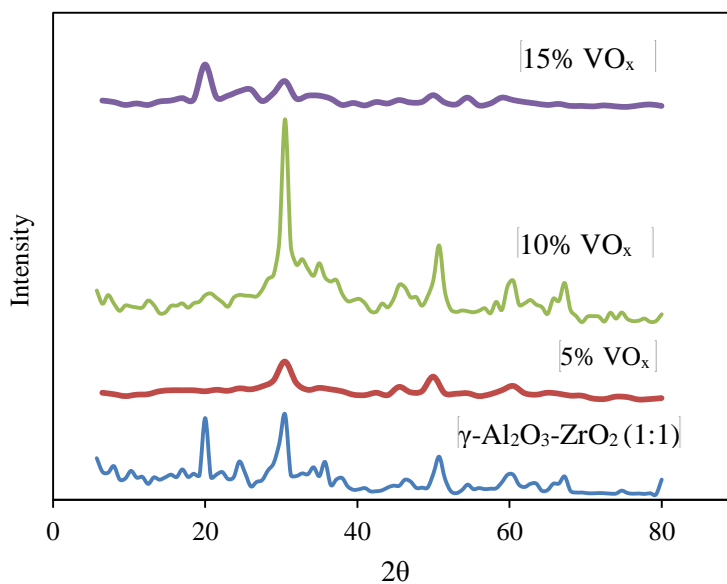
Figure 6.2. XRD patterns of $\gamma-Al_2O_3-ZrO_2$ (1:1) with various VO_x loading

At low VO_x loading of 5% only amorphous phase of VO_x species was formed [18] while at higher loadings of 10% and 15% crystal phase detected indicating formation of poly vanadate and crystalline VO_x. In all samples, γ-Al_2O_3 and ZrO_2 phases enhances catalyst thermal stability [52]. Moreover, ZrO_2 contents introduced crystal phase to the catalyst in comparison with catalyst sample without ZrO_2 [19], this crystal phase is not detected by XRD and may reduce oxygen carrying capacity and catalyst activity by enhancing metal crystal agglomeration.

6.1.3. Raman spectroscopy

Nature of vanadium oxide on support surface further investigated by using Raman spectroscopy. The Raman spectra of catalyst samples are shown in Figure 6.3. Sharp peaks at 132 cm^{-1} are arise due to vibration of V_6O_{13} [53], while peaks in the range of 200 to 600 cm^{-1} are from vibration of crystalline V_2O_5. These crystalline V_2O_5 species are formed as a result of V-O-V bond, and peaks at 995 cm^{-1} are due to V=O bond. It can be clearly seen that sample with 15% VO_x loading (Figure 6.3a) the sample exhibits sharp peaks in the range of crystalline V_2O_5. Increasing metal loading to certain level leads to poly-vanadate species. On the contrary, the poly-vanadate peaks almost disappeared in samples with 5 and 10% VO_x loading (Figure 6.3b and c). These findings are in line with the TPR results, where sample (c) gives the lowest H_2 consumption and activity relative to the others in (a and b).

It is reported in literature that vanadium loading forms monolayer on support surface [54]. This monolayer consists mainly from V-O and V=O bonds which are responsible from isolated vanadium species formation on support surface. ZrO_2 addition has little impact on metal support interaction especially at low vanadium loading.

Increasing ZrO_2 contents in the support can results in monolayer coverage at higher vanadium loading levels that can enhance vanadium species isolation on support surface [55-61]. This can be attributed to the stronger V-O-Al bonds than V-O-Zr bonds [54]. Surface vanadium oxide layer on oxide supports is more likely to form than crystalline V_2O_5 due to surface mobility of vanadium oxide and the lower surface free energy of crystalline V_2O_5 ($8–9 \times 10^{-6}$ J cm^{-2}) relative to supports ($Al_2O_3 \sim 68–70 \times 10^{-6}$ J cm^{-2}; $ZrO_2 \sim 59–80 \times 10^{-6}$ J cm^{-2}; $TiO_2 \sim 28–38 \times 10^{-6}$ J cm^{-2})[62].
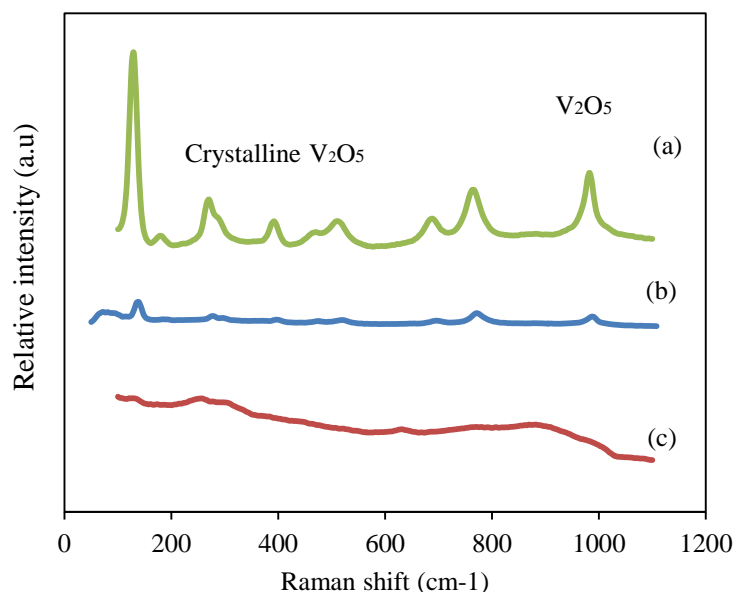
Figure 6.3. Raman spectroscopy of catalyst samples (a) 15% VO_x/γ-Al_2O_3-ZrO_2(1:1) (b) 10% VO_x/γ-Al_2O_3-ZrO_2(1:1) (c) 5% V_2O_5/γ-Al_2O_3-ZrO_2(1:1)

6.1.4. FTIR spectroscopy

Figure 6.4 shows FTIR spectra of the different VO_x containing VO_x/γ-Al_2O_3-ZrO_2(1:1) catalyst samples. Vanadium related species vibrations appear between 750 to 1400 cm^{-1}, and the band at 934 cm^{-1} can be attributed to Al–O–V vibrations and due to

significant interaction between γ–Al_2O_3 and vanadium [66, 51]. The band at 1052 cm^{-1} is relative to the V=O stretching mode and the vibration at 754 cm^{-1} can be attributed to the V–O–V stretch [58]. This observation is also consistent to the Raman analysis which confirms the presence of isolated and polymeric VO_x on catalyst surface. On the other hand, Zr-O related vibrations recorded before 640 cm^{-1} wavenumber. Comparison of the FTIR spectra of VO_x/γ-Al_2O_3-ZrO_2 catalyst with bulk V_2O_5 spectra shows that the absorptions at 980 and 1010 cm^{-1} can be attributed to V_2O_5 crystallites [49]. Therefore as mentioned earlier, the FTIR and Raman confirm the presence of isolated and poly vanadate species with crystalline phase.
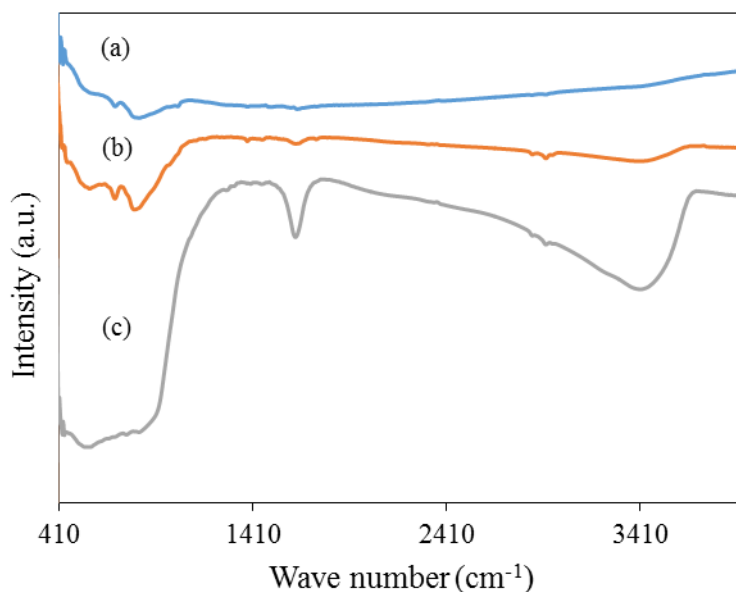
Figure 6.4. FTIR spectra of catalyst samples (a) 15% VO_x/γ-Al_2O_3-ZrO_2(1:1) (b) 10% VO_x/γ-Al_2O_3-ZrO_2(1:1) (c) 5% V_2O_5/γ-Al_2O_3-ZrO_2(1:1)

6.1.5. Catalyst acidity

The NH$_3$-TPD experiments were conducted to determine the total acidity and acid strength of the prepared catalysts. Ammonia was used for acidity measurement of the catalyst samples due to its strong basicity and small molecular size. Furthermore, ammonia allow to determine the total acidity and strength of acid sites for wide range of temperatures [19]. The acidity of the VO$_x$/γ-Al$_2$O$_3$-ZrO$_2$ catalyst significantly affects metal support interaction which also determines the reducibility of the VO$_x$ species. Generally, higher the reducibility of ODH the catalyst facilitates the ethane conversion but lowers ethylene selectivity due to uncontrolled O$_2$ release. For all the experiments, samples were saturated with ammonia at 120 °C. The ammonia desorptions were conducted in the temperature range of 120-500 °C with a heating rate of 10 °C/min under argon flow. Figure 6.5 shows the ammonia desorption profiles on different VO$_x$ containing VO$_x$/γ-Al$_2$O$_3$-ZrO$_2$(1:1) catalysts. One can easily see in this Figure 6.5, ZrO$_2$ affect metal-support interaction specially at low and intermediate metal loading[53]. Introduction of zirconia to alumina as created additional week acid sites indicated by new peaks at higher temperature of 270 °C (Figure 6.5). The multiples peaks indicates second order adsorption[38].

It can be noticed that increasing VO$_x$ loading also decrease sample acidity but further increasing the percentage 15% acidity increased again. This can be attributed to acidic properties of agglomerated VO$_x$ species at high loading. Total acidity of the catalysts were calculated by calibrating TCD signal to volume of NH$_3$ desorbed. Data was collected using 0.2 g for all samples during TPD test. The area under the curve calculated using numerical integration to be used in total acidity calculations. Equation 6.1 shows samples total acidity calculations.

$$\text{total acidity (ml NH}_3/\text{g)} = \frac{a}{w\beta} \qquad\qquad (6.1)$$

where, (1) a is the area under the curve (ml NH$_3$ $^{\circ}$C/min), (2) w is sample weight and (3) β is the heating rate $^{\circ}$C/min. Total acidity was found to be 5.73, 5.5 and 4.78 for 5%, 10% and 15% VO$_x$ containing catalysts, respectively. As mentioned earlier, increasing metal loading reduces samples acidity by blocking acid sites[56]. However, introduction of ZrO$_2$ also decreased total acidity but in the same time samples acidity is almost constant when metal loading is increased.
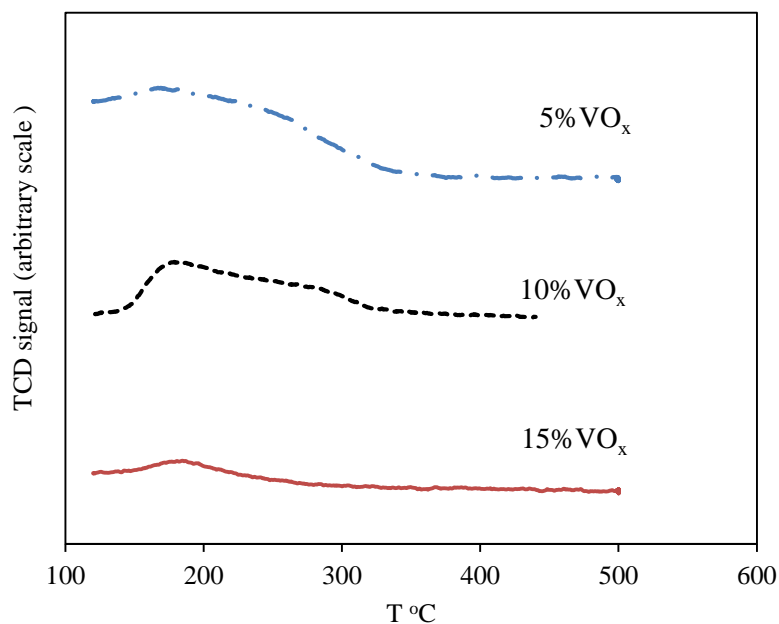
Figure 6.5. NH$_3$-TPD profile of VO$_x$/γ-Al$_2$O$_3$-ZrO$_2$ (1:1) catalyst

6.1.6. Reducibility and oxygen carrying capacity

TPR characterization is an important technique for oxygen free ODH given TPR simulates the actual ODH reaction as shown in Equations 6.2 and 6.3.

$$V_2O_5 + 2\,H_2 \rightarrow V_2O_3 + 2\,H_2O \tag{6.2}$$

$$2CH_3\text{-}CH_3 + V_2O_5 \rightarrow V_2O_3 + 2CH_2=CH_2 + 2H_2O \tag{6.3}$$

$$V_2O_3 + O_2 \rightarrow V_2O_5 \tag{6.4}$$
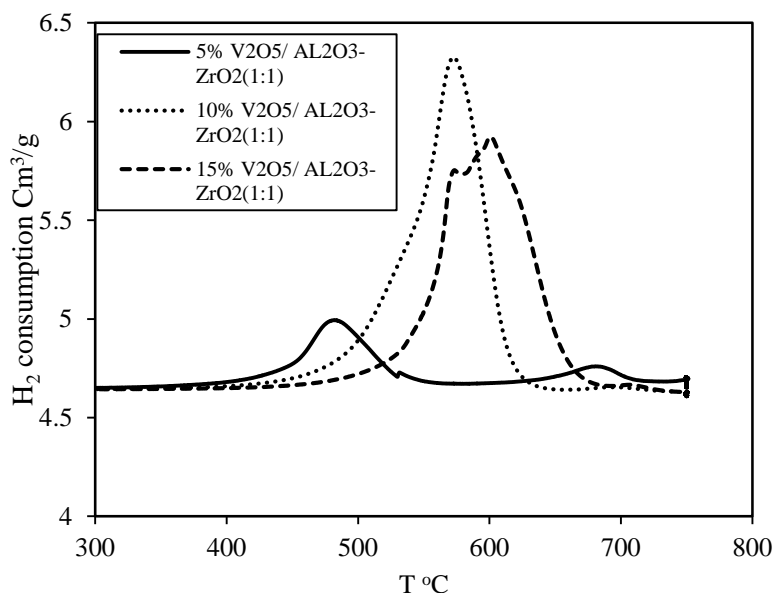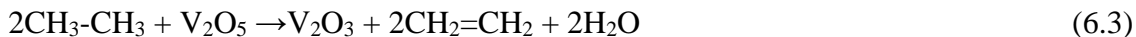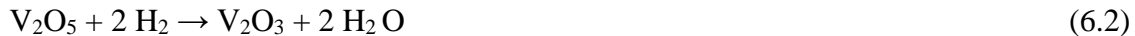
Figure 6.6. TPR profile for catalyst $VO_x/\gamma\text{-}Al_2O_3\text{-}ZrO_2$ (1:1) with various VOx loading

TPR provides indication of catalyst activity and the temperature range of this activity. Additionally, TPR can be utilized to estimate O_2 carrying capacity and redox properties of the catalysts. TPR results are shown in Figure 6.6 in which plots of H_2 consumption versus temperature for catalysts with 5%, 10% and 15% VO_x loading on the support. All the samples give a major single peak which indicate that the reduction proceed by a single step [66,53]. The 5% VO_x sample shows lowest oxygen consumption. The sample with 10% VO_x loading gives the highest H_2 consumptions per gram of catalyst. Sample with 15% VO_x gives lower H_2 consumption due to formation of crystal phase of VO_x as reported in XRD patterns. It can be seen that increasing VO_x contents shifted the

reduction temperature toward right direction. This can be attributed to formation of crystalline VO_x species which are difficult to reduce at low temperature. Introduction of ZrO_2 reduced support surface acidity and that enhance the formation of isolated mono-vanadate species on support surface [53] . ZrO_2 also affects metal support interaction specially at high VO_x loading [52]. During vanadium oxide reduction, oxygen vacancies are formed at the surface, as the reduction proceeds concentration of these vacancies surpasses a certain value, they aggregate and part of vanadium oxide may shear edges producing new structure (non-isolated species). This may also occur as a result of increasing vanadium loading[54]. TPR results can give indication of catalyst oxygen carrying capacity and oxygen releasing rate since oxygen carrying capacity of the catalyst can be determined according to Equations 6.2, 6.3 and 6.4 that is two moles of hydrogen reduce one mole of oxygen, and oxygen released during the reduction can be calculated.

Reduction/oxidation cycles can confirm catalyst ability to be regenerated and also its thermal stability. Reduction/oxidation properties of catalyst samples were examined by repeating TPR cycles. Figure 6.7 shows repeated cycles for the sample with the highest activity (10% VO_x/γ-Al_2O_3-ZrO_2 (1:1)), same trend obtained in all samples although H_2 consumption slightly decreased at cycles number 3, 4 and 5 and then become constant.

Calcination temperature directly affect reduction/oxidation properties, and since in the present study all samples were calcinated at the same temperature, only composition effect considered to analyze catalyst reduction and oxidation ability.
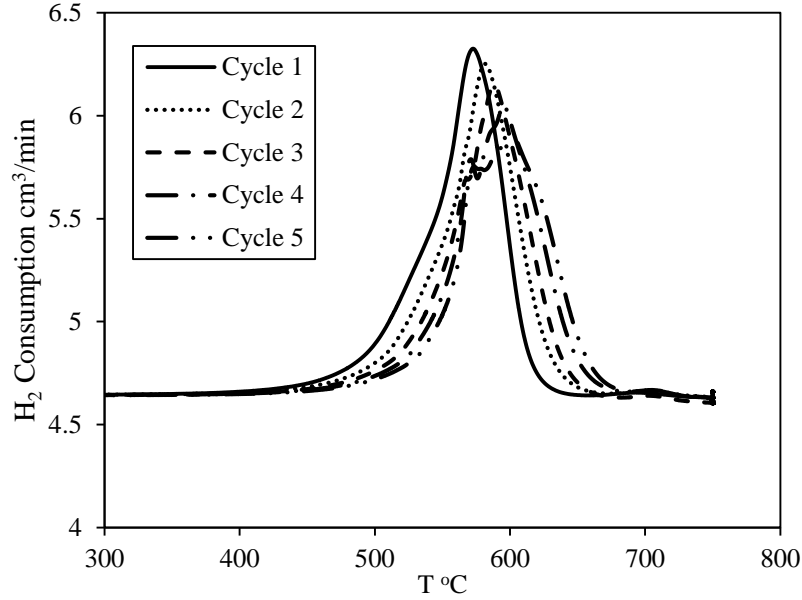
Figure 6.7. TPR/TPO cycles of $10\%\,VO_x/\gamma\text{-}Al_2O_3\text{-}ZrO_2$ (1:1) catalyst

$$\text{Metal reduced (f)}\% = \frac{Mw_v \times V_{H_2}}{v \times V_g \times W_o} \times 100\% \qquad (6.5)$$

where, (1)W_v is the amount of reduced vanadium (g),(2) MW_v is the molecular weight of vanadium (g/mol), (3)V_{H_2} is the volume of reacted hydrogen (cm^3 at STP), (4)V_g is the molar volume of gas(mol/cm^3 at STP), (5) W_o is initial weigh of vanadium and (6) v is the stoichiometric number of hydrogen based on the following reaction stoichiometry.

Figure 6.8 shows the percentage of vanadium reduces over TPR reduction/oxidation cycles, reacted hydrogen is calculated by calculating the TPR peak. The reduced vanadium is calculated as in Equation 6.5. Calculations were based on the assumption of V_2O_5 is the initial reducible catalyst species present on the support [19]. As can be seen from Figure 6.8 stable behavior and medium H_2 consumption was obtained and sample gives good stability in term of metal reduction.
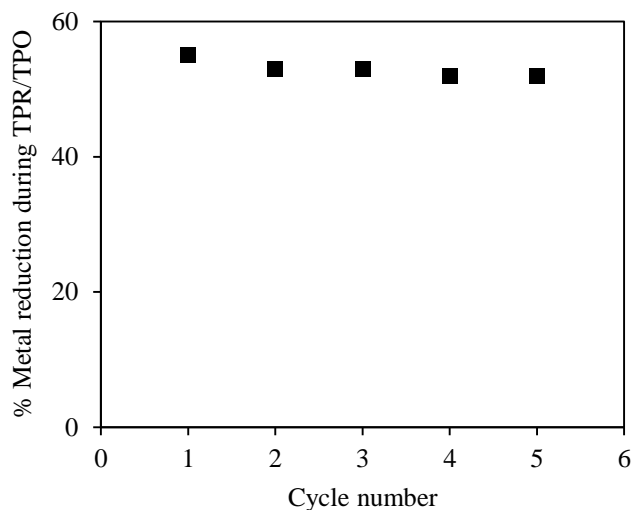
Figure 6.8. Percentage of vanadium reduction during TPT/TPO cycles

6.1.7. TPR kinetics modeling

During the TPR, the metal oxide reduction usually involves several steps. The overall reduction rate depends on one or combination of diffusion of reducing agent (H_2/C_2H_6), adsorption, surface reaction and desorption of the gaseous product (H_2O/CO_x). Depending on the nature of the reducible species, one of the above steps or their combination can control the overall reaction. Since the TPR experiments were carried out in conditions similar to what in [65], the external transport limitation can be assumed to be negligible because concentration variation of the gas phase reactant in the bulk phase and the oxygen carrier surface is negligible. Intraparticle diffusion was considered negligible due to small particle size of the samples. Therefore, the intrinsic TPR kinetics can be formulated considering an overall reaction rate being a function of the solid material reduction $f(\alpha)$ [36] and the compositions of the gas phase:

$$\frac{d\alpha}{dt} = K(T)f(\alpha)f(P_{H_2}, P_{H_2O}) \tag{6.6}$$

where, α is the progress of the reaction which can be expressed in many forms. In this study, the degree of reduction and oxidation of the catalyst sample is defined using the hydrogen and oxygen consumption data, for the reactions. Based on TPR profile analysis, the transient solid conversion (α) during each solid-state reaction can be written as:

$$\alpha(t) = \frac{\Delta n_t}{\Delta n_{total}} \qquad (6.7)$$

where, (1) Δn_t is the moles of H_2 or O_2 consumed at time t (min), (2) Δn_{total} is the total moles of H_2 or O_2 consumed it the whole reduction or oxidation cycle. The function f (P_{H2}, P_{H2O}) can be considered as constant if all the TPR experiments were carried out at same feed flow rate, hydrogen partial pressure, hydrogen essentially free of water, and differential conversion.

In this case Equation 6.6 can be written as:

$$\frac{d\alpha}{dt} = K(T)f(\alpha) \qquad (6.8)$$

and the rate constant can be defined by Arrhenius Equation:

$$k(T) = k_o Exp\left[\frac{-E_{app}}{R}\left(\frac{1}{T} - \frac{1}{T_m}\right)\right] \qquad (6.9)$$

where, (1) E_{app} is the activation energy, (2) k_o is the pre-exponential factor and (3) T_m the centering temperature to minimize cross-correlation between parameters. The function of the degree of conversion f (α) depends on the model applied in the determination of the kinetics.

The accessibility of the metal oxide grains in TPR experiments depends on support material properties. Thus, shape, size, and pore size distribution are all factors affecting

reducibility of oxide sites. Regarding metal support-interaction, there is a preferred orientation of the active component, which mainly depends on the chemical nature of the support material. In this study function $f(\alpha)$ assumed to take account for catalyst material properties.

Avarmi-Erofeev model (see Table 6.2) describes the function $f(\alpha)$ in reduction and oxidation of supported oxides proceeds via nucleation and crystal growth as follow:

$$f(\alpha) = n(1 - \alpha)(-\ln[1 - \alpha])^{\frac{n-1}{n}} \tag{6.10}$$

where, n is the Avrami exponent indicative of reduction mechanism of crystal dimensions growth. The value of n may vary depending on the mechanism of the reduction of the metal species [65], each value has certain meaning. In the present study n equals to 1 gives the best fit indicating random nucleation. Substituting Equations 6.9 and 6.10 in 6.8 then the final model equation cab be written as:

$$\frac{d(\alpha)}{dt} = nk_o Exp\left[\frac{-E_{app}}{R}\left(\frac{1}{T_o+\beta t} - \frac{1}{T_m}\right)\right](1 - \alpha) \tag{6.11}$$

where, (1) T_o the initial temperature, (2) β is the heating rate °C/min.

Table 6.2. Avrami-Erofeev models

Value of n	Mechanism	Model formulation
n	Avrami-Erofeev model	$f(\alpha) = n(1 - \alpha)(-\ln[1 - \alpha])^{\frac{n-1}{n}}$
1	Random nucleation	$f(\alpha) = (1 - \alpha)$
2	2-dimensional nuclei growth (2D Avrami-Erofeev model)	$f(\alpha) = 2(1 - \alpha)(-\ln[1 - \alpha])^{\frac{1}{2}}$
3	3-dimensional nuclei growth (3D Avrami-Erofeev model)	$f(\alpha) = 3(1 - \alpha)(-\ln[1 - \alpha])^{\frac{2}{3}}$

Kinetic parameters in Equation 6.11 was evaluated using Mathematica parametric NDSolve and FindFit functions. Regression achieved using 150 data points from TPR experiment collected every 2 seconds starting from room temperature up to 750 $^\circ$C and heating rate (β) of 10 $^\circ$C/min with 147 degree of freedom. A good regression results were obtained as can be seen in Figure 6.9. Table 6.3 shows kinetic parameters values.

Table 6.3. Estimated kinetic parameters within 95% confidence interval

Sample	k_o	E (kJ/mol)	R^2	Cor	AIC
5% VO_x	12×10^{-4}	124 ± 6.2	0.99	0.56	-23034
10% VO_x	9.3×10^{-4}	162 ± 8.1	0.99	0.78	-29034
15% VO_x	3.6×10^{-4}	181 ± 9	0.99	0.81	-31678

Activation energies obtained with good regression as indicated by R^2 and AIC statistics. The AIC is used as a measure of the relative quality of a statistical model to data set. Large negative AIC indicates good fitting as can be seen from Figure 6.9. Moreover activation energy is affected by nucleation and crystal growth processes. In fact activation energy being a difference between activation energy for nucleation and activation energy for particle growth. As discussed earlier, activation energy depends on metal type and support materials and in this occasion VO_x species has high interaction with the support and requires more energy to be reduced [65-69]. Furthermore, in comparison with catalysts activation energy for TPR reaction reported in [65], these values are higher which indicates VO_x on the Al_2O_3-ZrO_2 are more difficult to be reduced. VO_x species on the support can be presented in many forms such as isolated VO_x, poly vanadate and crystalline form. Increasing vanadium loading can affect formation of these species and therefore activation

energy varies with VO_x percentage. Reducibility of VO_x species varies depending on the type and therefore reaction or reduction rate [32]. Thus activation energy depends on the reducibility. For this catalyst, activation energy is higher than other supported metal oxides [65]. Activation energy for Ni reported to be 54.5 kJ/mol when alumina was used as support keeping in mind Ni is more active than V. Furthermore, crystalline VO_x formed during synthesis shifted the reduction temperature to higher range (see Figure 6.6) which explain increased activation energy for reduction [67].
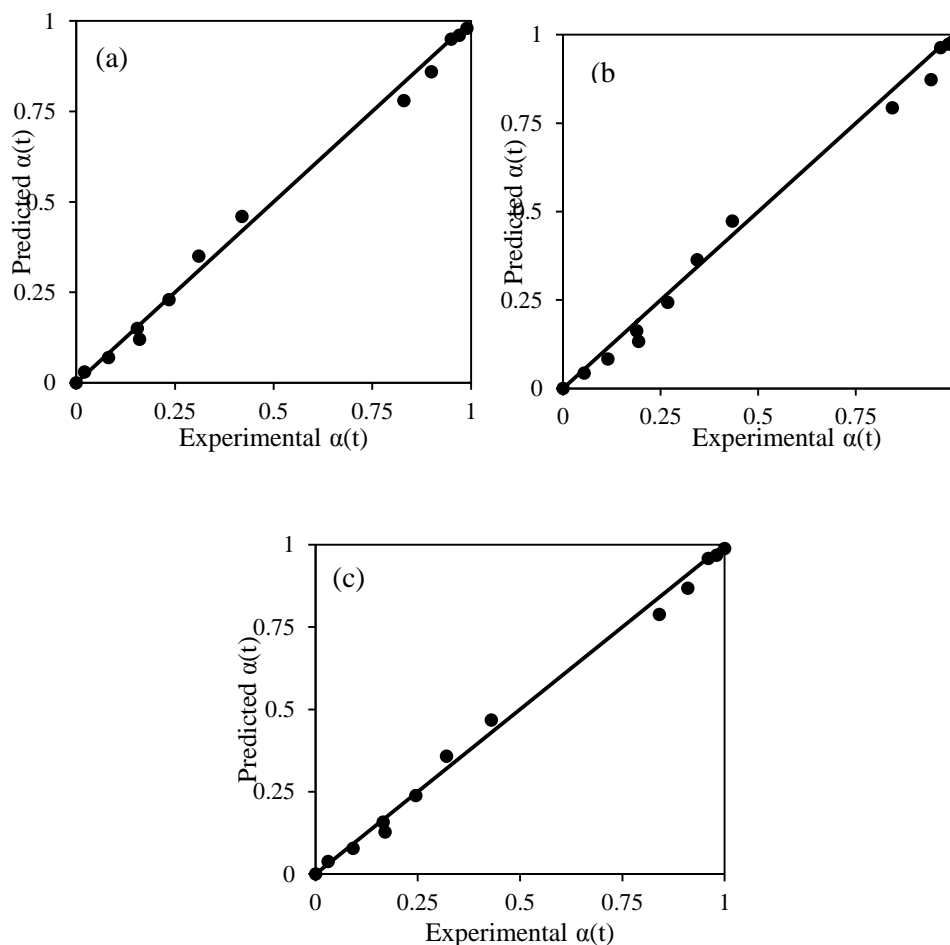
Figure 6.9. Predicted degree of reduction versus experimental values for (a) 5% VO_x (2) 10% VO_x (3) 15% VO_x supported on γ-Al_2O_3-ZrO_2 (1:1)

6.2. ODH of ethane in a fluidized CREC Riser Simulator

The fluidized ODH of ethane experiments carried out in a CREC Riser Simulator using pure ethane (99.95% purity) as feed. All the experiments were conducted at atmospheric pressure and constant catalyst to feed ratio of 0.2 g cat/ml feed. The temperature was varied between 525 and 600 $^{\circ}$C while reaction time was adjusted from 20 to 50 seconds. After each run the catalysts were regeneration by circulating air for 10 minutes.

Figures 6.10 and 6.11 display the ethane conversion and product selectivity of ODH of ethane using the VO_x/γ-Al_2O_3-ZrO_2 catalyst samples. Figure 6.10 shows ethane conversion for VO_x/γ-Al_2O_3-ZrO_2 (1:1) catalyst sample at 45 seconds and 575 $^{\circ}$C. The highest conversion was obtained 5.7% at 10% VO_x consisting with TPR data which gives highest H_2 consumption at temperature from 500 to 650 $^{\circ}$C. Sample with 5% VO_x gives lowest conversion due to low VO_x contents and 15% has lower activity due to crystalline VO_x phase as mention earlier.

Furthermore, ethylene selectivity is shown in Figure 6.11. 5% VO_x containing sample only active in temperature range from 450 to 530 $^{\circ}$C and that explains low selectivity and conversion. Intermediate VO_x contents of 10% has a controlled oxygen release and thus minimum combustion of the feed and ethylene occurs. Consequently, the ethylene selectivity with this catalyst shows is highest (88.4%) and the lower CO_x selectivity is lowest as shown in Figure 6.11.
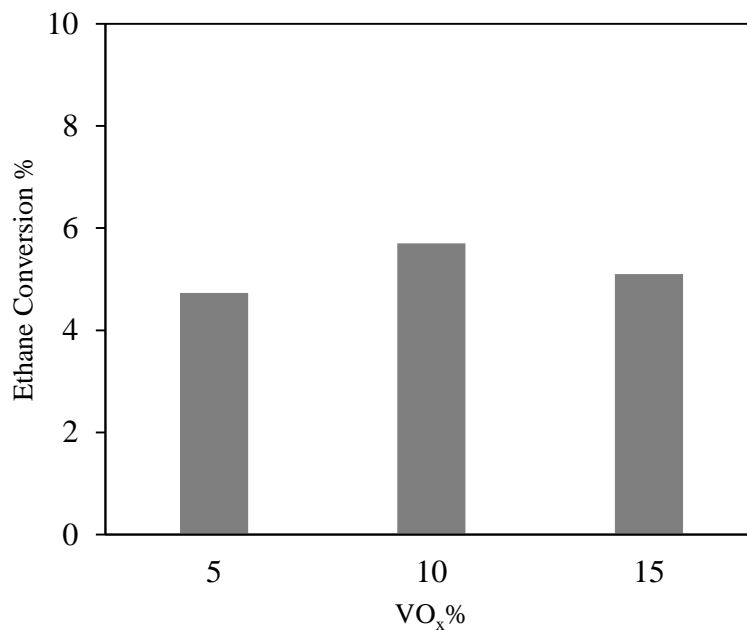
Figure 6.10. Ethan conversion at various VO_x supported on γ-Al_2O_3-ZrO_2 (1:1)

(feed=2ml, T=575 ^{o}C, t=45 sec w=0.4 g)
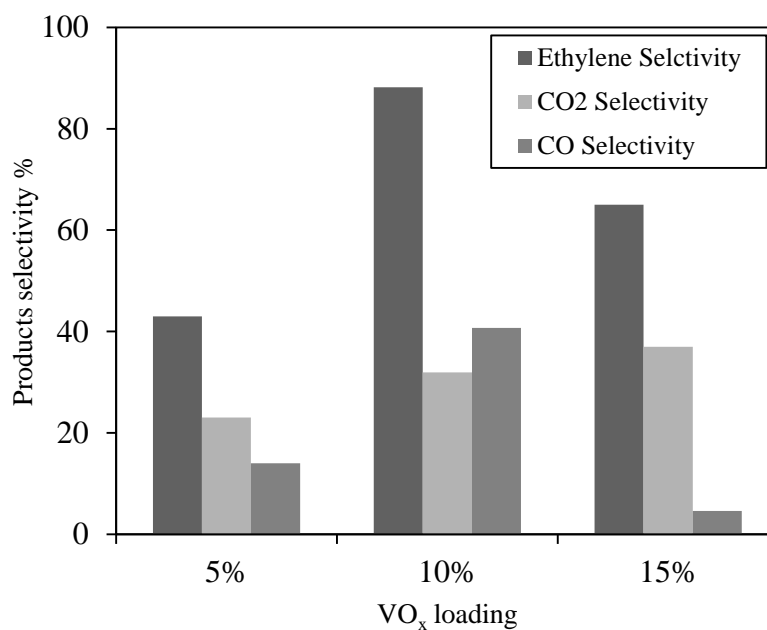
Figure 6.11. Products selectivity at various VO_x supported on γ-Al_2O_3-ZrO_2 (1:1)

(feed=2ml, T=575 ^{o}C, t=45 sec w=0.4 g)

Figure 6.12 shows the effects of temperature on conversion and selectivity for 10% VO_x/γ-Al_2O_3-ZrO_2 (1:1) catalysts. ZrO_2 contents in 10% VO_x/γ-Al_2O_3-ZrO_2 (1:1) also contributed into increasing ethylene selectivity up to at 575°C reaction temperature and lowering conversion. However ethylene selectivity decreases by increasing VO_x content.
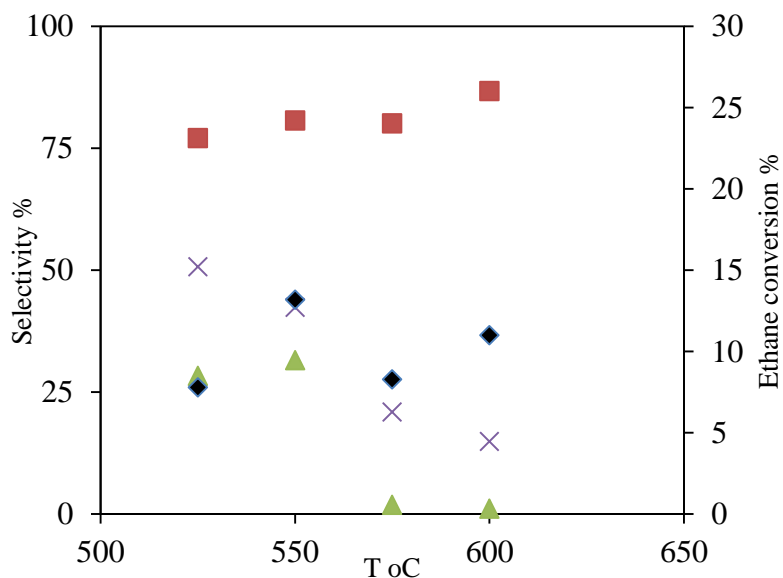
Figure 6.12. Effect of temperature on C_2H_6 conversion and C_2H_4 selectivity for 10% VO_x/γ-Al_2O_3-ZrO_2 (1:1), ♦Ethane conversion,■ Ethylene selectivity×CO_2 selectivity, ▲CO selectivity (t=45 sec, w=0.4, feed= 2 ml)

CO_x selectivity for 10% VO_x/γ-Al_2O_3-ZrO_2 (1:1) is shown in Figure 6.12. Highest CO_2 selectivity obtained was 50.7% at 525°C and for CO highest selectivity was 31.5% at 550°C, but in general ethylene selectivity slightly increased by increasing reaction temperature. Catalyst activity mainly depends on surface VO_x species nature which affects both activity and selectivity. Figure 6.12 shows conversion increases and decreases during ODH reaction, which can be related to reaction conditions and catalyst surface active sites. As mentioned earlier, it is required to optimize the types of VO_x species on the support

surface. This severely affects catalyst activity and selectivity During ODH reaction as can be seen from Figure 6.13, which is a schematic representation of the reaction. Isolated VO_x species which contains V=O bond can be converted into polymeric phase with V-O-V bond. Literature reported that there are two main reason to convert isolated VO_x into polymeric. Either during synthesis low pH level or by thermal treatment [54]. The other cause of polymerization of isolated VO_x species is reduction during ODH reaction when feed consume O_2 from catalyst surface. These vacancies lead to formation V-O-V bond instead which will results in polymerizing vanadium species on the surface [54].
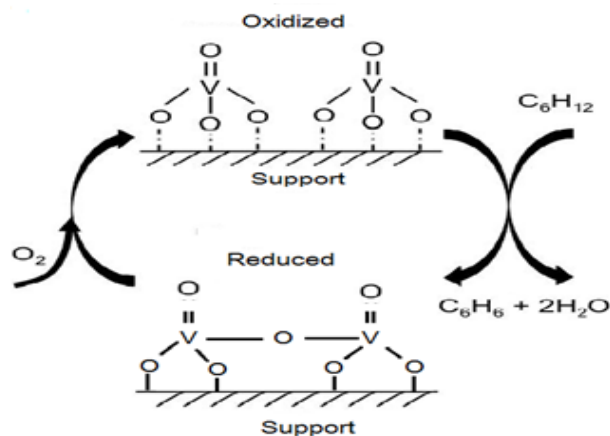
Figure 6.13. Ethane ODH over supported V_2O_5

Time effect also is shown in Figure 6.14 at constant reaction temperature. Increasing ethylene selectivity up to 90.8% at 50 seconds reaction time. Highest CO_2 selectivity obtained was 40.8% at 20 sec reaction time and for CO highest selectivity was 14.9% at 50 sec, but in general again ethylene selectivity slightly increased by increasing reaction time. Figure 6.15 show catalyst stability over reaction/regeneration cycles. Catalyst stability can be attributed to the thermal stability of Al_2O_3-ZrO_2 support and also VO_x stability on the surface [18, 53]. VO_x thermal stability was also confirmed by TPR
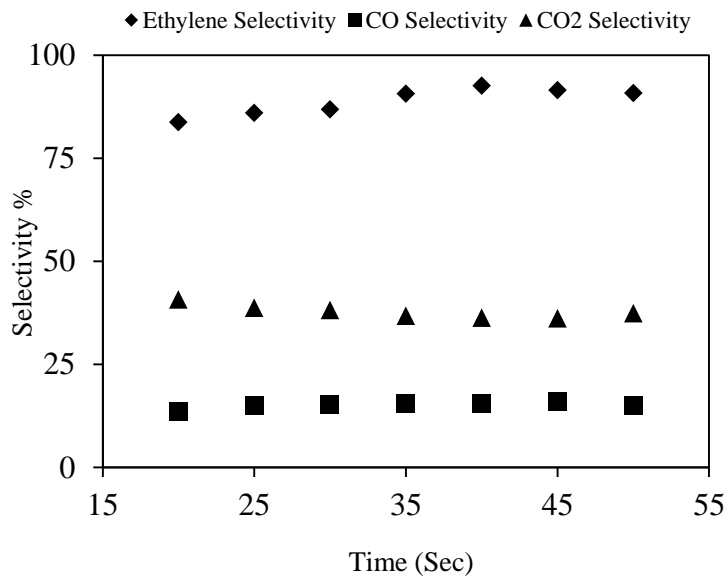
Figure 6.14. Effect of time on C_2H_6 conversion and product selectivity for 10% VO_x/γ-Al_2O_3-ZrO_2 (1:1) (T=575 ^oC, w=0.4, feed= 2 ml)
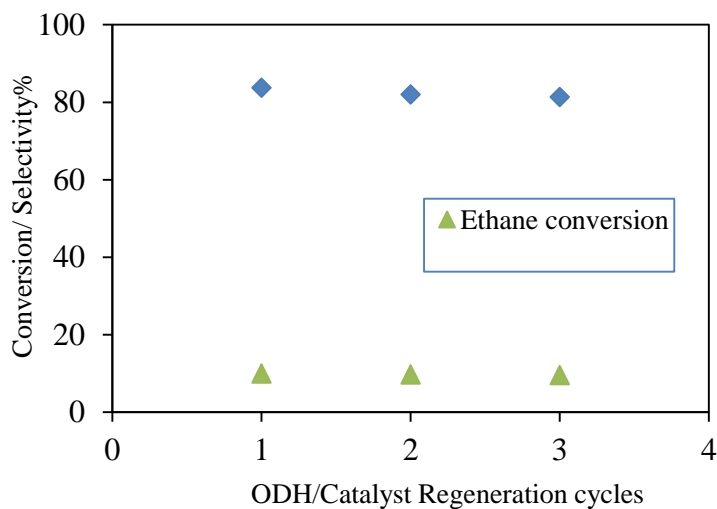
Figure 6.15. Conversion and selectivity over reaction/regeneration cycles for 10% VO_x/γ-Al_2O_3-ZrO_2 (1:2) (t=45 sec T=575 ^oC w=0.4 feed= 2 ml)

reduction/oxidation cycles (Figure 6.7), in which consistent peaks was obtained over 3 cycles.

Metal reduction directly affects feed conversion [32,44]. By decreasing acidity vanadium reducibility decreased which explains the low conversion of ethane. However ZrO_2 enhanced metal support interaction which leads to good selectivity to ethylene by the dehydrogenation process. Furthermore ZrO_2 affected V_2O_5 reduction as can be seen from XRD and TPR profile. This can also affect the nature of VO_x species on support surface and types of bond between these species. However a qualitative measure is required to specify the percentage of VO_x in the samples (i.e. %V^{5+}, % V^{4+}, etc.).

V-Support interaction and V loading determine type of the bonds and thus what type of VO_x species exist on support surface[52]. There are several types of VO_x species such as isolated vanadium oxide species, dimeric vanadium oxide species, two-dimensional vanadium oxide chains and V_2O_5 crystals. Samples of VO_x/γ-Al_2O_3-ZrO_2 contain isolated, dimeric and crystalline V_2O_5 as shown in Raman analysis before. These VO_x species contain V=O terminal bond with V-O-V and V-O-support bond, V-O-V bond is associated with polymeric VO_x species and previous studies showed V-O-V has no effect in ODH reaction[69].

The following are the conclusions of this Chapter 6:

i. XRF confirms catalyst compositions of the targeted VO_x loading. The increasing of VO_x loading shows slight decrease of the surface area of the catalysts.

ii. XRD and Raman analysis indicate the presence of V_2O_5 and ZrO_2 in the VO_x/γ-Al_2O_3-ZrO_2 catalysts. XRD pattern of VO_x/Al_2O_3-ZrO_2 showed that VO_x are present in crystalline phase due to the ZrO_2 modification. Raman spectra confirmed

the existence of isolated and polyvanadate species. NH_3-TPD measurement indicates weak acid sites on the VO_x/γ-Al_2O_3-ZrO_2.

iii. The TPR results showed two peaks due to reduction of V_2O_5 which occurs in two steps at low ZrO_2 contents. Increasing ZrO_2 contents decreased metal reduction. Also TPR/TPO cycles shows catalyst stability.

iv. Activation energy from TPR kinetics indicated lower reducibility at high VO_x loading with random nucleation mechanism.

v. The fluidized bed conditions enhanced the conversion of the ethane due to intense gas-solid mixing. The VO_x/γ-Al_2O_3-ZrO_2 shows a good performance in terms of ethylene selectivity even after ten repeated reduction runs. VO_x/γ-Al_2O_3-ZrO_2 catalyst gives good ethylene selectivity at 10% VO_x loading. Ethylene selectivity stable in reaction temperature range.

CHAPTER 7

KINETICS MODELING

This chapter presents the phenomenological kinetics modeling of the fluidized bed ODH of ethane to ethylene in gas phase oxygen fee conditions. In this the regard, the best performing catalyst (10 wt% VOx on Al_2O_3/ZrO_2 = 1:1) was selected for the kinetics experiments in the CREC Riser Simulator. The Langmuir-Hinshelwood type kinetics models were developed considering all the series-parallel reactions. The reducibility of the catalysts is also incorporated in kinetic models in order to take into account of the depletion of the oxygen concentration due to the gas (ethane)-solid (catalyst) reaction.

7.1. The reaction network

The network of ethane ODH reaction consists both desired and undesired reactions. According to open literature, following the are major reactions in a gas phase ODH of ethane [28, 29]:

Desired reaction

$$C_2H_6 + 1/2O_2 \leftrightarrow C_2H_4 + H_2O \tag{7.1}$$

Undesired reaction

$$C_2H_6 + (1.5 + x)\, O_2 \leftrightarrow 2\, CO_x + 3H_2O \tag{7.2}$$

$$C_2H_4 + (4x - 2)\, O_2 \leftrightarrow 2CO_x + 2\, H_2O \tag{7.3}$$
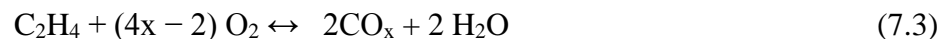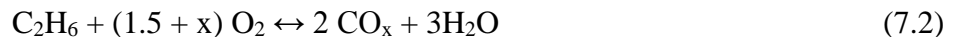
In oxygen-free environment, the ODH reaction proceeds by a gas (ethane)-solid(metal oxide) reaction, as expressed in Equation 7.4, producing ethylene as desired product.

$$C_2H_6 + MO_x \leftrightarrow C_2H_4 + H_2O + MO_{x-1} \qquad\qquad (7.4)$$

However, the feed ethane and desired product ethylene may further react with solid phase oxygen to give carbon oxides (CO_x). Therefore, the overall reaction network should contain all the series-parallel reactions (Figure 7.1) [29].
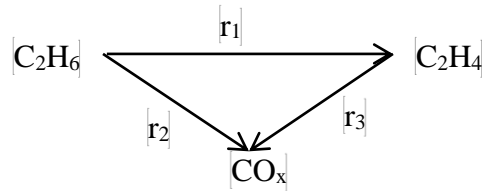
Figure 7.1. ODH of ethane reaction network

The reaction network represent three reactions (1) ethane selective oxidation to ethylene, (2) ethane non-selective oxidation (combustion) to CO_x and (3) ethylene combustion to CO_x. In the context of the present study, the product analysis of ODH of ethane in a CREC riser simulator using $VO_x/\gamma\text{-}Al_2O_3\text{-}ZrO_2$ catalysts also shows ethylene, CO_2, CO and H_2O as major products which further support the above reaction network.

7.1.1. Rate equations

In literature, there are kinetic studies of ODH of ethane reactions and only a few these studies which considered the Eley-Rideal and Langmuir−Hinshelwood models for ethane ODH to ethylene [3,18,22]. According to these studies hydrocarbon feed reacts with lattice oxygen from the catalyst to produce alkene and water. The reduced catalyst is then re-oxidized with molecular oxygen to recover oxygen consumed by the feed.

In catalytic ODH reaction, it is assumed that there are three types of oxygen one can consider: adsorbed, surface lattice and subsurface lattice oxygen. Kinetic model should take into account for these types of oxygen as in Langmuir−Hinshelwood mechanism. In Langmuir−Hinshelwood mechanism, both of the reactants adsorbed on the catalyst surface as shown in Figure 7.2 [39]. The other reactant in the gas-phase may react directly in one step (Eley-Rideal) or may sample several surface sites before reacting(L-H) [23,24]. Equations 7.5, 7.6 and 7.7 show a simple representation of Langmuir−Hinshelwood rate expression.

$$a_{(g)} + S_{(s)} \rightleftharpoons a\text{-}S_{(s)} \tag{7.5}$$

$$b_{(g)} + S_{(s)} \rightleftharpoons b\text{-}S_{(s)} \tag{7.6}$$

$$a\text{-}S_{(s)} + b\text{-}S_{(s)} \rightarrow \text{Products} \tag{7.7}$$
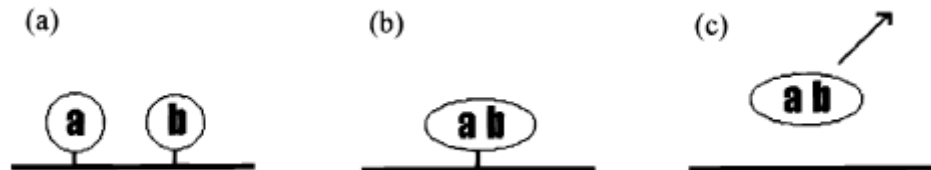
Figure 7.2. Steps of Langmuir−Hinshelwood mechanism (a) reactants adsorption (b) Surface reaction (c) products desorption

In the context of present study, rate of formation of all product species in ethane ODH reaction over 10 wt % $VO_x/\gamma\text{-}Al_2O_3\text{-}ZrO_2$ catalyst is described using Langmuir−Hinshelwood rate expression. The model takes into account the adsorption on the catalyst surface and the reactions with the lattice oxygen of the catalyst to form the products. The generalized model can be expressed as follows:

$$r_i = \frac{k_i^k K_i^A p_i}{1 + \sum_j^n K_j^A P_j} \tag{7.8}$$

where, r_i is the rate of reaction of component i (mol/(g_{cat}.min), k_i^k the kinetic constant for component i (mol/(g_{cat}.min), K_i^A the adsorption constant for component i (in units of atm^{-1}), and P the partial pressure of component i (atm) and n is the total number of chemical species.

The rate Equation 7.8 is valid if the catalyst is reduced completely and all the oxygen carried by the catalyst is consumed at reaction temperature. However, it is important to consider the variation of oxygen content of the catalyst with time during the reaction. Such variation of oxygen content can be expressed in terms of degree of reduction of the catalysts. In several studies, the degree of reduction of the catalyst is modeled as activity decay [42]. In the context of present study, TPR data is modeled using activity decay function (α).

We assumed reaction of C_2H_6 with adsorbed oxygen is the one responsible of producing ethylene as in Equation 7.6 and free released oxygen leads to combustion of C_2H_6 and C_2H_4 Equations 7.2 and 7.3. During the ODH experiments in CREC Riser Simulator, the products concentration was much less than ethane concentration, or in other words ethane concentration at any time is greater than products concentration. Therefore, it can be assumed that no product re-adsorption occurs. A similar conclusion was given in [43]. Therefore, Equation 7.8 can be written for each component as:

$$r_1 = \frac{k_{C2H6}^k K_{C2H6}^A P_{C2H6}}{1 + K_{C2H6}^A P_{C2H6}} \alpha \tag{7.9}$$

$$r_2 = \frac{k_2^* K_{C2H6}^A P_{C2H6}}{1+K_{C2H6}^A P_{C2H6}} \alpha \qquad (7.10)$$

$$r_3 = \frac{k_3^* K_{C2H4}^A P_{C2H4}}{1+K_{C2H6}^A P_{C2H6}} \alpha \qquad (7.11)$$

where,

$$k_2^* = k_2^{CO2} + k_2^{CO} \qquad (7.12)$$

$$k_3^* = k_3^{CO2} + k_3^{CO} \qquad (7.13)$$

In addition, adsorption constants and kinetic constants are lumped together and Equations 7.10, 7.11 and 7.12 become:

$$r_1 = \frac{k_1' P_{C2H6}}{1+K_{C2H6}^A P_{C2H6}} \alpha \qquad (7.14)$$

$$r_2 = \frac{k_2' P_{C2H6}}{1+K_{C2H6}^A P_{C2H6}} \alpha \qquad (7.15)$$

$$r_3 = \frac{k_3' P_{C2H4}}{1+K_{C2H6}^A P_{C2H6}} \alpha \qquad (7.16)$$

where,

$$k_1' = k_{C2H6}^k x K_{C2H6}^A \qquad (7.17)$$

$$k_2' = k_2^* x K_{C2H6}^A \qquad (7.18)$$

$$k_3' = k_3^* x K_{C2H4}^A \qquad (7.19)$$

7.2. TPR model development

During the ODH of ethane reaction, the catalyst starts reacting with the reducing agent (hydrogen/ethane/ethylene) at certain temperature and the rate increases with temperature until a maximum value. The catalyst reduction during ODH reactions can be modeled using the TPR data given the same reduction steps occurs in TPR except it uses hydrogen as reducing agent. During TPR, hydrogen is consumed and the consumption of hydrogen is measured within certain temperature range. Catalyst reaction (consumption) with hydrogen makes a specific curve represents catalyst finger print according to catalyst properties. A single or a multiple peak curve can be obtained depending on the nature of metal oxide on catalyst surface [19,20]. The model is mainly a modified standard normal distribution function in Equation 7.20 representing the H_2 consumption in the temperature range which catalyst is active as can be seen in Figure 7.3.

$$\emptyset(x) = \frac{\exp\left[\frac{-(x-\mu)^2}{2\sigma^2}\right]}{2\sqrt{\pi}} \tag{7.20}$$

where, σ is the variance and μ is the mean, this equation represents the rate of oxygen release by a specific catalyst and by simple modification it can fit the case as follow:

$$V_{H_2} = a_1 + b_1 \times \exp\left[\frac{-(T-T_m)^2}{2c_1^2}\right] \tag{7.21}$$

where, (1) V_{H2} is H_2 consumption cm^3/min, (2) a_1 is the initial amount of H_2 consumption at low temperature, (3) b_1 equal the highest consumption minus a (4) c_1 is a constant $^\circ K$ (5) T_m Temperature of the maximum consumption. This model is also valid for all catalysts with TPR profile similar to vanadium oxide supported catalysts, except these parameters mentioned that are unique for the specific catalyst. For multiple peaks, study suggests that

there is more than one metal oxide phases working as active site. Therefore, data must be de-convoluted before fitting the model. The ratio of the accumulated oxygen released by the catalyst to the total oxygen capacity of the catalyst could be released at very high temperature, and (α) can be written as;

$$\alpha = \frac{\int_0^T a_1 + b_1 \exp\left[\frac{-(T-T_m)^2}{2c_1^2}\right] dT}{\int_0^{1000} a_1 + b_1 \exp\left[\frac{-(T-T_m)^2}{2c_1^2}\right] dT} \qquad (7.22)$$
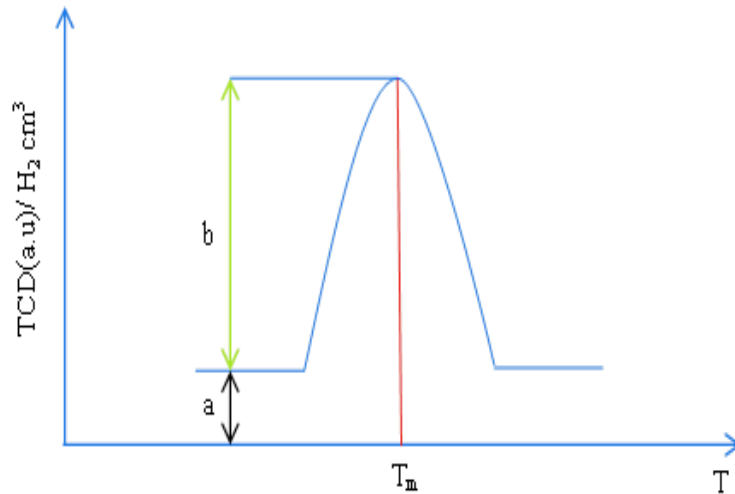
Figure 7.3. TPR model parameters graphical representation

7.3.   Mathematical model development

7.3.1. Assessment of mass transfer limitations

Overall reaction rate of ethane disappearance and formation of produces involves diffusion, adsorption and intrinsic reaction steps. Depending on the nature of the reducible species, one of the above steps or their combination can control the overall reaction. The external mass transfer can be assessed from Sherwood number and Froessling's

dimensionless correlations[44]. External mass transfer effect can be negligible if the following condition is satisfied:

$$W_{C_2H_6g} \gg r'_{A(obs)} \tag{7.23}$$

$$W_{C_2H_6g} = k_g(C_{C_2H_6}g - C_{C_2H_6}s) \tag{7.24}$$

$$Sh = 2 + 1.1Sc^{0.33}Re^{0.5} \tag{7.25}$$

$$k_g = \frac{Sh \times D_{AB}}{d_p} \tag{7.26}$$

$$r_i = \frac{V}{W}\frac{d\left(\frac{P_i}{RT}\right)}{dt} \tag{7.26}$$

where, (1) $W_{C2H6,g}$ is radial flux of ethane (mol/s.cm^2) (2) *Sh, Sc*, and *Re* are Sherwood, Schmidt, and Reynolds numbers, respectively, (3) k_g is the external mass transfer coefficient (cm/s),(4) $r'_{A(obs)}$ is the observed reaction rate (mol/g solid. s), (5) $C_{C2H6,g}$ is the bulk concentration of ethane, (6) C_{As} is the surface concentration of ethane (mol/L), (7) D_{AB} diffusivity cm^2/s. Values of these parameters are shown in .

Reaction rate $r'_{A(obs)}$ was calculated at higher conversion of ethane using and found to be 1.3 $\times 10^{-5}$(mol/g solid. s). $W_{C2H6,g}$ was found equal to 0.00123 mol/s.cm^2 and according to this values $W_{C2H6,g} >> r'_{A(obs)}$ and thus condition in is satisfied and the external mass transfer cab be considered negligible.

Intraparticle diffusion was assessed using the Weisz-Prater criterion [44] :

$$C_{wp} = \frac{r'_{A(obs)}\rho_p R_p^2}{D_{eff}C_{As}} < 1 \tag{7.27}$$

where, (1) $r'_{A(obs)}$ is the observed reaction rate (mol/g solid. s), (2)ρ_p is the particle density (g/cc), (3)Rp is the particle radius(cm), (4) D_{eff} is the effective diffusivity (cm^2/s), (5) C_{AS} is the concentration of gaseous reactant at the surface of solid particles (mol/L). Values also can be found in Table 7.1. C_{wp} also found to be 0.0000688 mmol/cm^3 and the value is much less than 1, therefore intraparticle mass transfer also is negligible for this reaction.

Table 7.1. Parameters used to evaluate mass transfer limitations

Parameter	Value	Remarks
$r'_{A(obs)}$ (mol/g solid. s)	1.3×10^{-5}	Calculated at highest conversion
D_{AB}(cm^2/s)	0.00027	from Fuller's correlation [45]
$C_{C2H6,s}$ (mol/cm^3)	0.0	
$C_{C2H6,g}$ (mol/cm^3)	0.0137	
Sh	2	the lowest value of Sh equals 2, which occurs at stagnant fluid conditions around the solid particle
R_p^2 cm	0.006 cm	Estimated from pulse chemisorption using AutoChem II Analyzer
ρ_p (g/cm^3)	0.545	
D_{eff}(cm^2/s)	0.1 D_{AB}	

7.3.2. Kinetic model formulation

CREC riser simulator is considered mixed batch reactor as reported in [46]. Thus reaction rate can be expressed as:

$$\eta r_i = \frac{V}{W} \frac{d\left(\frac{P_i}{RT}\right)}{dt} \tag{7.28}$$

where, (1) V is the reactor volume (cm^3), (2) W is the catalyst (g), (3) p_i the partial pressure of species i, (4) R the gas constant in (cm^3. atm. K^{-1}·mol^{-1}), (5) T the reactor temperature (K), and (6) t is the time (seconds). Moreover, from assessment of mass transfer limitation in Section 7.3.1, η is the effectiveness factor which will be taken as 1. Then the rate equation can be expressed as:

$$\frac{dP_i}{dt} = \frac{WRT}{V} r_i \tag{7.29}$$

$$\frac{dP_i}{dt} = \frac{WRT}{V} r_i \alpha \tag{7.30}$$

At this stage reaction network in Figure 7.1 can be written in term of ordinary differential equations (ODEs). This set of ODEs represent the change in partial pressure of reactant and products inside the reactor as a function of time and this set should be solved simultaneously using experimental initial conditions.

$$\frac{dP_{C2H6}}{dt} = -\frac{WRT}{V} (r_1 + r_2) \tag{7.31}$$

$$\frac{dP_{C2H4}}{dt} = \frac{WRT}{V} (r_1 - r_3) \tag{7.32}$$

$$\frac{dP_{C2H6}}{dt} = \frac{4WRT}{V} (r_2 + r_3) \tag{7.33}$$

Temperature effect was included in reaction constants and expressed according to Arrhenius relationship given in Equation 7.34. This allowed us to evaluate activation energies $E_i{}'$ and pre-exponential factors $k_o{}'$ which are the actual E_i and k_o multiplied by adsorption constant $K_i{}^A$.

$$k'_i = k'_o \text{Exp}\left[\frac{-E'_i}{R}\left(\frac{1}{T} - \frac{1}{T_m}\right)\right] \tag{7.34}$$

where, T_m is the average reaction temperature [42], which in this case equals to 562 °C. Subsisting Equations 7.28-7.30 and 7.34 in 7.31-7.33 E_i' k_o' can be obtained using Mathematica "FindFit" fit built-in function after solving the ODE's set in Equations 26-28 using Parametric parametric "NDSolve".

7.3.3. Estimation of TPR model parameters

The model given in Equation 7.22 was fitted to TPR experimental data in Figure 7.4 using Mathematica built-in function "FindFit". Parameters values are shown in Table 7.2 together with the model statistical analysis using coefficient of determination (R^2) and Akaike information criterion (AIC).

Coefficient of determination R^2 was found to be 0.961 which indicates a good regression as seen in Figure7.5. Akaike information criterion (AIC) also was used as a measure of the relative quality of a statistical model to data set. According to literature, the large negative value of AIC indicates goodness of fitting. Table 7.2 reports the R^2 and AIC value of the TPR model fitting. One can see that the R^2 is high and large negative values of AIC, indicating excellent fitting of the TPR model Equation 7.22.

7.3.4. Estimation of kinetic parameters

The kinetics parameter were evaluated by a nonlinear regressions analysis using ODH of ethane experimental form as developed in CREC Riser Simulator and implemented in Mathematica. The set of ODEs in Equations 7.31-7.33 representing the kinetic models was solved simultaneously using "NDSolve" before it was fitted to experimental data. Upon solving ODEs the partial pressure of each species becomes a function of time.
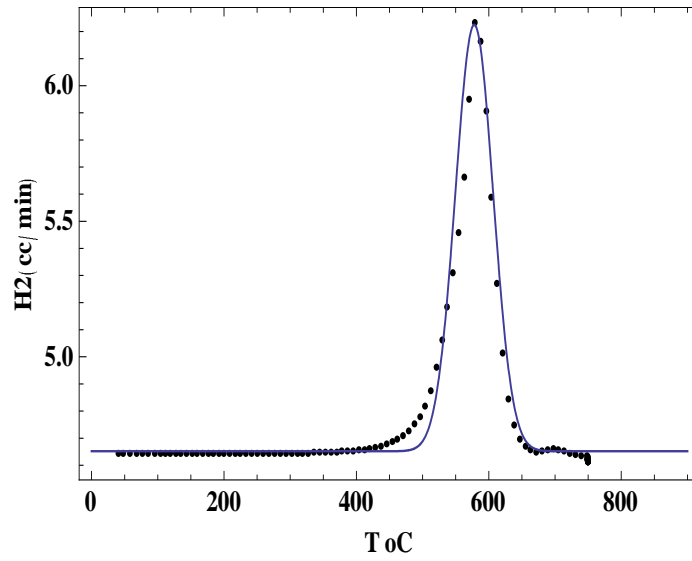
Figure 7.4. Model predicted H_2 consumed and experimental data at various temperature

Table 7.2. Fitted model parameters using equation with confidence interval of 95%

Parameter	a	b	c	AIC	R^2
Value	4.65	1.44	38	-286	0.999
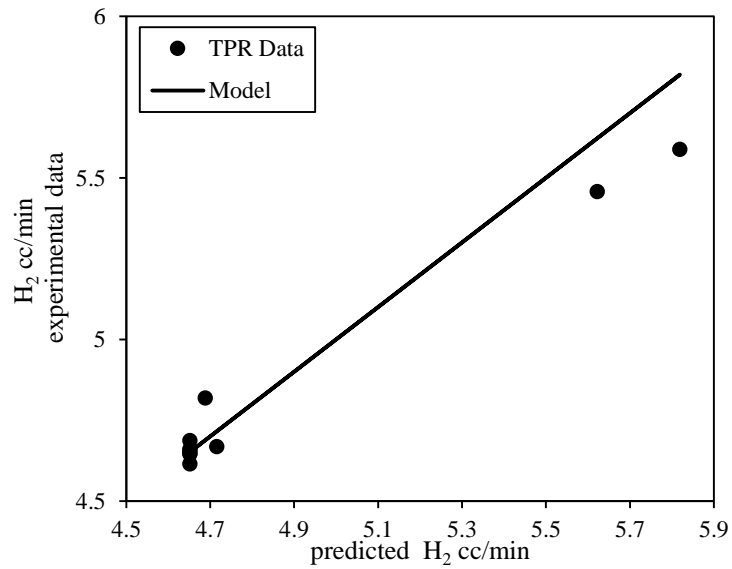
Figure 7.5. Plot of model predicted H_2 consumed and experimental data

Temperature effect appears when reaction data was collected at several reaction temperatures (525, 550,575 and 600 °C). Using Arrhenius relation components, activation energies 'E$_i$' and pre-exponential factors "k$_o$" were estimated. Furthermore, catalyst weight "w" was taken as 0.4 g with reactor volume "v" of 53 cm^3.

Activity function (α) in Equation 7.22 was estimated at each temperature. The value of α was varied from 0 to 1 in a way that if all O$_2$ carried by the catalyst is consumed during reaction that means α is 1 and all metal reduced by 100%. However, in the real case as shown in TPR result for the same catalyst, metal reduction is always less than 100% therefore α is always less than 1. Table 7.3 shows kinetic parameters estimation with statistical adjusted R^2.

Table 7.4 shows that activation energies E$_i$' and pre-exponential factors k$_o$ were estimated by plotting reaction constants at each temperature as shown in Figure 7.6. However, as mentioned before these activation energies and pre-exponential factors are multiplied by adsorption constant. Since K^A$_{C2H6}$ was estimated already, Equation 7.17 used again to calculate the observed k$_{C2H6}$ and the corresponding activation energy and pre-exponential factor as shown in Figure 7.6.

Table 7.3. Estimated kinetic model parameters with 95% confidence interval

Parameter	T=525 °C	T=550 °C	T=575 °C	T=600 °C
k'$_1$ (mol/g$_{cat}$.s.atm)	0.162	0.1811	0.2114	0.2147
k'$_2$ (mol/g$_{cat}$.s.atm)	0.0168	0.0174	0.0279	0.1285
k'$_3$ (mol/g$_{cat}$.s.atm)	0.0860	0.0885	0.0891	0.1212
K^A$_{C2H6}$ (atm^{-1})	0.0960	0.0978	0.0991	0.0996
α	0.502	0.529	0.56	0.592
R^2	0.94	0.95	0.95	0.94

Table 7.4. Activation energies and pre-exponentials factor (R^2 of 0.99) for all parameters

Parameter	Value	95% CI
k'_{o1} (J/g.s.atm)	0.991	±0.10901
k'_{o2} (J/g.s.atm)	2.95	±0.3245
k'_{o3} (J/g.s.atm)	2.17	±0.2387
k_{o1} (J/g.s)	0.997	±0.10967
E_1 (kJ/mol)	28.4	±3.124
E'_2 (kJ/mol)	74	±8.14
E'_3 (kJ/mol)	306.4	±33.704
σ^*		2.3×10^{-3}
Data points		112
Degree of freedom		105

*$\sigma =[\sum(X_{experimental}- X_{estimated})^2]^{1/2}/(m - p)$, where m is the number of data points and p is the number of model parameters.

Table 7.5. Kinetic parameters correlation matrix

	k'_{o1}	k'_{o2}	k'_{o3}	k_{o1}	E'_1	E'_2	E'_3	E_1
k'_{o1}	1							
k'_{o2}	-0.33	1						
k'_{o3}	0.43	-0.845	1					
k_{o1}	0.69	0.43	-0.023	1				
E'_1	0.15	-0.44	0.57	0.62	1			
E'_2	0.041	0.53	-0.3	0.02	-0.51	1		
E'_3	-0.002	0.11	-0.42	-0.01	0.58	-0.9	1	
E_1	-0.089	0.25	-0.11	0.83	0.67	-0.24	0.12	1
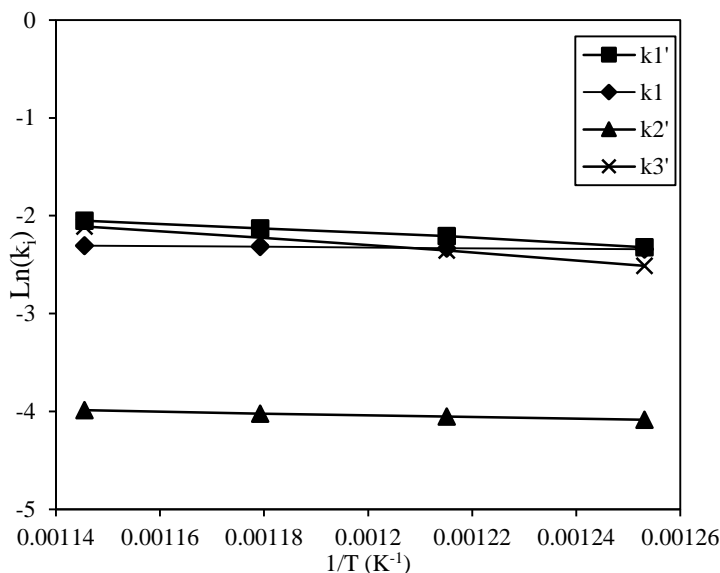
Figure 7.6. Plot of reaction constants versus temperature inverse

Activation energy is defined as the energy barrier required accomplishing a certain reaction. Thus by comparing the values of activation energies given in Table 7.4 , it can be seen that the activation energy for the formation of CO_x from ethane (reaction 2 in Figure 7.1) is lower than that required for the formation of ethylene and that is why it is difficult to control the selectivity to ethylene. On the other hand, activation energy in reaction 3 in Figure 7.1 is relatively high thus this reaction is difficult to occur. Furthermore, when actual activation energy for ODH (reaction 1 in Figure 7.1) to produce ethylene was calculated, it was found that this energy is less than the activation energy for the same reaction over 10% VO_x/Al_2O_3 catalyst [29] and this can explain the improved catalyst selectivity when compared to the un-modified version of the catalyst.

Figure 7.7 shows component partial pressure at various temperatures during ODH reaction in CREC riser simulator reactor together with the model predicted values. As can be seen in Figure 7.7, the model is in good agreement with experimental data. It is obvious

that Langmuir-Hinshelwood mechanism successfully represented ethane ODH reaction over 10% wt VO_x/Al_2O_3-ZrO_2. However, there is a slight deviation from experimental data at some points and this can be attributed to Langmuir-Hinshelwood nature which account mainly for adsorption and surface reaction. In contrast in some studies [18], it is reported that the participation of catalyst oxygen in both the selective and unselective steps of the reaction sequence indicating that ethane reduces the catalytic surface and creates oxygen vacancies, readily replenished by gaseous di-oxygen. Such fact should be considered by the proposed model together with the metal support interaction and redox properties. Figure 7.8 also shows overall plot of predicted components partial pressures versus experimental data. Figure 7.9 shows plot of model predicted product selectivity versus conversion at different reaction temperatures. Trend of data is consistent with the proposed reaction network.
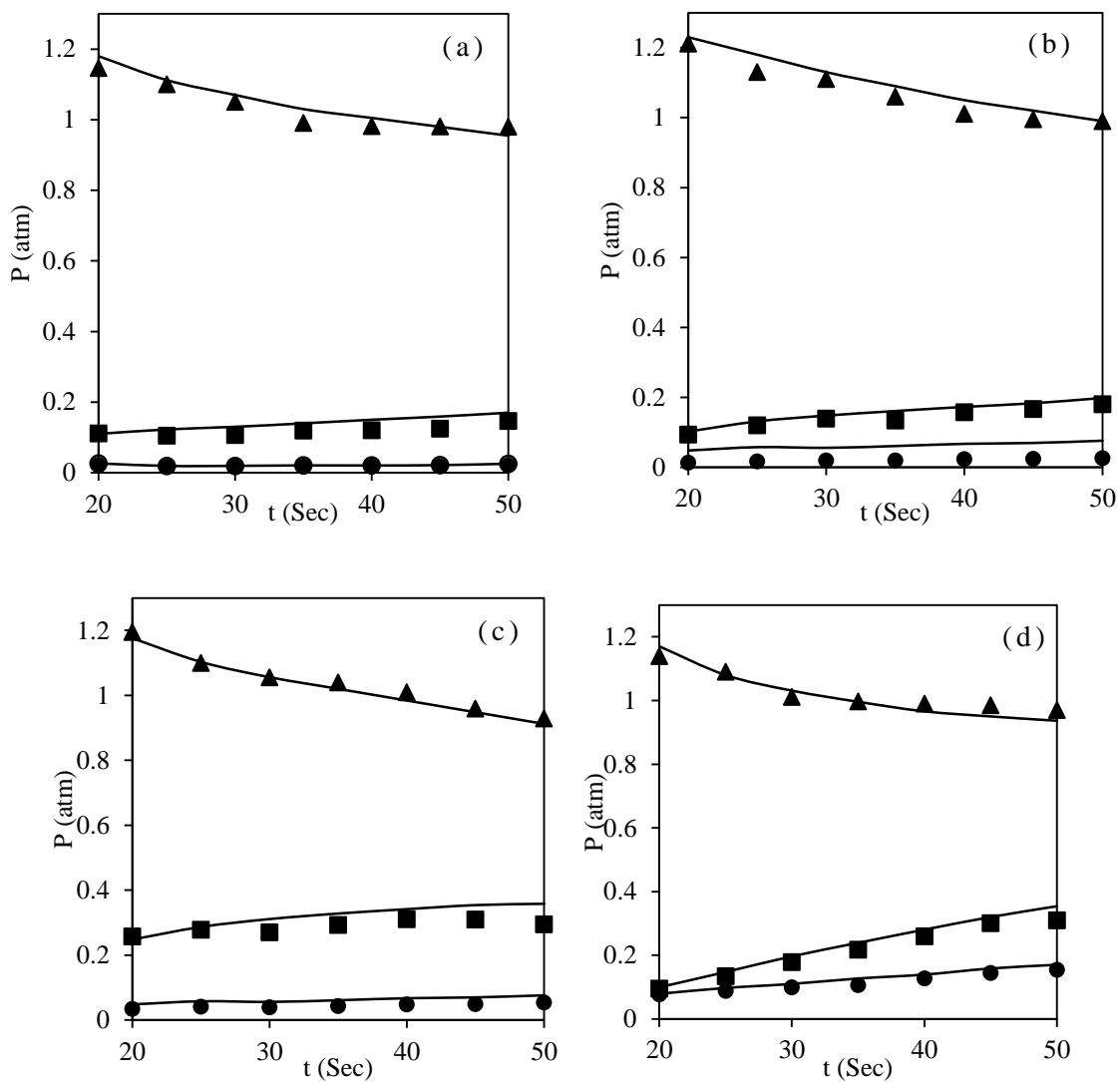
Figure 7.7. Experimental components partial pressure and predicted values versus time

(a)T=525°C, (b)T=550°C ,(c)T=575°C ,(d)T=600°C (feed =2ml ,w=0.4g, v=53

cm^3)(▲ ethylene ,■CO$_2$, ●CO, —— model)
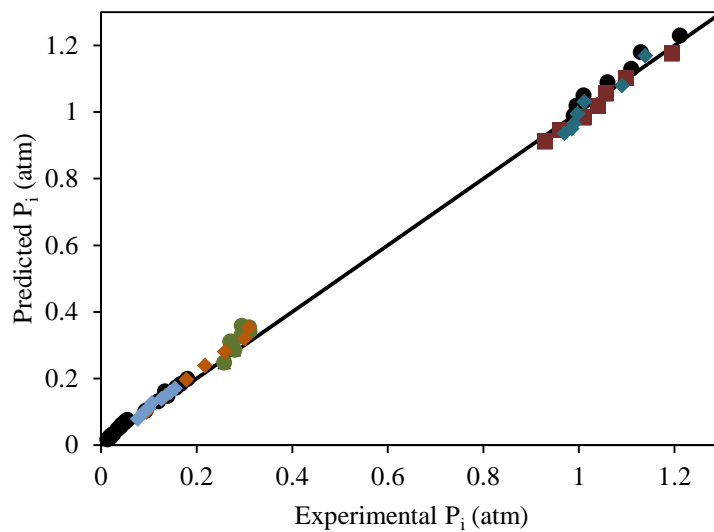
Figure 7.8. Model prediction results and experimental data (w=0.4g, feed=2 ml)
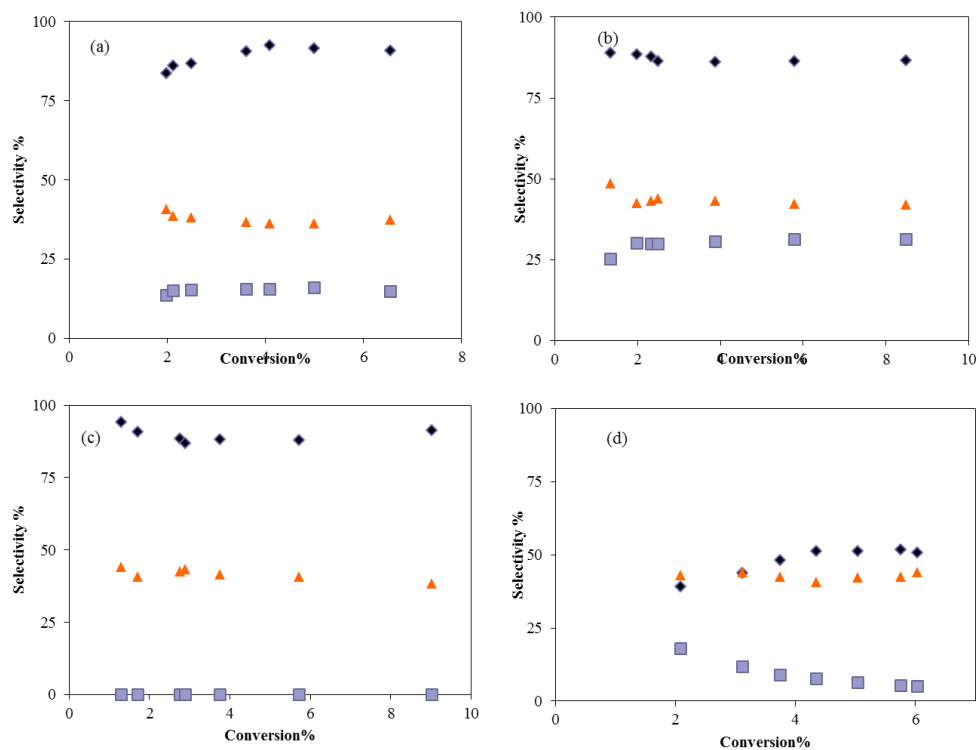
Figure 7.9. Overall predicted product selectivity versus conversion at (a) 525 ^{o}C, (b), 550

^{o}C (c) 575 ^{o}C, (d) 600 ^{o}C (♦ethylene, ▲CO$_2$, ■CO), consecutive reaction/regeneration

cycles, [Regeneration for 10 min at reaction temperature]

One may be interested in making a comparison between estimated kinetic parameters in this study and those in the literature. However there is only a few studies that reported fluidized bed ODH of ethane to ethylene kinetics. Therefore similar studies are used to compare the kinetic parameters as reported in Table 7.6. The dissimilarity between reported kinetic parameters and the values reported in the present study can be attributed to several reasons including different experimental set-up, different catalysts, reaction mechanism and the proposed network. It is reasonable to compare kinetic parameters in the present study to those were reported in Sameer et.al [19] because fluidized conditions was used, however catalyst is modified by ZrO_2. As can be seen in Table 7.6, activation energy of C_2H_4 formation is 88 kJ/mol, which is much higher than the calculated value in the present study (28.4 kJ/mol). This can be attributed to different

Table 7.6. Reported activation energy C_2H_4 of ethylene formation in ethane ODH

Catalyst	Activation energy of C_2H_4 formation kJ/mol	Reference	Notes
10 wt% VO_x/γ-Al_2O_3-ZrO_2 (1:1)	28.4	Present study	Fluidized bed ,oxygen free environment
10 wt% VO_x/c-Al_2O_3	88	12	Fluidized bed ,oxygen free environment
1.4 wt % VO_x/γ-Al_2O_3	94	16	Fixed bed reactor using O_2 supply
28.4 wt % VO_x/SiO_2	86	17	Fixed bed reactor using O_2 supply

catalyst compositions and properties which can be seen from XRD, TPR results. Furthermore, although both studies adopted Langmuir-Hinshelwood mechanism to express reaction rate, in the present study the L-H rate equation was modified assuming product partial pressure is very low in comparison with ethane partial pressure. Ethane ODH kinetic over VO_x based catalyst also investigated at fixed bed reactor and activation energy of C_2H_4 formation was found to be 94 kJ/mol as reported in Table 7.6 [46]. However, a different reaction network was proposed, by considering CO_x gases are only produced from ethane. Additionally, Mars-Van Krevelen mechanism was used to describe the reaction.

Following are the conclusions of kinetics modeling:

i.   The gas phase oxygen free ODH of ethane in fluidized bed proceeds with series-parallel reaction network forming ethylene, water and carbon oxides as major products. A Langmuir-Hinshelwood type model together with catalyst activity decay model (oxygen depletion) based on TPR results described the reaction rates adequately.

ii.   The model was found to be in a good agreement with experimental data. Reactants and products partial pressure during ODH reaction were predicted satisfactory.

iii.   The formation of ethylene requires lest amount of activation energy of 28.4 kJ/mol which is consistent to the experimental data (more selective product).

CHAPTER 8

OPTIMIZATION

Optimization and mathematical modeling are powerful tools to solve different problems which arise in chemical engineering. Problems as designing a plant, determining the number of units for a specific task, assigning raw materials to different production processes and deciding the production planning or production targets are some of the issues that can be solved through mathematical modeling. In other words, the mathematical formulations are used to make decisions at different levels, from the synthesis and design of the process up to its operation and scheduling. In the present study the objective is to optimize the operating conditions in CREC riser reactor, which is in this case study can be considered a batch unit. A batch unit operates in a non-continuous manner, receiving feed at certain times and after a processing time, producing products or intermediates. Semi-continuous units are characterized by a processing rate for each product; they are operated continuously with periodic startups and shutdowns.

The aim of this section is to optimize ODH of ethane to ethylene in fluidized bed reactor over $10\%VO_x/Al_2O_3$-ZrO_2 catalyst to determine the optimum conditions to achieve higher ethylene yield. As mentioned before literature review revealed that there are no much studies conducted. It is required to investigate this case study and to model the reaction to optimize ethylene yield. Kinetic model was utilized in optimization of ethane ODH reaction over $10\%VO_x/Al_2O_3$-ZrO_2 catalyst. In kinetic model in chapter 6 reaction network was assumed in the way that consider all possible reactions and the rate equation

as well established using Langmuir-Hinshelwood kinetics rate expression. Furthermore catalyst decaying performance was taken into account via modeling TPR experimental data for $10\% VO_x/Al_2O_3\text{-}ZrO_2$ catalyst in order to consider as much catalytic properties.

On the other hand in this study a mathematical model is developed based on temperature programmed reduction characterization technique. The objective is to correlate catalyst properties (metal loading, oxygen carrying capacity) to its performance during oxidation reaction. The model explicitly is a function of temperature and implicitly is a function of metal loading and other catalyst properties.

Oxygen releasing consumes hydrogen, this consumption of hydrogen measured with in certain temperature range. Catalyst reaction (consumption) with hydrogen makes a specific curve represents catalyst finger print according to catalyst properties. A single or a multiple peak curve can be obtained depending on the nature of metal oxide on catalyst surface [25,26]. The model is manly a modified standard normal distribution function

8.1. Optimization model development

There are a general steps in solving an optimization problems:

1. Analyze the process itself so that the process variables and specific characteristics of interest are defined; that is, make a list of all of the variables.
2. Determine the criterion for optimization, and specify the objective function in terms of the variables defined in step 1 together with coefficients. This step provides the performance model.
3. Using mathematical expressions, develop a valid process or equipment model that relates the input-output variables of the process and associated coefficients.

4. If the problem formulation is too large in scope: (a) break it up into manageable parts or (b) simplify the objective function and model.

5. Applying a suitable optimization technique to the mathematical statement of the problem.

8.1.1. Formulation of optimization program

Hypothesis:

    i.   Reaction pathways are irreversible as shown in Figure 7.1 in chapter 7.

    ii.   Rate of production of ethylene follows Langmuir-Hinshelwood kinetics.

    iii.   Catalyst composition controlling the O_2 release.

    iv.   Catalyst restore its performance after regeneration.

    v.   Catalyst properties represented by TPR mathematical model.

The objective function represents such factors as profit, cost, energy, and yield in terms of the key variables of the process being analyzed. The process model and constraints describe the interrelationships of the key variables [70]. In this study the objective function is ethylene partial pressure inside the reactor. The explicit decision variables are Temperature, time and catalyst weight with the implicit catalyst characteristics.

This section deals with development of the optimization model for ethane ODH reaction over VO_x/Al_2O_3 catalyst. Optimization strategy is to quantify the best solution to a problem within constraints. The optimization models consist of:

    i.   Variables: all types may be present.

    ii.   Parameters: the parameters are fixed to values.

    iii.   Constraints: the limitation on the variables value.

95

iv.   Mathematical relationships or equations: the mathematical expressions can

include equalities, inequalities and logical conditions. In general the model

equalities are usually include mass balances, energy balances, equilibrium

relations and engineering relations. The model inequalities often consists of

allowable operating limits, specification, performance requirement and

bounds on availability's.

The general form of such an optimization model is:

$\max f(x, y, p)$

such that,

$h(x, y, p) = 0$
$g(x, y, p) \leq 0$

$x \in X \leq R^n$ $(x$ is a vector of continuous variables)

$y \in Y = \{0,1\}$ $(y$ is a vector of binary variables)

p

                          $(p$ is a vector of parameters)

- Variables

The continuous variables, x, are real numbers that may represent time, temperature,

pressure and catalyst weight

- Objective Function

In this work the objective for the model is to maximize ethylene partial pressure

- Constraints

h(x,y,p) are the equality constraints which correspond to reaction rates , reaction

constants and partial pressure of each components

$g(x,y) \leq 0$ are the inequality constraints which correspond to limitation on time, temperature and catalyst weight

The model for ethane ODH reaction optimization is as follow:

Max

$$\frac{dP_{C2H6}}{dt} = -\frac{WRT}{V}(r_1 + r_2) \tag{8.1}$$

s.t

$$\frac{dP_{C2H4}}{dt} = \frac{WRT}{V}(r_1 - r_3) \tag{8.2}$$

$$\frac{dP_{C2H6}}{dt} = \frac{4WRT}{V}(r_2 + r_3) \tag{8.3}$$

$$r_1 = \frac{k_1' P_{C2H6}}{1 + K_{C2H6}^A P_{C2H6}} \alpha \tag{8.4}$$

$$r_2 = \frac{k_2' P_{C2H6}}{1 + K_{C2H6}^A P_{C2H6}} \alpha \tag{8.5}$$

$$r_3 = \frac{k_3' P_{C2H4}}{1 + K_{C2H6}^A P_{C2H6}} \alpha \tag{8.6}$$

$$\alpha = \frac{\int_0^T a + b \times Exp[\frac{-(T-T_m)^2}{2*c^2}]}{\int_0^{1000} a + b \times Exp[\frac{-(T-T_m)^2}{2*c^2}]} \tag{8.7}$$

$$K_i = k_{i,0} Exp\left[\frac{-E_i}{R} \times \left(\frac{1}{T} - \frac{1}{T_m}\right)\right] \tag{8.8}$$

$$525 < T < 600 \tag{8.9}$$

$$20 < t < 120 \tag{8.10}$$

$$0 < W < 1 \tag{8.11}$$

Model established in form of non-linear program NLP with inequality constraints. Model non-linearity appears from the rate Equations 8.4, 8.5 and 8.6 where components partial pressure appears in both numerator and the denominator. And as mentioned earlier; model can be considered as a function of reaction temperature T and time t with catalyst weight. However catalyst properties (metal loading, oxygen carrying capacity) included also with in the term α. GAMS software was used to optimize the objective function using CONOPT solver.

8.1.2. Reaction and kinetic parameters

Reaction conditions as presented in chapter 4 where temperature vitiated between 525-600 ^{o}C , reaction time 20-50 seconds and catalyst weight in ODH reaction experiment was fixed at 0.4g. However these conditions reflected in the constraints with slight differences in order to explore wider range of conditions in optimization process. Kinetic parameters k_o and E_i values can be found in chapter 6 where kinetic model regression achieved and these values estimated. Similarly TPR model α associated parameters also can be found in chapter 6.

8.1.3. Undergoing optimization using GAMS

Nonlinear models created with GAMS must be solved with a nonlinear programming (NLP) algorithm. Currently, there is a large number of different solvers available and the number is growing. The most important distinction between the solvers is whether they attempt to find a local or a global solution. Solvers that attempt to find a global solution (so called Global Solvers) can usually not solve very large models. As a contrast most local solvers can work with much larger models. In the present study

CONOPT solver was used. The algorithm used in GAMS/CONOPT is based on the GRG

algorithm first suggested by Abadie and Carpentier (1969).

8.2.   Results and discussion

Reactor conditions optimized using GAMS software. Nonlinear solver used in order

to maximize ethylene production and thus to minimize CO_x, also to production and to

specify reactor conditions that achieve this objective under number of constraints. Solution

using GAMS gives zero errors, NONOPT and bounds.   Table 8.1 shows the model

parameters value, ethane conversion and ethylene selectivity calculated using Equations

8.12 and 8.13.   Moreover new reaction network appears according to optimum solution

where there is no CO_x gases produced directly from ethane as shown in Figure 8.1.

Table 8.1. Optimized kinetics parameters using GAMS software

Parameter	Value
P_{C2H6} (atm)	0.602
P_{C2H4} (atm)	0.836
P_{COx} (atm)	0.103
r_1 (mol/gcat.s.atm)	0.172
r_2 (mol/gcat.s.atm)	0
r_3 (mol/gcat.s.atm)	0.043
W (g)	0.2
T (^{o}C)	600
t (sec)	20
α	0.569
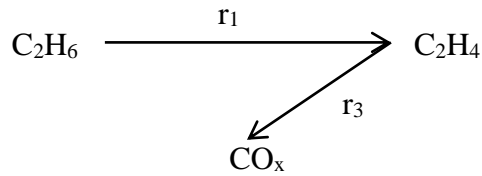
Figure 8.1. Optimized reaction network

Equations 8.12 and 8.13 used to calculate ethane conversion and product selectivity:

$$\text{Conversion of ethane} = \frac{\text{Moles of ethane converted}}{\text{Moles of ethane fed}} \times 100\ \% \qquad (8.12)$$

$$\text{Selectivity of product i} = \frac{\text{Moles of product i}}{\text{M of ethane}} \times 100\ \% \qquad (8.13)$$

Optimized ethylene selectivity found to be 92% at 5.9 % ethane conversion ant the optimum conditions found to be 600 ºC reaction temperature, 20 seconds reaction period and 0.2 g catalyst weight.
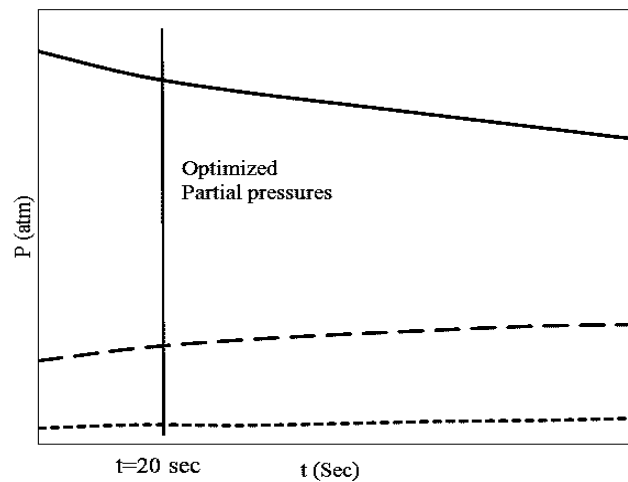
Figure 8.2. Plot of optimum partial pressure in time domain

These results consist with the observed conversion and selectivity trend during ODH reaction at various temperature where ethylene selectivity decreases with time and temperature due to CO_x formation temperature as can be seen in figure. In literature using different types of catalyst high selectivity to ethylene only achieved at low conversion. In other words selectivity decreases when conversion increased, this low selectivity can be attributed to thermodynamics limitation and selectivity control due to CO_x gases production [71]. Also these results eliminate reaction in Equation 7.2 in which ethane converted to CO_x by direct combustion. This is somehow is reasonable because combustion of ethane requires electrophilic oxygen O_2^- , on the other hand catalyst release nucleophilic oxygen (O^{2-} and O^-) to selectively oxidize the feed [72] .

CHAPTER 9

CONCLUSIONS AND RECOMMENDATIONS

A series of $VO_x/\gamma Al_2O_3$-ZrO_2 catalysts were synthesized, characterized and evaluated in a fluidized CREC Riser Simulator for ODH of ethane to ethylene in gas phase oxygen free reaction conditions. The phenomenological kinetics model was developed using Langmuir-Hinshelwood type rate expression. The optimum reaction conditions were determined using GAMS software and the reaction kinetics data obtained from the CREC Riser Simulator. Following are the conclusion of this research:

9.1. Effect of ZrO_2

i. XRD analysis show the presence of both V_2O_5 and ZrO_2 species on the VO_x/γ-Al_2O_3-ZrO_2 catalysts. XRD patterns also indicate that VO_x is present in the prepared catalyst in a crystalline phase, with the formation of this crystalline phase being promoted by the ZrO_2. Sample of VO_x/γ-Al_2O_3 catalyst display an amorphous phase only.

ii. TPR results show good V_2O_5 reduction activity at low ZrO_2 content (2;1 ratios). TPR/TPO oxidation-reduction cycles show good catalyst stability. Increasing ZrO_2 content decreases the percent of metal reduction.

iii. NH_3-TPD measurements show the existence of weak acid sites on the VO_x/γ-Al_2O_3-ZrO_2. The desorption kinetics suggests a medium range of interaction energies

involved between VO_x, and the support, with this likely enhancing metal reducibility.

iv. ODH of ethane in the presence of $VO_x/\gamma\text{-}Al_2O_3\text{-}ZrO_2$ and under free oxygen atmosphere shows that ethylene, CO and CO_2 are the major products.

v. Among the three samples, the catalyst with $\gamma\text{-}Al_2O_3\text{:}ZrO_2 = 2\text{:}1$ ratio gives the highest ethane conversion (37.9%). This result agrees with TPR analysis which shows best reducibility (highest H_2 consumption).

vi. The $VO_x/\gamma\text{-}Al_2O_3\text{-}ZrO_2$ catalyst ($\gamma\text{-}Al_2O_3\text{:}ZrO_2 = 2\text{:}1$) gives ethylene selectivity up to 90 % (at 600 °C) while the unmodified $VO_x/\gamma\text{-}Al_2O_3$ catalyst gives 42 % ethylene selectivity under same reaction conditions.

vii. ZrO_2 addition alters the acidity and structure of the support which influences the formation of VO_x (mono or poly). The ZrO2 also affects the metal support interaction and plays a vital role in lowering VO_x reducibility, therefore ethylene selectivity was increased due to controlled O_2 release.

9.2. Effect of VO_x reducibility

i. $VO_x/Al_2O_3\text{-}ZrO_2$ catalyst gives good ethylene selectivity at 10% VO_x loading. This ethylene selectivity was stable in reaction temperature range.

ii. XRF techniques was used to confirm catalyst composition and BET surface area was used to measure the surface area.

iii. XRD and Raman analysis indicates the presence of V_2O_5 and ZrO_2 in the $VO_x/Al_2O_3\text{-}ZrO_2$ catalyst. XRD pattern of $VO_x/Al_2O_3\text{-}ZrO_2$ showed that VO_x are present in crystalline phase, this phase introduced by ZrO_2. Raman spectra

confirmed the existence of isolated and polyvanadate species. NH_3-TPD measurement indicates weak acid sites on the VO_x/γ-Al_2O_3-ZrO_2.

iv. The TPR results showed two peaks due to reduction of V_2O_5 which occurs in two steps at low ZrO_2 contents.

v. Activation energy from TPR kinetics indicated lower reducibility at high VO_x loading with random nucleation mechanism.

9.3. ODH Kinetic modeling

i. The gas phase oxygen free ODH of ethane in fluidized bed proceeds with series-parallel reaction network forming ethylene, water and carbon oxides as major products. A Langmuir-Hinshelwood type model together with catalyst activity decay model based on TPR results described the reaction rates adequately.

ii. The model was found to be in a good agreement with experimental data. Reactants and products partial pressure during ODH reaction were predicted satisfactory.

iii. The formation of ethylene requires lest amount of activation energy of 28.4 kJ/mol which is consistent to the experimental data (more selective product).

9.4. Optimization of ethane ODH reaction

i. Based on kinetic studies of ODH of ethane to ethylene reaction in CREC-riser over VO_x/γ-Al_2O_3-ZrO_2 catalyst, an optimization model developed and TPR mathematical model utilized to describe catalyst activity behavior and properties such as metal loading percentage and type of materials. The optimization model also consistence with reaction data extracted from CREC- riser reactor.

ii.   ODH reaction conditions of ethane to ethylene reaction in CREC-riser over VO_x/γ-Al_2O_3-ZrO_2catalyst were optimized using the developed optimization model in GAMS software and higher Selectivity and conversion obtained using less amount of catalyst and higher reaction temperature for short period of time.

9.5.   Recommendations

i.   Further investigation of VO_x and ZrO_2 content and catalyst surface science to increase conversion.

ii.   Deferent methods of synthesis.

iii.   Different catalyst to feed ratios and fluidization speed.

iv.   Development of reaction rate expression after determination of adsorption constant experimentally.

v.   Development of optimization model to optimize different types of catalysts

References

[1] S. A. Mulla, O. V Buyevskaya, and M. Baerns, "A comparative study on non-catalytic and catalytic oxidative dehydrogenation of ethane to ethylene," vol. 226, pp. 73–78, 2002.

[2] M. Loukah, J. C. Vedrine, and M. Ziyad, "Oxidative dehydrogenation of ethane on V- and Cr-based phosphate catalysts," vol. 4, 1995.

[3] P. Ciambelli, P. Galli, L. Lisi, M. A. Massucci, P. Patrono, R. Pirone, G. Ruoppolo, and G. Russo, "TiO_2 supported vanadyl phosphate as catalyst for oxidative dehydrogenation of ethane to ethylene," vol. 203, pp. 133–142, 2000.

[4] J. E. Miller, M. M. Gonzales, L. Evans, A. G. Sault, C. Zhang, R. Rao, G. Whitwell, A. Maiti, and D. King-Smith, "Oxidative dehydrogenation of ethane over iron phosphate catalysts," Appl. Catal. A Gen., vol. 231, no. 1–2, pp. 281–292, May 2002.

[5] J. P. Bortolozzi, L. B. Gutierrez, and M. a. Ulla, "Synthesis of Ni/Al_2O_3 and Ni–Co/Al_2O_3 coatings onto AISI 314 foams and their catalytic application for the oxidative dehydrogenation of ethane," Appl. Catal. A Gen., vol. 452, pp. 179–188, Feb. 2013.

[6] L. Marchese, "Acid SAPO-34 Catalysts for Oxidative Dehydrogenation of Ethane," J. Catal., vol. 208, no. 2, pp. 479–484, Jun. 2002.

[7]   X. Lin, C. a. Hoel, W. M. H. Sachtler, K. R. Poeppelmeier, and E. Weitz, "Oxidative dehydrogenation (ODH) of ethane with O_2 as oxidant on selected transition metal-loaded zeolites," J. Catal., vol. 265, no. 1, pp. 54–62, Jul. 2009.

[8]   Y. Schuurman, V. Ducarme, T. Chen, W. Li, C. Mirodatos, and G. A. Martin, "Low temperature oxidative dehydrogenation of ethane over catalysts based on group VIII metals," Appl. Catal. A Gen., vol. 163, no. 1–2, pp. 227–235, Dec. 1997.

[9]   Y. Wu, J. Gao, Y. He, and T. Wu, "Preparation and characterization of Ni–Zr–O nanoparticles and its catalytic behavior for ethane oxidative dehydrogenation," Appl. Surf. Sci., vol. 258, no. 11, pp. 4922–4928, Mar. 2012.

[10]   H. Zhu, S. Ould-Chikh, D. H. Anjum, M. Sun, G. Biausque, J.-M. Basset, and V. Caps, "Nb effect in the nickel oxide-catalyzed low-temperature oxidative dehydrogenation of ethane," J. Catal., vol. 285, no. 1, pp. 292–303, Jan. 2012.

[11]   N. Haddad, E. Bordes-Richard, L. Hilaire, and a. Barama, "Oxidative dehydrogenation of ethane to ethene on alumina-supported molybdenum-based catalysts modified by vanadium and phosphorus," Catal. Today, vol. 126, no. 1–2, pp. 256–263, Aug. 2007.

[12]   L. Lisi, G. Ruoppolo, M. P. Casaletto, P. Galli, M. a. Massucci, P. Patrono, and F. Pinzari, "Vanadium-metal(IV)phosphates as catalysts for the oxidative dehydrogenation of ethane," J. Mol. Catal. A Chem., vol. 232, no. 1–2, pp. 127–134, May 2005.

[13] B. Solsona, J. M. López-Nieto, M. Alcántara-Rodríguez, E. Rodríguez-Castellón, and a. Jiménez-López, "Oxidative dehydrogenation of ethane on Cr, mixed Al/Cr and mixed Ga/Cr oxide pillared zirconium phosphate materials," J. Mol. Catal. A Chem., vol. 153, no. 1–2, pp. 199–207, Mar. 2000.

[14] Z. Wang, L. Chen, G. Zou, X. Luo, R. Gao, L. Chou, and X. Wang, "A novel $BaCl_2$–TiO_2–SnO_2 catalyst for the oxidative dehydrogenation of ethane," Catal. Commun., vol. 25, no. 3, pp. 45–49, Aug. 2012.

[15] Q. ZHOU, D. ZHOU, Y. WU, and T. WU, "Oxidative dehydrogenation of ethane over RE-NiO (RE=La, Nd, Sm, Gd) catalysts," J. Rare Earths, vol. 31, no. 7, pp. 669–673, Jul. 2013.

[16] Y. Brik, "Titania-Supported Cobalt and Cobalt–Phosphorus Catalysts: Characterization and Performances in Ethane Oxidative Dehydrogenation," J. Catal., vol. 202, no. 1, pp. 118–128, Aug. 2001.

[17] N. Haddad, E. Bordes-Richard, and a. Barama, "MoO_x-based catalysts for the oxidative dehydrogenation (ODH) of ethane to ethylene," Catal. Today, vol. 142, no. 3–4, pp. 215–219, Apr. 2009.

[18] A. Qiao, V. N. Kalevaru, J. Radnik, a. Srihari Kumar, N. Lingaiah, P. S. Sai Prasad, and a. Martin, "Oxidative dehydrogenation of ethane to ethylene over V_2O_5/Nb_2O_5 catalysts," Catal. Commun., vol. 30, pp. 45–50, Jan. 2013.

[19] S. Al-Ghamdi, M. Volpe, M. M. Hossain, and H. de Lasa, "$VO_x/c-Al_2O_3$ catalyst for oxidative dehydrogenation of ethane to ethylene: Desorption kinetics and catalytic activity," Appl. Catal. A Gen., vol. 450, pp. 120–130, Jan. 2013.

[20] Bakare, I.A., Shamseldin M., Razzak, S.A., Al-Ghamdi, S., **Hossain, M.M.**, de Lasa, H.I., Fluidized bed ODH of ethane to ethylene over $VOx-MoO_x/\gamma-Al_2O_3$ catalyst: Desorption kinetics and catalytic activity, Chemical Engineering Journal, doi:10.1016/j.cej.2014.09.114.

[21] B. Fu, J. Lu, P. C. Stair, G. Xiao, M. C. Kung, and H. H. Kung, "Oxidative dehydrogenation of ethane over alumina-supported Pd catalysts. Effect of alumina overlayer," J. Catal., vol. 297, pp. 289–295, Jan. 2013.

[22] X. Lin, K. R. Poeppelmeier, and E. Weitz, "Oxidative dehydrogenation of ethane with oxygen catalyzed by K–Y zeolite supported first-row transition metals," Appl. Catal. A Gen., vol. 381, no. 1–2, pp. 114–120, Jun. 2010.

[23] G. Tsilomelekis, A. Christodoulakis, and S. Boghosian, "Support effects on structure and activity of molybdenum oxide catalysts for the oxidative dehydrogenation of ethane," Catal. Today, vol. 127, no. 1–4, pp. 139–147, Sep. 2007.

[24] D. Ahchieva, M. Peglow, S. Heinrich, L. Mörl, T. Wolff, and F. Klose, "Oxidative dehydrogenation of ethane in a fluidized bed membrane reactor," Appl. Catal. A Gen., vol. 296, no. 2, pp. 176–185, Dec. 2005.

[25]   E. López, E. Heracleous, A. a. Lemonidou, and D. O. Borio, "Study of a multitubular fixed-bed reactor for ethylene production via ethane oxidative dehydrogenation," Chem. Eng. J., vol. 145, no. 2, pp. 308–315, Dec. 2008.

[26] Desislava Ahchieva , MirkoPeglow, Stefan Heinrich , LotharMorl,Tania Wolff, Frank Klose ," Oxidative dehydrogenation of ethane in a fluidized bed membrane reactor", Applied Catalysis A: General 296 (2005) 176–185.

[27]   Eduardo Lópeza, EleniHeracleous, Angeliki A. Lemonidou, Daniel O. Borio," Study of a multitubular fixed-bed reactor for ethylene production via ethane oxidative dehydrogenation", Chemical Engineering Journal 145 (2008) 308–315.

[28]   K. Chen, A. Khodakov, J. Yang, A. T. Bell, and E. Iglesia, "Isotopic Tracer and Kinetic Studies of Oxidative Dehydrogenation Pathways on Vanadium Oxide Catalysts," vol. 333, pp. 325–333, 1999.

[28]   K. Chen, E. Iglesia, and A. T. Bell, "Isotopic Tracer Studies of Reaction Pathways for Propane Oxidative Dehydrogenation on Molybdenum Oxide Catalysts," pp. 646–653, 2001.

[29]   M. D. Argyle, K. Chen, A. T. Bell, and E. Iglesia, "Ethane Oxidative Dehydrogenation Pathways on Vanadium Oxide Catalysts," pp. 5421–5427, 2002.

[30]   E. Heracleous, A. a Lemonidou, and J. a Lercher, "Mechanistic features of the ethane oxidative dehydrogenation by in situ FTIR spectroscopy over a MoO_3/Al_2O_3 catalyst," Appl. Catal. A Gen., vol. 264, no. 1, pp. 73–80, Jun. 2004.

[31] F. Klose, "Selective oxidation of ethane over a $VO_x/\gamma-Al_2O_3$ catalyst – investigation of the reaction network," Appl. Catal. A Gen., vol. 260, no. 1, pp. 101–110, Mar. 2004.

[32] R. Grabowski and J. Słoczyński, "Kinetics of oxidative dehydrogenation of propane and ethane on VO_x/SiO_2 pure and with potassium additive," Chem. Eng. Process. Process Intensif., vol. 44, no. 10, pp. 1082–1093, Oct. 2005.

[33] E. Heracleous and a Lemonidou, "Ni–Nb–O mixed oxides as highly active and selective catalysts for ethene production via ethane oxidative dehydrogenation. Part II: Mechanistic aspects and kinetic modeling," J. Catal., vol. 237, no. 1, pp. 175–189, Jan. 2006.

[34] E. Heracleous and a. a. Lemonidou, "Reaction pathways of ethane oxidative and non-oxidative dehydrogenation on $\gamma-Al_2O_3$ studied by temperature-programmed reaction (TP-reaction)," Catal. Today, vol. 112, no. 1–4, pp. 23–27, Mar. 2006.

[35] A. Dinse, S. Khennache, B. Frank, C. Hess, and R. Herbert, "Oxidative dehydrogenation of propane on silica (SBA-15) supported vanadia catalysts : A kinetic investigation," vol. 307, pp. 45–50, 2009.

[36] F. Rahman, K. F. Loughlin, M. a. Al-Saleh, M. R. Saeed, N. M. Tukur, M. M. Hossain, K. Karim, and A. Mamedov, "Kinetics and mechanism of partial oxidation of ethane to ethylene and acetic acid over MoV type catalysts," Appl. Catal. A Gen., vol. 375, no. 1, pp. 17–25, Feb. 2010.

[37]   Kung. H., "Oxidative deydrogenation of light (C_2 to C_4) Alkanes." pp. 1–38, 1994.

[38]   J. Gascón, R. Valenciano, C. Téllez, J. Herguido, and M. Menéndez, "A generalized kinetic model for the partial oxidation of n-butane to maleic anhydride under aerobic and anaerobic conditions," Chem. Eng. Sci., vol. 61, no. 19, pp. 6385–6394, Oct. 2006.

[39]   O. Rubio, J. Herguido, and M. Menéndez, "Oxidative dehydrogenation of n-butane on V/MgO catalysts—kinetic study in anaerobic conditions," Chem. Eng. Sci., vol. 58, no. 20, pp. 4619–4627, Oct. 2003.

[40]   V. Balcaen, I. Sack, M. Olea, and G. B. Marin, "Transient kinetic modeling of the oxidative dehydrogenation of propane over a vanadia-based catalyst in the absence of O_2," Appl. Catal. A Gen., vol. 371, no. 1–2, pp. 31–42, Dec. 2009.

[41]   K. Fukudome, N. Ikenaga, T. Miyake, and T. Suzuki, "Oxidative dehydrogenation of propane using lattice oxygen of vanadium oxides on silica," Catal. Sci. Technol., vol. 1, no. 6, p. 987, 2011.

[42]   J. Herguido, M. Mene, and J. Santamarı, "Oxidative Dehydrogenation of n -Butane in a Two-Zone Fluidized-Bed Reactor," pp. 90–97, 1999.

[43]   E. A. Mamedov and V. C. Corberfin, "A : Oxidative dehydrogenation of lower alkanes on vanadium oxide-based catalysts . The present state of the art and outlooks," vol. 127, 1995.

[44] S. A. Al-ghamdi, M. M. Hossain, and H. I. De Lasa, "Kinetic Modeling of Ethane Oxidative Dehydrogenation over VO_x/Al_2O_3Catalyst in a Fluidized-Bed Riser Simulator," 2013.

[45] E. Nouri, M. Shahmiri, H. R. Rezaie, and F. Talayian, "The effect of alumina content on the structural properties of ZrO_2-Al_2O_3 unstabilized composite nanopowders," pp. 1–8, 2012.

[46] A. Ajbar and E. Ali, "Dynamic Modeling and Control of a Fluidized Bed Reactor for the Oxidative Dehydrogenation of Ethylbenzene to Styrene Department of Chemical Engineering ," vol. 10, no. 2, p. 9661, 1998.

[47] S. E. Pheng, N. Aishah, and S. Amin, "[ENE06] Optimization of ethylene yield in oxidative coupling of methane over Li / MgO catalyst," pp. 574–578, 2004.

[48] Y. Amini, M. Fattahi, F. Khorasheh, and S. Sahebdelfar, "Neural network modeling the effect of oxygenate additives on the performance of Pt–Sn/γ-Al_2O_3 catalyst in propane dehydrogenation," Appl. Petrochemical Res., vol. 3, no. 1–2, pp. 47–54, Jun. 2013.

[49] F. Klose, T. Wolff, H. Lorenz, a Seidelmorgenstern, Y. Suchorski, M. Piorkowska, and H. Weiss, "Active species on γ-alumina-supported vanadia catalysts: Nature and reducibility," J. Catal., vol. 247, no. 2, pp. 176–193, Apr. 2007.

[50] M. Argyle, "Effect of Catalyst Structure on Oxidative Dehydrogenation of Ethane and Propane on Alumina-Supported Vanadia," J. Catal., vol. 208, no. 1, pp. 139–149, May 2002.

[51]   A. M. Elfadly, A. M. Badawi, F. Z. Yehia, Y. A. Mohamed, M. A. Betiha, and A. M. Rabie, "Selective nano alumina supported vanadium oxide catalysts for oxidative dehydrogenation of ethylbenzene to styrene using CO_2 as soft oxidant," Egypt. J. Pet., vol. 22, no. 3, pp. 373–380, Dec. 2013.

[52]   E. Nouri, M. Shahmiri, H. R. Rezaie, and F. Talayian, "The effect of alumina content on the structural properties of ZrO_2 -Al_2O_3 unstabilized composite nanopowders," pp. 1–8, 2012.

[53]   Y. H. Kim and H. Lee, "Redox Property of Vanadium Oxide and Its Behavior in Catalytic Oxidation," vol. 20, no. 12, 1999.

[54]   I. E. Wachs, "Catalysis science of supported vanadium oxide catalysts.," Dalton Trans., vol. 42, no. 33, pp. 11762–9, Sep. 2013.

[55]   J. R. Sohn, S. G. Cho, Y. Il Pae, and S. Hayashi, "Characterization of Vanadium Oxide – Zirconia Catalyst," vol. 177, no. 0076, pp. 170–177, 1996.

[56]   Anna G. and Aftanas G., "The global approach to TPD and isothermal adsorption – desorption kinetics .," Proceedings on, Tatranské Matliare (SK), 26 – 30 May, 2003.

[57]   D. Sun, R. Narita, F. Sato, Y. Yamada, and S. Sato, "Catalytic Dehydration of 1,2-Propanediol into Propanal over Ag-Modified Silica;Alumina," Chem. Lett., vol. 43, no. 4, pp. 450–452, 2014.

[58]   P. Liu, K. Zhu, Y. Gao, Q. Wu, J. Liu, J. Qiu, Q. Gu, and H. Zheng, "Ultra-long VO2 (A) nanorods using the high-temperature mixing method under hydrothermal

conditions: synthesis, evolution and thermochromic properties," CrystEngComm, vol. 15, no. 14, p. 2753, 2013.

[59]   X. . Wang, H. . Li, Y. . Fei, X. Wang, Y. . Xiong, Y. . Nie, and K. . Feng, "XRD and Raman study of vanadium oxide thin films deposited on fused silica substrates by RF magnetron sputtering," Appl. Surf. Sci., vol. 177, no. 1–2, pp. 8–14, Jun. 2001.

[60]   R. Bulánek, P. Čičmanec, and M. Setnička, "Possibility of VO_x/SiO_2 Complexes Speciation: Comparative Multi-wavelength Raman and DR UV-vis Study," Phys. Procedia, vol. 44, pp. 195–205, Jan. 2013.

[61]   I. E. Wachs, "i," vol. 157, pp. 67–90, 1997.

[62]   P. O. F. We, J. A. T. Solid, and S. Interface, "J. HABER, T. MACHEJ and T. CZEPPE," vol. 151, pp. 301–310, 1985.

[63]   M. A. Bañares, M. V Mart, X. Gao, J. L. G. Fierro, and I. E. Wachs, "Dynamic behavior of supported vanadia catalysts in the selective oxidation of ethane In situ Raman , UV − Vis DRS and reactivity studies," vol. 61, pp. 295–301, 2000.

[64]   A. Auroux, Top. Catal. 4 (1) (1997) 71–89.

[65]   Mohammad M. Hossain , Hugo I. de Lasa Reactivity and Stability of Co-Ni/Al_2O_3 Oxygen carrier in multicycle CLC , AIChE Journal July 2007 Vol. 53, No. 7.

[66]   N.W. Hurst , S.J. Gentry , A. Jones , Catal. Rev. Sci. Eng. 1982, 24 ,233.

[67]   M. A. Bañares, M. V Mart, X. Gao, J. L. G. Fierro, and I. E. Wachs, "Dynamic behavior of supported vanadia catalysts in the selective oxidation of ethane In situ Raman , UV − Vis DRS and reactivity studies," vol. 61, pp. 295–301, 2000.

[68] Richardson JT, Scates RM, Twigg MV. X-ray diffraction of hydrogen reduction of NiO/a-Al$_2$O$_3$ steam reforming catalysts, Appl CatalA: General. 2004;267:35–46.

[69]   Kanervo JM, Krause AOI. Kinetics analysis of temperature-programmed reduction: behavior of a CrO$_x$/Al$_2$O$_3$ catalyst. J PhysChem B. 2001; 105:9778–9784.

[70]   L. L. F. Edgar, David M. Himmelblau, Optimization of chemical processes, Second. McGraw-Hill, 2001.

[71]   B. Mitra, I. E. Wachs, and G. Deo, "Promotion of the propane ODH reaction over supported V$_2$O$_5$/Al$_2$O$_3$ catalyst with secondary surface metal oxide additives," J. Catal., vol. 240, no. 2, pp. 151−159, Jun. 2006.

[72]   A. Comite, a. Sorrentino, G. Capannelli, M. Di Serio, R. Tesser, and E. Santacesaria, "Oxidative dehydrogenation of propane using V$_2$O$_5$/TiO$_2$/SiO$_2$ catalysts prepared by grafting titanium and vanadium alkoxides on silica," J. Mol. Catal. A Chem., vol. 198, no. 1–2, pp. 151−165, May 2003.

Vitae

Name   : Abd Alwadood Hassan Elbadawi

Nationality   : Sudanese

Date of Birth   : 3/11/1990

Email   : abdulwadoodhassan@gmail.com

Address   : King Fahd University of Petroleum & Minerals, Dhahran

Academic Background   : B.Sc. Chemical Engineering – University of Khartoum

Abd Alwadood H. Elbadawi is a M.S student at department of chemical engineering at King Fahd University of Petroleum and Minerals and research assistant at the research institute center of research excellence in corrosion. He went to University of Khartoum where he was awarded Bachelor of Science in chemical engineering. Currently is a member of research project in chemical engineering department funded by KACST on ethane conversion into ethylene. He also presented research papers in international conferences and presented a poster in the 23rd ISCRE & 7th APCRE , Bangkok , Thailand , September 2014.

Research Outcomes

Journal Papers (in progress):

1- **AbdAlwadood H. Elbadawi**, Mohammed S.Ba-Shammakh, Sameer Al-Ghamdi, Shaikh A. Razzak, Mohammad M. Hossain, Hugo I. de Lasa, "Fluidizable $VO_x/\gamma-Al_2O_3$-ZrO_2 Catalysts for ODH of Ethane to Ethylene in a Gas Phase Oxygen Free Environment".

2- **AbdAlwadood H. Elbadawi**, Mohammed S.Ba-Shammakh, Sameer Al-Ghamdi, Shaikh A. Razzak, Mohammad M. Hossain, Hugo I. de Lasa, "Fluidized-bed ODH of Ethane to Ethylene over $VO_x/\gamma-Al_2O_3$-ZrO_2 Catalyst: Effect of VO_x Reducibility on Catalyst Activity".

3- **AbdAlwadood H. Elbadawi**, Sameer A. Al-Ghamdi,Mohammad M. Hossian." Kinetic Modeling of Ethane Oxidative Dehydrogenation over 10% VO_x/Al_2O_3-ZrO_2 Catalyst in a Fluidized-Bed Riser Simulator".

4- **AbdAlwadood H. Elbadawi**, Mohammed S.Ba-Shammakh, Sameer Al-Ghamdi, Mohammad M. Hossain," An Optimization Model for ODH of Ethane to Ethylene on on VO_x/Al_2O_3 catalyst in a fluidized bed CREC Riser Simulator".

Conferences Contribution:

1- **AbdAlWadood H.E**, Mogahid Osman, Sameer Al-Ghamdi, Mohammed Ba-Shammakh, Shaikh A.Razzak, , Hugo I. de Lasa, Hossain, M.M. (2014), Fluidized-bed ODH of ethane to ethylene over V_2O_5-Nb/La-Al_2O_3 catalysts, 23rd Canadian symposium on catalysis, Edmonton, Alberta, Canada, May- 2014.

2- **AbdAlWadood Elbadawi**, Mogahid Osman, Mohammed Ba-Shammakh, Shaikh A. Razzak, Hossain, M.M. Hugo I. de Lasa (2014), Oxidative dehydrogenation of ethane to ethylene over V_2O_5/La-Al_2O_3 catalysts, 64th Canadian Chemical Engineering Conference, October 19-22, 2014, Niagra Falls, Ontario, Canada.

3- Idris A. Bakare, **AbdAlwadood H. Elbadawi**, Shaikh A. Razzak, Sameer Al-Ghamdi, Hugo I. de Lasa, Mohammad M. Hossain ," Fluidized bed ODH of ethane to ethylene over VO_x-MoO_x/γ-Al_2O_3 catalyst: Desorption kinetics and catalytic activity ", 23rd ISCRE & 7th APCRE , Bangkok , Thailand , September 2014.

4- **AbdAlWadood Elbadawi**, Mogahid Osman, Mohammed Ba-Shammakh, Shaikh A. Razzak, Hossain, M.M. Hugo I. de Lasa (2014), Oxidative dehydrogenation of ethane to ethylene over V_2O_5/La-Al_2O_3 catalysts, AIChE Annual Meeting, November 16-21, 2014, Hilton Atlanta, GA, USA.